Copyright Warning & Restrictions

The copyright law of the United States (Title 17, United States Code) governs the making of photocopies or other reproductions of copyrighted material.

Under certain conditions specified in the law, libraries and archives are authorized to furnish a photocopy or other reproduction. One of these specified conditions is that the photocopy or reproduction is not to be "used for any purpose other than private study, scholarship, or research." If a, user makes a request for, or later uses, a photocopy or reproduction for purposes in excess of "fair use" that user may be liable for copyright infringement,

This institution reserves the right to refuse to accept a copying order if, in its judgment, fulfillment of the order would involve violation of copyright law.

Please Note: The author retains the copyright while the New Jersey Institute of Technology reserves the right to distribute this thesis or dissertation

Printing note: If you do not wish to print this page, then select "Pages from: first page # to: last page #" on the print dialog screen

ABSTRACT

DEVELOPMENT OF NOVEL PROTEIN DIGESTION AND QUANTITATION METHODS FOR MASS SPECTROMETRIC ANALYSIS

by
Yongling Ai

Proteins are the workhorses of biology, playing multifaceted roles in maintaining cellular function, signaling, and response to environmental cues. Understanding their abundance and dynamics is pivotal for unraveling the complexities of biological processes, which underpins the foundations of molecular and cellular biology. Accurate measurement of protein quantities provides insights into cellular homeostasis, facilitates the discovery of biomarkers, and sheds light on the molecular mechanisms of diseases, bridging the gap between the molecular intricacies of proteins and their functional consequences in health and disease. The evolution of protein quantitation methodologies, from classical colorimetric assays to sophisticated mass spectrometry-based approaches, has expanded the analytical precision and dynamic range, enabling the detection of proteins at low abundance levels. The development of targeted proteomic techniques has further refined the quantitation process, allowing researchers to investigate specific proteins or post-translational modifications with high sensitivity and accuracy. However, bottom-up targeted proteomic analysis and quantitation often requires overnight tryptic digestion to ensure complete protein cleavage into peptides, which may significantly hamper experimental efficiency and induce some chemical modifications during the long digestion process. In addition, isotope-labeled internal standards are needed for the absolute quantitation of the target proteins. Syntheses of those standards are time-consuming and costly, and some of standards might not be available or difficult to synthesize if the

surrogate peptides contain post-translational modifications (PTMs). Therefore, developing new technologies to speed up the sample preparation process like digestion and standard-free quantitation strategies is essential and holds the promise of unlocking deeper insights into biology, driving innovation in diagnostics, and advancing the development of targeted therapies.

Accordingly, the goal of this work is to develop novel methods for the ultrafast tryptic digestion of proteins and standard-free quantitation for peptides and proteins absolute quantitation without building the calibration curve. Three projects are included here with two novel technologies, i.e., ultrafast microdroplet digestion and coulometric mass spectrometry, showing the different applications. Firstly, the investigation of tryptic protein digestion in microdroplets and in bulk solution is conducted to comprehensively evaluate the microdroplet digestion versus bulk overnight digestion by examining digestion efficiency. Secondly, standard-free coulometric mass spectrometry (CMS) is applied for the absolute quantitation of tryptophan-containing peptides and amyloid beta-peptide fragments. Thirdly, coulometric mass spectrometry is further extended for the absolute quantitation of protein mixture sample, host cell proteins as well as deamidation modification. The successful application of those emerging technologies shows the potential for fast and cost-efficient quantitation of peptides and proteins in clinical and pharmaceutical settings.

DEVELOPMENT OF NOVEL PROTEIN DIGESTION AND QUANTITATION METHODS FOR MASS SPECTROMETIC ANALYSIS

by
Yongling Ai

A Dissertation
Submitted to the Faculty of
New Jersey Institute of Technology
in Partial Fulfillment of the Requirements for the Degree of
Doctor of Philosophy in Chemistry

Department of Chemistry and Environmental Science

December 2023

.

APPROVAL PAGE

DEVELOPMENT OF NOVEL PROTEIN DIGESTION AND QUANTITATION METHODS FOR MASS SPECTROMETRIC ANALYSIS

Yongling Ai

Dr. Hao Chen, Dissertation Advisor — Date
Professor of Chemistry and Environmental Science, NJIT

Dr. Omowunmi Sadik, Committee Member — Date
Chair of Chemistry and Environment Science
Distinguished Professor of Chemistry and Environment Science, NJIT

Dr. Somenath Mitra, Committee Member — Date
Distinguished Professor of Chemistry and Environmental Science, NJIT

Dr. Yuanwei Zhang, Committee Member — Date
Assistant Professor of Chemistry and Environmental Science, NJIT

Dr. Zhi Wei, Committee Member — Date
Professor of Computer Science, NJIT

BIOGRAPHICAL SKETCH

Author: Yongling Ai

Degree: Doctor of Philosophy

Date: December 2023

Undergraduate and Graduate Education:

- Doctor of Philosophy in Chemistry,
  New Jersey Institute of Technology, Newark, NJ, 2023

- Master of Science in Pharmaceutical Analysis,
  China Pharmaceutical University, Nanjing, P.R. China, 2018

- Bachelor of Science in Pharmacy,
  Chongqing Medical University, Chongqing, P. R. China, 2015

Major: Chemistry

Presentations and Publications:

Publications:

Ai, Y.; Fnu, P. I. J.; Zhao, P.; Hassan, M. T.; Sharma, A.; Hao, G.; Zhou, Z.; Chen, H., Development of Coulometric Mass Spectrometry for Absolute Chemical Quantitation. *Encyclopedia of Analytical Chemistry* **2023,** accepted.

Ai, Y.; Gunawardena, H. P.; Li, X.; Kim, Y.-I.; Dewald, H. D.; Chen, H., Standard-Free Absolute Quantitation of Antibody Deamidation Degradation and Host Cell Proteins by Coulometric Mass Spectrometry. *Analytical Chemistry* **2022,** *94* (36), 12490-12499.

Ai, Y.; Xu, J.; Gunawardena, H. P.; Zare, R. N.; Chen, H., Investigation of Tryptic Protein Digestion in Microdroplets and in Bulk Solution. *Journal of the American Society for Mass Spectrometry* **2022,** *33* (7), 1238-1249.

Ai, Y.; Zhao, P.; Fnu, P. I. J.; Chen, H., Absolute Quantitation of Tryptophan-Containing Peptides and Amyloid β-peptide Fragments by Coulometric Mass Spectrometry. *Journal of the American Society for Mass Spectrometry* **2021,** *32* (7), 1771-1779.

Li, Y.; Castaneda-Bagatella, D., M. T.; Kakkad, D.; Ai, Y.; Chen, H.; Champagne, P., Synthetic and Mechanistic Study on the Conjugate Isothiocyanation of Enones with Trimethylsilyl Isothiocyanate. *Organic and Biomolecular Chemistry* **2023,** accepted.

Fnu, P. I. J.; Hassan, M. T.; Yaroshuk, T.; Ai, Y.; Chen, H., Absolute Quantitation of Peptides and Proteins by Coulometric Mass Spectrometry after Derivatization. *International Journal of Mass Spectrometry* **2023,** *495*, p117153.

Yu, S.; Reddy, O.; Abaci, A.; Ai, Y.; Li, Y.; Chen, H.; Guvendiren, M.; Belfield, K. D.; Zhang, Y., Novel BODIPY-Based Photobase Generators for Photoinduced Polymerization. *ACS Applied Materials and Interfaces* **2023**, *15* (38), 45281-45289.

Gunawardena, H. P.; Ai, Y.; Gao, J.; Zare, R. N.; Chen, H., Rapid Characterization of Antibodies via Automated Flow Injection Coupled with Online Microdroplet Reactions and Native-pH Mass Spectrometry. *Analytical Chemistry* **2023**, *95* (6), 3340-3348.

Liu, C.; Wang, Q.; Hivick, B. E.; Ai, Y.; Champagne, P. A.; Pan, Y.; Chen, H., Capture of Electrochemically Generated Fleeting Carbazole Radical Cations and Elucidation of Carbazole Dimerization Mechanism by Mass Spectrometry. *Analytical Chemistry* **2020,** *92* (23), 15291-15296.

Presentations:

Ai, Y.; Gunawardena, H. P.; Li, X.; Kim, Y.-I.; Dewald, H. D.; Chen, H., Standard-Free Absolute Quantitation of Antibody Deamidation Degradation and Host Cell Proteins by Coulometric Mass Spectrometry. Presented at 70th American Society of Mass Spectrometry annual conference, June 6-9, 2022, Minneapolis, MN.

Ai, Y.; Gunawardena, H. P.; Li, X.; Kim, Y.-I.; Dewald, H. D.; Chen, H., Standard-Free Absolute Quantitation of Antibody Deamidation Degradation and Host Cell Proteins by Coulometric Mass Spectrometry. Presented at 2022 Eastern Analytical Symposium and Exposition annual conference, November 13-15, Plainsboro, NJ.

Ai, Y.; Zhao, P.; Fnu, P. I. J.; Chen, H., Absolute Quantitation of Tryptophan-Containing Peptides and Amyloid β-peptide Fragments by Coulometric Mass Spectrometry. Presented at 69th American Society of Mass Spectrometry annual conference, June 6-9, 2021, Philadephia, PA.

Ai, Y.; Zhao, P.; Fnu, P. I. J.; Chen, H., Absolute Quantitation of Tryptophan-Containing Peptides and Amyloid β-peptide Fragments by Coulometric Mass Spectrometry. Presented at 2021 American Chemiscal Society (ACS) Spring Meetings and Expositions, June 6-9, Philadephia, PA.

TO MY PARENTS:

Jun Ai (Daddy) and Bingqiong Zhong (Mummy)
Thank you for your unconditional love and consistent support throughout this journey.

ACKNOWLEDGMENTS

I am grateful to Professor. Hao Chen for his guidance, everlasting patience, constant support, and encouragement as my dissertation advisor. Besides being an outstanding advisor, he is a friend who encouraged and allowed me to grow as an independent researcher through this Ph.D. journey.

I would also like to thank my committee members: Professor Omowunmi Sadik, Professor Somenath Mitra, Professor Yuanwei Zhang, and Professor Zhi Wei, for spending their time and sharing their expertise on completing my Ph.D..

I would like to express my appreciation for the funding provided by the Department of Chemistry and Environmental Science. Also, I am grateful for the research funding from the National Science Foundation (grant # CHE-1915878) and the National Institutes of Health (grant #1R15GM137311- 01).

I want to express my special thanks to the former graduates Dr. Pengyi Zhao and Dr. Qi Wang, for sharing their research experiences, interview tips and encouragement over numerous chats.

My gratitude goes to my friends at NJIT: Shupei Yu, Yanmei Li, Chen Wu, Pham Dung, Xiaokai Zhang, Nengyi huang. Thank you for being friends of mine and encouraging me to finish this journey.

Finally, sincerely thank my family members for their unconditional love and constant support, motivating me to pursue my dreams, and cheering me up during this journey.

TABLE OF CONTENTS

TABLE OF CONTENTS
(Continued)

Chapter **Page**

TABLE OF CONTENTS
(Continued)

Chapter **Page**

TABLE OF CONTENTS
(Continued)

LIST OF TABLES

LIST OF TABLES
(Continued)

Table **Page**

LIST OF FIGURES

LIST OF FIGURES
(Continued)

Figure **Page**

LIST OF FIGURES
(Continued)

Figure **Page**

LIST OF FIGURES
(Continued)

Figure **Page**

LIST OF FIGURES
(Continued)

Figure **Page**

LIST OF FIGURES
(Continued)

Figure **Page**

LIST OF FIGURES
(Continued)

Figure **Page**

LIST OF FIGURES
(Continued)

Figure **Page**

LIST OF SCHEMES

CHAPTER 1

INTRODUCTION

1.1 Microdroplet Reaction

1.1.1 Acceleration of reaction in charged microdroplets

Most chemical reactions are conventionally run in bulk phase. Recent studies have shown that significant reaction acceleration can be achieved at the air/solution interface of microdroplets.[1-6] The unique environment of microdroplets can drive reactions that are thermodynamically unfavorable in bulk phase. In 2011, examination of the reaction between a ketone (ketosteroid) and hydrazine (Girard T reagent) to form the hydrazone using reactive desorption electrospray ionization (DESI) clearly showed reaction acceleration in microdroplets in air compared to the corresponding reaction in the bulk phase (Figure 1.1).[7] Since then, the focus of this type of study has been divided between investigating the mechanism of this acceleration phenomenon in microdroplets and leveraging it for organic synthesis. To accelerate reactions, a variety of microdroplet formats have been developed, including preparative electrospray,[8] thin-film deposition,[9-11] microdroplets in sprays,[1, 2, 12, 13] the fusion of microdroplets,[14, 15] various levitated droplet experiments,[16, 17] and multiphase microdroplet reactions.[18] Based on how microdroplets have been generated and used as reaction vessels, the microdroplet reaction methodologies used so far can be broadly classified into five categories (Figure 1.2): (a) reactions in sprays, (b) reactions occurring during microdroplet collisions, (c) reactions occurring when microdroplets splash onto surfaces, (d) reactions in individual levitated microdroplets, and (e) reactions in thin films.[5]

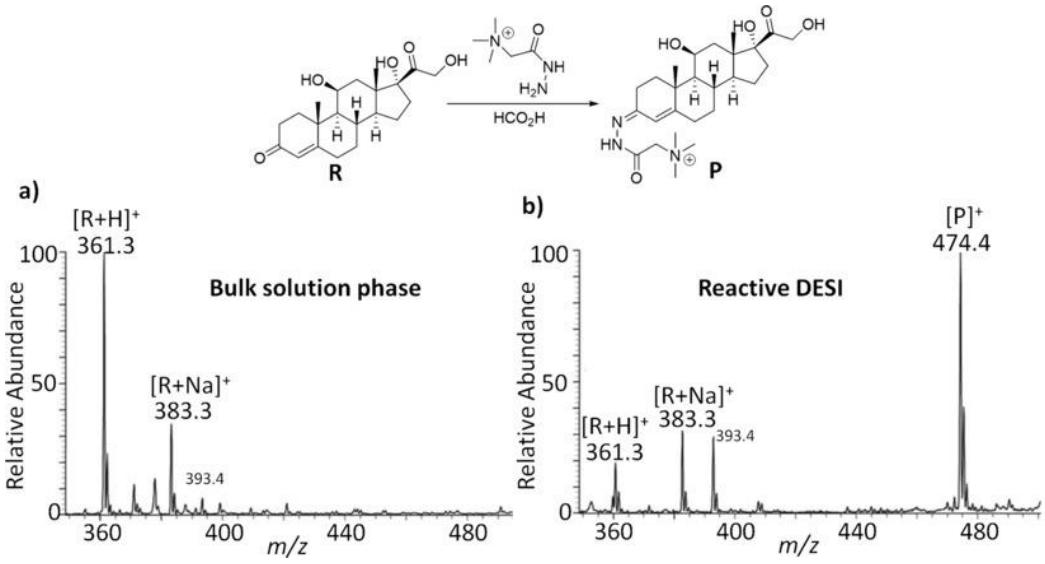

Figure 1.1 Mass spectra of the reaction mixture of Girad's reagent T with ketosteroid (R) to form the charge-labeled hydrazine product (P) recorded a) after 5 min in bulk solution, with no detectable product ions, or b) immediately in a reactive DESI experiment, showing dominant product ions.

Source: Yan, X.; Bain, R. M.; Cooks, R. G., Organic reactions in microdroplets: Reaction acceleration revealed by mass spectrometry. Angewandte Chemie International Edition ***2016,*** *55 (42), 12960-12972.*

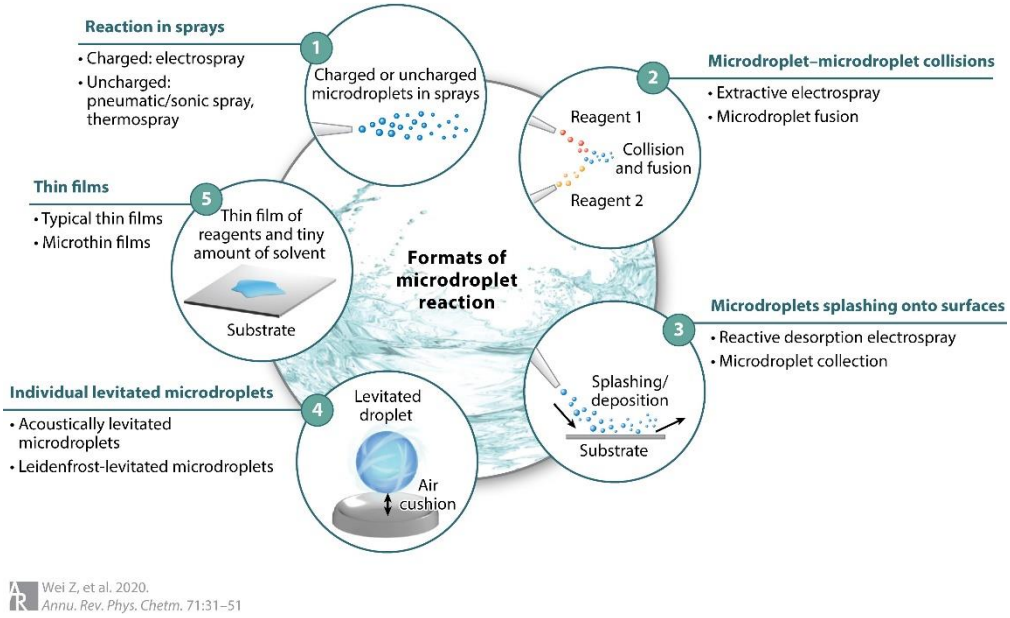

Figure 1.2 Five typical formats of microdroplet reactions.

Source: Wei, Z.; Li, Y.; Cooks, R. G.; Yan, X., Accelerated reaction kinetics in microdroplets: Overview and recent developments. Annual Review of Physical Chemistry ***2020,*** *71, 31-51.*

The exact mechanism behind reaction acceleration in microdroplets remains to be fully understood. Reactions in confined volumes (droplets/thin films) have been found to

be much more efficient than in the corresponding bulk-solution-phase on the same scale. There are many differences in the physical properties for the bulk phase and microdroplets, such as the significantly reduced dimensions of droplets and their greatly increased surface areas. Some studies reported that the interface plays a major role in acceleration, and the solvent-binding energy of reagents, intermediates, and products is crucial. For instance, Figure 1.3 compares the energetics of an ionic reaction with a neutral reagent across bulk phase, small droplet and free gas phase species.[6] The orders of magnitude difference in reaction rates between bulk solution and the gas phase is attributed to solvation.[19] Small droplets represent an intermediate case of partial solvation, leading to significant acceleration compared to bulk phase. The reaction efficiency in microdroplets depends on the cumulative effects of these and other properties of the droplets. Droplets formed by different methods might also exhibit varied properties. For example, droplets are charged to various extents before and after solvent evaporation, and these properties as well as the internal structure and surface distribution of solute will contribute to the observed reactivity. Several major factors that can be concluded from available experimental data to contribute to reaction acceleration are *in situ* evaporation with associated increases in reagent concentrations as solvent is depleted from the droplets, 2) the *in situ* acidity or basicity of droplets in the ionization source, and 3) the confinement of reagents in small-volume reactors, especially the fact that small-volume reactors have large surface-to-volume ratios.[6] Microdroplet reactions are expected to influence many fields such as chemical derivatization,[20-23] reaction mechanistic studies,[24-27] high-throughput reaction screening,[28] accelerated organic synthesis in preparative electrospray,[1, 8, 29] the determination of protein unfolding kinetics and H/D exchange for metabolomic labeling,[14] ultrafast biomolecular reactions[7] as well as rapid small-scale, green and sustainable synthesis.[30, 31]

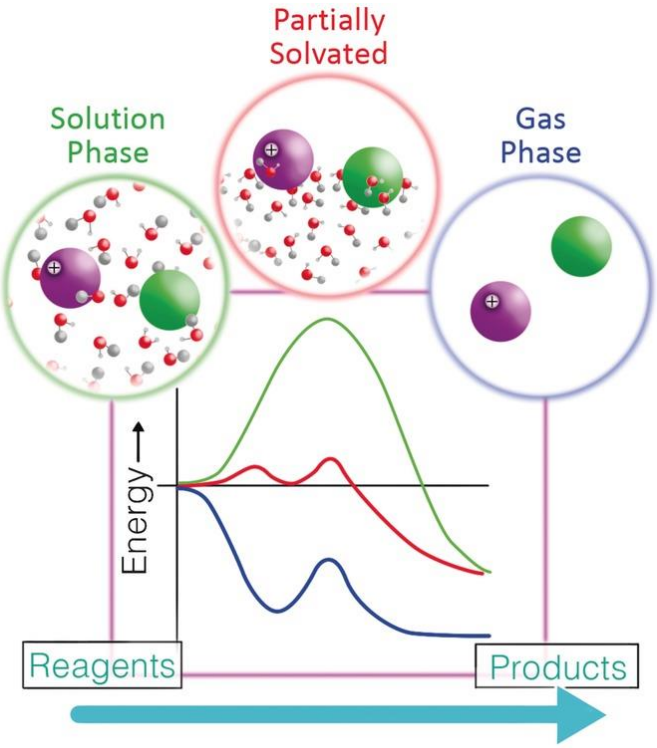

Figure 1.3 Energetics associated with incomplete solvation underlies acceleration of reactions occurring at the interface.

Source: Yan, X.; Bain, R. M.; Cooks, R. G., Organic reactions in microdroplets: Reaction acceleration revealed by mass spectrometry. Angewandte Chemie International Edition ***2016,*** *55 (42), 12960-12972.*

1.1.2 Ultrafast microdroplet digestion

Protein digestion is an essential step in both bottom-up and middle-down proteomics strategies and has a large impact on the quality of protein identification, characterization, and quantification.[32, 33] The vast majority of proteomics experiments rely on digestion of the protein into peptides prior to MS analysis. In a typical procedure, the protein solution is mixed with a proper quantity of an enzyme, such as trypsin, and incubated overnight at 37 °C.[33] To facilitate digestion, proteins are typically denatured before the digestion to destroy the compact, globular structure and expose more proteolytic cleavage sites.[34] Commonly used methods include the application of external stress or additives, such as heat, radiation, or urea.[35, 36] In addition, reductive alkylation is commonly used to break down disulfide bonds.[35] Over the years, novel techniques have been developed to improve

protein digestion and increase throughput and reproducibility. To further expedite protein digestion, various attempts have been taken to reduce the incubation time from overnight to several minutes, such as increasing the digestion temperature,[37, 38] using columns or porous materials for trypsin immobilization,[39-42] addition of organic solvents,[43, 44] applying microwave energy[45] or focused ultrasonic field,[46] or some combination of these.[47] Recently, ultra-fast enzymatic reactions in aqueous microdroplets containing both trypsin and protein were reported in 2020.[48] Several model proteins such as myoglobin, cytochrome c as well as therapeutic antibody subunits were digested within less than 1 ms using a homemade electrosonic spray ionization (ESSI) setup (Figure 1.4) to produce tiny (~9 μm ID) microdroplets. The higher sequence coverage achieved from microdroplet digestion compared to that obtained from bulk-phase digestion suggests the superiority of microdroplets in improving protein enzymatic digestion, especially for large or protease-resistant proteins.

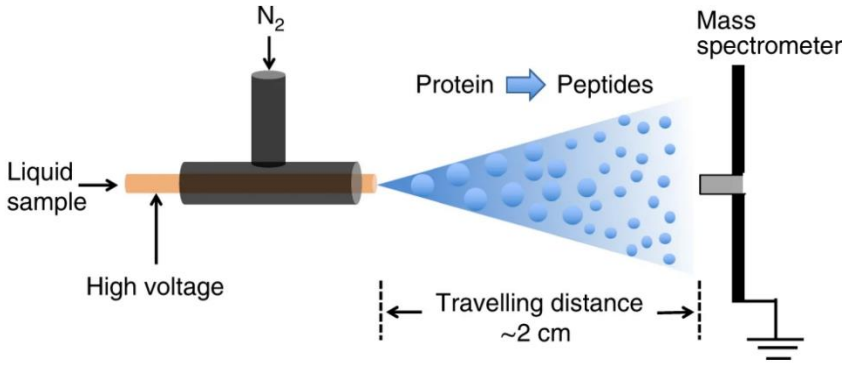

Figure 1.4 Schematic of the experimental apparatus for the online proteolysis by microdroplet chemistry coupled with mass spectrometry (ESSI-MS).

Source: Zhong, X.; Chen, H.; Zare, R. N., Ultrafast enzymatic digestion of proteins by microdroplet mass spectrometry. Nature communications ***2020,*** *11 (1), 1049.*

In addition, ultrarapid pepsin digestion of proteins in charged microdroplets at low pH was also reported. Extremely accelerated peptic digestion of cytochrome c as well as an in-house produced protein RocC was completed within milliseconds, displaying sequence coverage of 100% and 98.1% separately.[49] Furthermore, most recently, a rapid

online digestion platform named online microdroplet-assisted enzymatic digestion (MAED) was developed.[50] It involves the integration of intact protein separation with real time enzymatic digestion in microdroplets (Figure 1.5). Various protein standards, including an antibody standard, were characterized in a bottom-up manner without prior digestion, and high sequence coverages were obtained. Moreover, a more complex sample, mouse brain extract, was also digested with successful protein identifications. Compared with the conventional bottom-up approach, a more comprehensive characterization could be obtained particularly for low molecular weight proteins. It has been suggested that the integration of online microdroplet chemistry allows the fusion of top-down and bottom-up approaches which will be much faster than the traditional proteomics strategies.

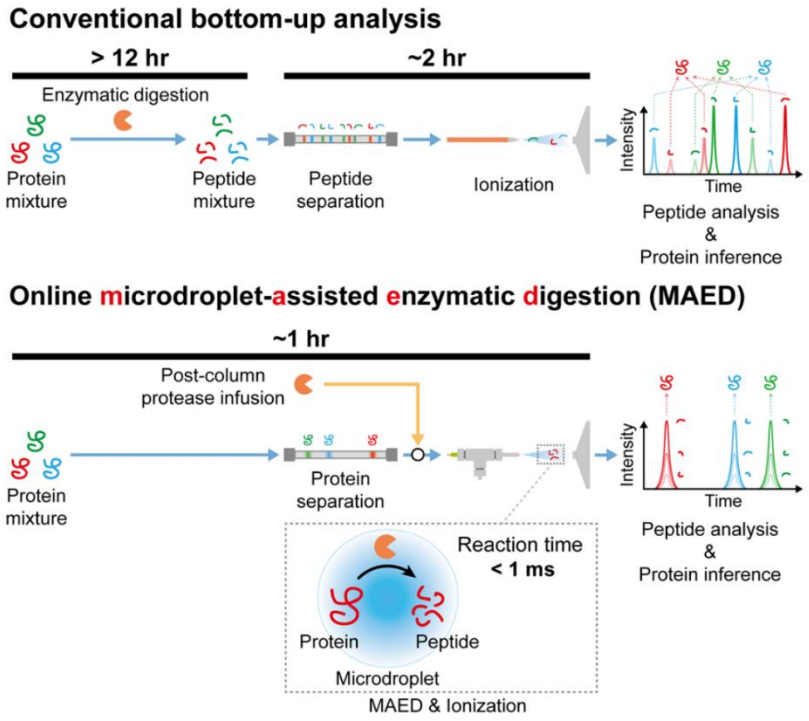

Figure 1.5 Schematic illustration comparing the workflow of conventional bottom-up analysis and online MAED.

Source: Ma, C.-H.; Chen, C.-L.; Hsu, C.-C., Real-time bottom-up characterization of protein mixtures enabled by online microdroplet-assisted enzymatic digestion (MAED). Chemical Communications ***2023,*** *59 (84), 12585-12588.*

1.2 Mass Spectrometry Based Protein Quantification

1.2.1 Relative quantitation in mass spectrometry-based proteomics

Nowadays, with the technical advances of mass spectrometry (MS) and the improvement of (bio)informatics computing resources and algorithm design, liquid chromatography/mass spectrometry (LC/MS) has emerged as a powerful tool for accurate and reliable quantitation rather than mere protein identification, especially in large-scale proteomics study. As the most prevalent quantitation platform for protein analysis, MS overcomes the limitations of immunoassayed based methods by offering greater specificity, speed, analyte dynamic range, sample throughput and multiplexing capabilities.[51-54] Most of these MS-based quantitation strategies provide information on relative alteration of protein abundance in a proteome-wide scale through isotope labeling strategies or label-free approaches based on ion counting or peak intensity.

For relative quantification, samples to be compared are differentially labeled with stable isotopes. After labeling, these samples are combined and analyzed using quantitative MS. The intensity ratio of heavy to light peptides is measured to determine the relative change in protein abundance. Various labeling methods have been developed, including chemical, proteolytic, isobaric, and metabolic labeling techniques. The most popular method of chemical labeling would be the isotope-coded affinity tags (ICAT) approach, where a compound containing stable isotope is attached to cysteine (Cys) residues in proteins.[55, 56] Different isotopomers of the compound, each having a unique mass, are utilized to label different samples. After this differential labeling, the samples are combined and undergo protease digestion followed by affinity-purification of Cys-containing peptides. In addition to the original ICAT methods, strategies have been reported for chemical labeling of carboxyl, amino, or thiol moieties.[57-62] In the hydrolysis-coupled labeling method, proteins are digested with protease in the presence of ^{18}O-labeled water,

leading to the incorporation of ^{18}O at the carboxyl end of each peptide.[63, 64] An alternative method for *in vitro* labeling involves using an isobaric tag such as tandem mass tags (TMTs) and isobaric tags for relative and absolute quantitation (iTRAQ). Each tag has an identical mass but contains stable isotopes at unique atomic positions to generate a reporter ion with a unique mass-charge ratio upon fragmentation.[65, 66] An obvious advantage of these in vitro labeling methods is that they can be applied to tissue samples, where *in vivo* labeling is challenging or practically unfeasible. On the other hand, they require intricate steps for sample handling and labeling. Besides, the samples to be compared are forced to be combined at later stages of the process, potentially allowing variations in earlier steps to affect accuracy of quantification. stable isotope labeling by amino acids in cell culture (SILAC) is another method for labeling, involving the *in vivo* metabolic incorporation of stable isotopes, where cells are cultivated in a medium supplemented with an appropriate stable isotope labeled nutrient for growth, enabling the whole proteome to be labeled.[67-70] An obvious advantage of these metabolic labeling methods compared to the chemical and hydrolytic methods is that protein samples can be combined at much earlier stage in the procedure, such as during cell harvesting. Accordingly, the effect of experimental errors can be minimized. On the other hand, achieving stable isotope labeling in animal and metabolically inactive cells can be challenging or sometimes unfeasible. These methods have been widely implemented in relative quantification in proteomics studies.

1.2.2 Absolute quantitation in mass spectrometry-based proteomics

Several labeling and label-free approaches based on either elementary or molecular mass spectrometry with their own strengths and limitations have been developed for protein absolute quantitation. As a complementary alternative to better-established molecular MS-based quantitative approaches, ICP-MS could also be used for absolute quantitative

proteomics via inorganic standards[71, 72] by means of the naturally ICP-detectable heteroatoms or artificial elemental labeling.[73, 74] For the molecular MS-based absolute quantitative strategies, compared to the labeling techniques, label free absolute quantitation in global profiling reduces cost and time investment but might require internal standards for MS signal normalization and suffer from compromised quantification accuracy and reproducibility.[75-78] For absolute quantitation through labeling, a known amount of isotope-labeled authentic standard is mixed with the analyte, and the mixture is introduced into mass spectrometer. Isotope dilution mass spectrometry is the most used approach to determine the absolute concentration of a protein in a complex mixture.[79]

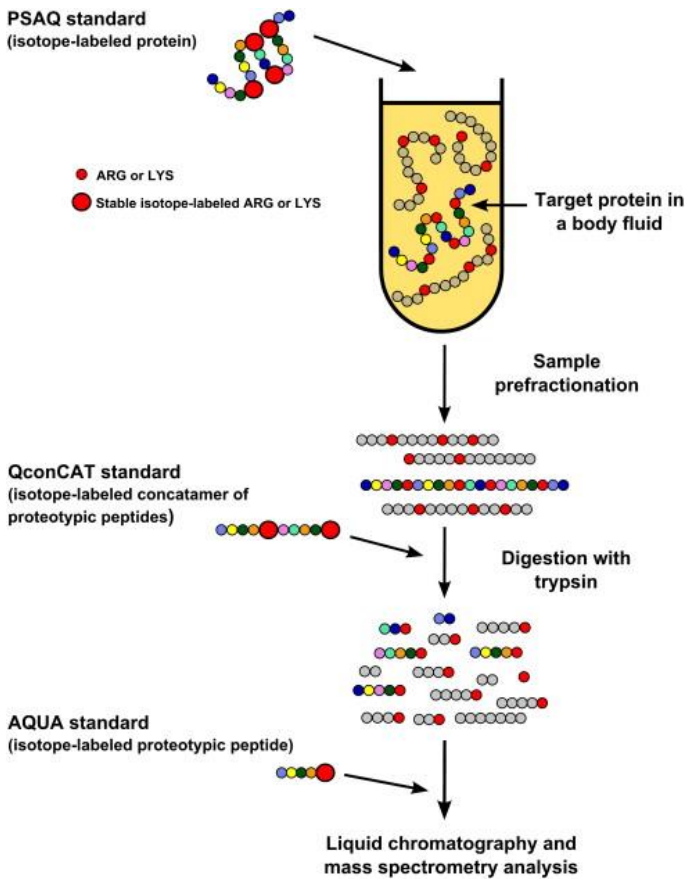

Figure 1.6 Isotope-dilution strategies for targeted MS-based absolute quantification of proteins.

Source: Brun, V.; Masselon, C.; Garin, J.; Dupuis, A., Isotope dilution strategies for absolute quantitative proteomics. Journal of proteomics ***2009,*** *72 (5), 740-749.*

Depending on the quantitation standard used, isotope dilution-based quantitation is further divided into absolute quantification (AQUA), quantification concatemer (QconCAT) and protein standard absolute quantification (PSAQ) strategies (Figure 1.6).[79] AQUA is one of the earliest methods developed and is still in wide use,[80] which involves the use of stable isotope labeled (SIL) synthetic peptides that are identical to native peptides of interest spiked into the sample before protein digestion or, alternatively, right before LC/MS analysis.[81] Quantification can be carried out either by MRM, PRM or SIM mode[76, 82] on the basis of the measured intensity ratio between the natural and labeled peptides, which are easily detected as pairs of signals separated by a known and constant mass difference Δm (Figure 1.7).[83] Because the concentration of the labeled peptide added to the sample is known, the amount of the natural peptide can be calculated from the signal ratio. In contrast with AQUA peptides, which needs to be chemically synthesized, purified and quantified one by one, QconCAT utilizes synthetic DNA that encodes a concatenated series of peptides of interest and released after proteolysis, which provides an efficient way of multiplex absolute quantification.[84] Unlike AQUA and QconCAT, both of which are based on labeled peptides, PSAQ uses heavy isotope–labeled proteins that are purified and quantified before being spiked into complex samples. Compared to AQUA and QconCAT, PSAQ is more accurate since the protein standards can be added at the very beginning of analytical process to correct the error over sample preparation steps and enzymatic digestion efficiency prior to LC/MS quantification.[85-89] Accordingly, the most suitable standard should be selected based on the purpose of the experiment, or on whether it intends to quantify a limited set of targets including their post-translational modifications, obtain highly accurate data for a single unique protein, or to determine the absolute or stoichiometric abundance of a broad range of proteins.

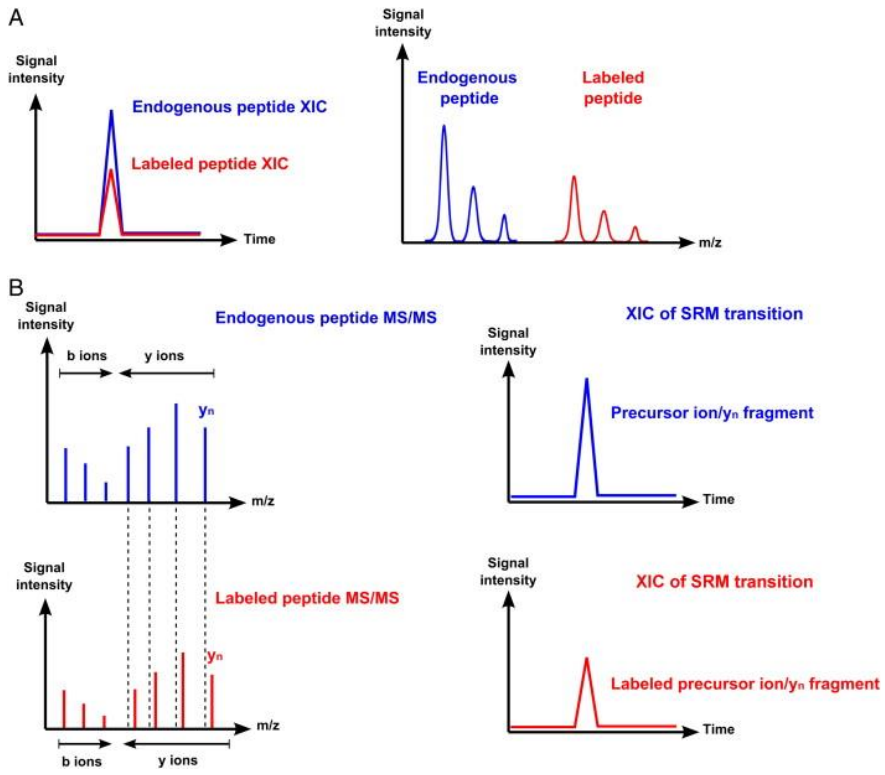

Figure 1.7 Mass spectrometry methodologies for absolute quantification of proteins. (A) Absolute quantification using LC–MS. (B) Absolute quantification using LC–SRM (Selected Reaction Monitoring).

Source: Brun, V.; Masselon, C.; Garin, J.; Dupuis, A., Isotope dilution strategies for absolute quantitative proteomics. Journal of proteomics ***2009,*** *72 (5), 740-749.*

1.3 Coulometric Mass Spectrometry

1.3.1 Introduction of coulometric mass spectrometry

Hyphenation of electrochemistry (EC) and mass spectrometry has been very popular and widely used for many applications as EC can benefit from the identification and the quantitation of reaction products by means of a mass spectrometer. Numerous interesting and attractive studies have been published so far including drug metabolism study, protein structural analysis, and electrochemical reaction mechanism elucidation,[90-95] as well as the capture of elusive reaction intermediates[96-105] and for electro-synthetic reaction screening.[106-108] As a new application of EC/MS techniques, coulometric mass spectrometry (CMS) has been developed and employed for absolute quantitation of

electrochemical reactive target molecules without using any standards or establishing a calibration curve. Although the traditional coulometric approach could also achieve standard-free quantitation based on Faraday's law, the complete electrochemical oxidation or reduction conversion is often challenging. Since MS is coupled following EC, it allows for the measurement of the oxidation or reduction conversion yield and is ideal for monitoring the reaction products, further confirming and validating the reaction mechanism and electron transfer. Theoretically, CMS quantitation can be applicable for analytes that contain an electroactive functional group with known electrochemical activities. Once the electrochemical reaction is triggered, the total electric charge responsible for oxidizing/reducing analyte substance in coulombs, Q, is directly proportional to the quantity of the oxidized/reduced substance: $Q=nzF$, where n is the moles of analyte, z is the number of electrons transferred per molecule for the redox reaction, and F is the Faraday constant (9.65×104 C mol^{-1}). Q can be directly measured from the integration of Faradaic current over time. The moles of the analyte that is oxidized or reduced can be calculated as $n= Q/zF$. On the other hand, electroactive species shows reduced intensities in the acquired MS spectra upon oxidation/reduction, and the relative MS intensity change upon redox reaction, Δi, can reflect the redox conversion yield. From the acquired MS spectra before and after electrolysis, Δi can be measured in two ways: the relative change in the target analyte peak intensity (relative to a reference peak) or the relative change in the target analyte peak area in the extracted ion chromatogram (EIC) upon electrolysis. Thus, the amount of analyte converted, in combination with the conversion yield, can be used to calculate the total amount of analyte. In other words, Total amount of analyte = (amount of the oxidized/reduced analyte) / (the oxidation/reduction yield) = $(Q/zF)/\Delta i = Q/(zF\Delta i)$.[109]

1.3.2 Small molecule quantitation with coulometric mass spectrometry

Small molecule quantitation by MS has been widely carried out, mainly relying on structural similarities or isotope-labeled compounds as the internal standard due to MS signal fluctuations and the ion suppression effect from the matrices. In addition, MS-based absolute quantitation approaches require the construction of a calibration curve. Although liquid chromatography (LC) in combination with electrochemical detection has been well established for the trace determination of electroactive compounds in mixtures and complex matrices such as the quantitation of carbohydrates, and neurotransmitters, ascorbic acid, uric acid and phenothiazines,[110-113] based on the generated electric current response which is proportional to the quantity of analytes, authentic target compounds and the calibration curve are still needed. The traditional coulometric approach has been known for the direct quantitation of electroactive compounds based on Faraday's law. The absolute quantity of the analytes could be easily calculated if the targets undergo complete oxidation or reduction. However, full redox conversion is often difficult to achieve and control for multiple reasons. Therefore, CMS had applied for the absolute quantitation of analytes under partial electrolysis with the conversion yield being measured by MS.[109] Several electroactive small organic molecules (Figure 1.8), such as dopamine (DA), norepinephrine (NE), rutin (RN), and uric acid (UA), were successfully quantified using CMS. The obtained quantitation error ranged from −2.6% to +4.6%.[109, 114]

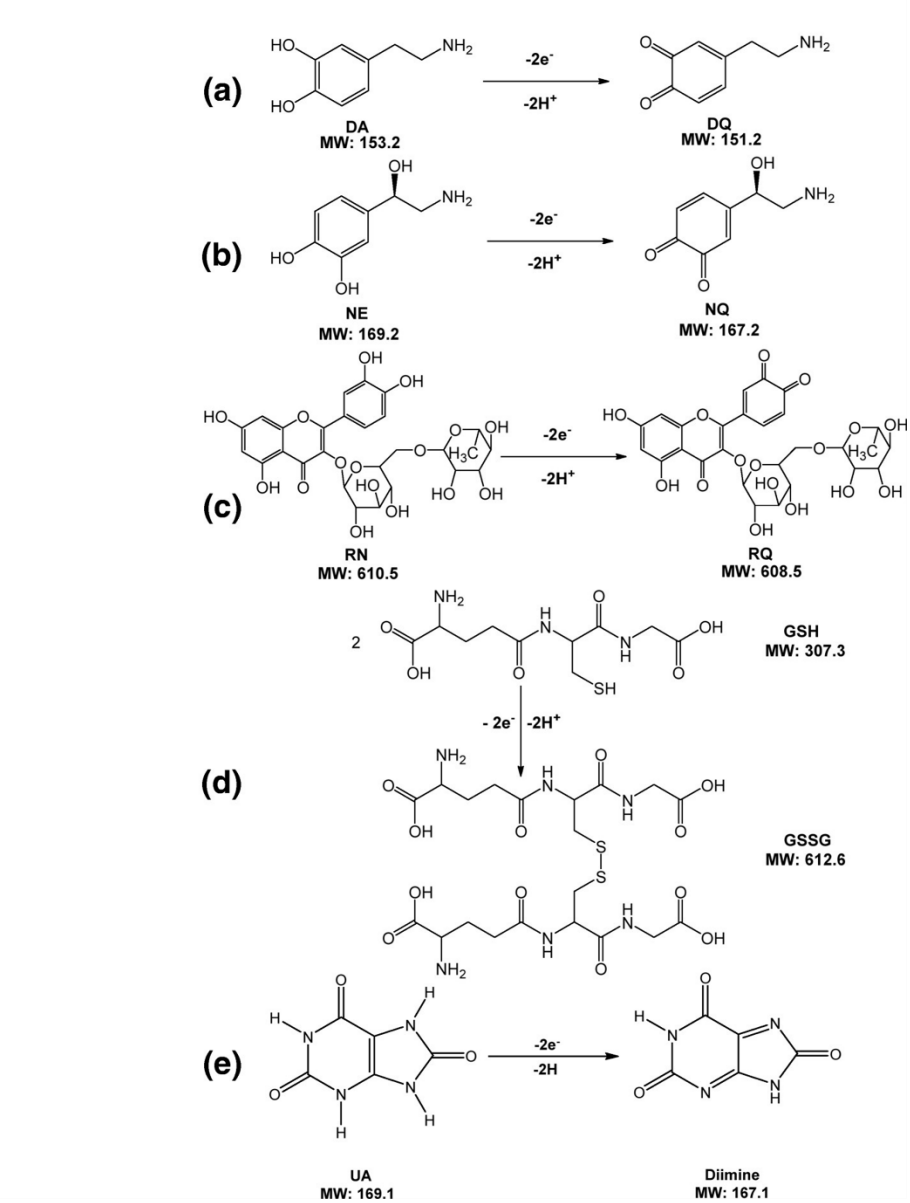

Figure 1.8 Equations showing the electrochemical oxidation of (a) DA, (b) NE, (c) RN, (d) UA, and (e) 5-HT.

Source: Xu, C.; Zheng, Q.; Zhao, P.; Paterson, J.; Chen, H., A new quantification method using electrochemical mass spectrometry. Journal of The American Society for Mass Spectrometry ***2019,*** *30 (4), 685-693.*

1.3.3 Peptide and protein quantitation with coulometric mass spectrometry

In addition to the quantitation of small molecules, CMS has been demonstrated to quantify peptides without using peptide standards or isotope-labeled peptide standards.[109, 115] Among the 20 naturally occurring amino acids, four are oxidizable: cysteine (C),[116]

tyrosine (Y),[117] tryptophan (W),[117] and methionine (M),[118] listed in the order of their increasing oxidation potential. Glutathione (GSH), a thiol-containing peptide, was first quantified with CMS based on the electrochemical oxidation conversion of thiols into disulfides (Figure 1.9a).[109] The oxidized GSH product glutathione disulfide (GSSG) was confirmed from MS. The integrated current area and the measured oxidation yield were combined to successfully quantify the amount of native GSH with a measurement error of 4.6%. Another oxidizable residue, tyrosine, with a relatively low oxidation potential and relatively high abundance in proteins was investigated and showed a reproducible and stable electric current for all the examined tyrosine containing peptides. Under an appropriate oxidation potential (e.g., 1.00–1.05 V vs. Ag/AgCl), the phenol side chain of a peptide tyrosine residue can be oxidized into a semiquinone by losses of two electrons and two protons (Figure 1.9b), in which a mass shift of 2 Da occurs, which can be readily monitored by MS analysis.[115]

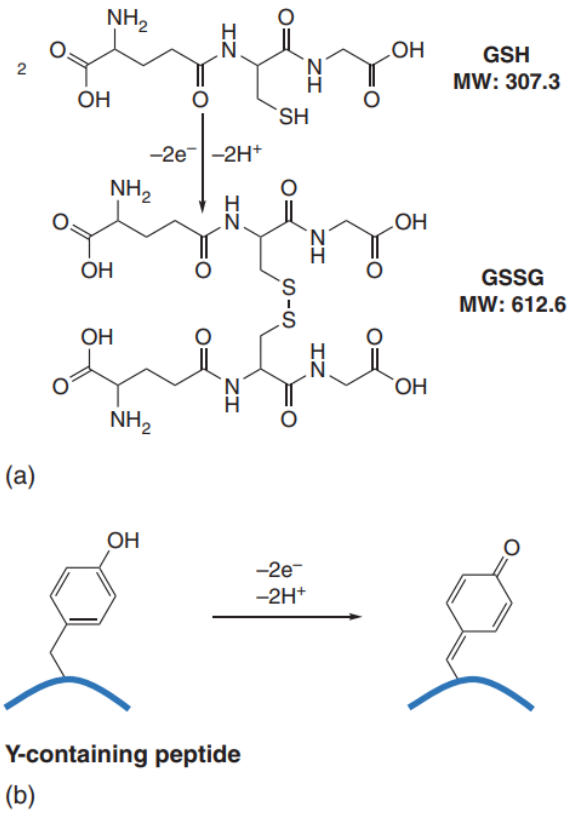

Figure 1.9 Equation showing the electrochemical oxidation of (a) GSH and (b) a tyrosine-containing peptide.

Sources: Xu, C.; Zheng, Q.; Zhao, P.; Paterson, J.; Chen, H., A new quantification method using electrochemical mass spectrometry. Journal of The American Society for Mass Spectrometry ***2019,*** *30 (4), 685-693.*
Zhao, P.; Zare, R. N.; Chen, H., Absolute quantitation of oxidizable peptides by coulometric mass spectrometry. J. Am. Soc. Mass Spectrom. ***2019,*** *30 (11), 2398-2407.*

MS-based absolute quantitation of protein concentration in biological samples plays an important role in clinical and pharmaceutical studies such as the evaluation and validation of clinical biomarker candidates[119] and biotherapeutic bioanalysis/drug metabolism and pharmacokinetics (DMPK).[120] Popular methods for absolute protein quantitation by MS involve the digestion of target proteins and employ isotope-labeled peptide internal standards to quantify chosen surrogate peptides, which has been widely used and considered as the gold standard in regulated bioanalysis.[121] Although these methods have gained success, the synthesis of isotope-labeled peptides is time-consuming and costly. Therefore, it is only feasible to quantify a limited number of proteins at a time

given the high cost and complexity of the sample preparation. Thus, the development of methods for accurate protein quantitation without using isotope-labeled standards is largely needed. To circumvent this limitation, CMS has been applied for protein quantitation by selecting a surrogate peptide containing electrochemically active residue (e.g., tyrosine, and cysteine) to present the corresponding proteins (Figure 1.10). Several model proteins such as β-casein, and apomyoglobin as well as a recombinant human IgG2 kappa mAb that binds specifically to the human epidermal growth factor receptor were successfully quantified based on tyrosine-containing surrogate peptides and validated with traditional IDMS method with good accuracy.[122] The basic workflow of CMS quantitation is very similar to the commonly used target proteomics quantitation (e.g., selected reaction monitoring [SRM]/parallel reaction monitoring [PRM]) including protein extraction, selective enrichment, tryptic digestion, chromatographic separation, and MS detection.

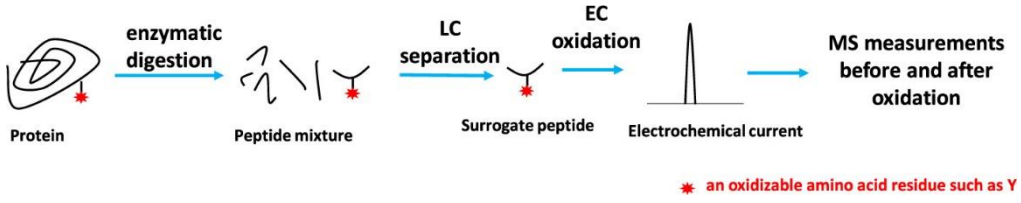

Figure 1.10 Schematic showing absolute quantitation of protein by CMS.

Source: Zhao, P.; Wang, Q.; Kaur, M.; Kim, Y.-I.; Dewald, H. D.; Mozziconacci, O.; Liu, Y.; Chen, H., Absolute Quantitation of Proteins by Coulometric Mass Spectrometry. Anal. Chem. ***2020,*** *92 (11), 7877-7883.*

CHAPTER 2

COMPARISON OF ULTRAFAST MICRODROPLET PROTEIN DIGESTION AND TRADITIONAL BULK OVERNIGHT DIGESTION

A version of this work has been published in the *Journal of the American Society for Mass Spectrometry* as the article: Ai, Y.; Xu, J.; Gunawardena, H. P.; Zare, R. N.; Chen, H., Investigation of Tryptic Protein Digestion in Microdroplets and in Bulk Solution. *Journal of the American Society for Mass Spectrometry* **2022,** *33* (7), 1238-1249.

2.1 Introduction

Numerous studies in the past decade have shown that reaction rates can be dramatically accelerated if reactions are conducted in microdroplet rather than in bulk solution.[1, 5, 123, 124] The reaction acceleration has mainly been attributed to the special reaction environment at the air−liquid surface of microdroplet where partial solvation of the reagents, the presence of a strong electric field, enhanced concentration of solute, rapid desolvation, and surface excess charge accumulation could be the influencing factors to speed up the reaction.[5, 125-129] This "catalytic" feature allows microdroplet chemistry to have impactful applications including rapid chemical derivatization,[7, 14, 23, 94, 130] reaction kinetic studies,[14] high-throughput reaction screening,[28] nanomaterial preparation,[131-133] and the rapid, green and sustainable synthesis or degradation.[5, 30, 49, 124, 134-137] However, most of these reactions involved small organic molecules, large molecule protein reactions in microdroplets are rare, except enzymatic digestion of proteins.[49, 134, 135] The microdroplet digestion of proteins is very fast and completes in submillisecond time scale (e.g., within 250 μs).[134]

Protein digestion is an important step for bottom-up proteomics research, as large proteins can be cleaved into small peptides that can be easily analyzed with mass spectrometry (MS). Traditional digestion of proteins is time-consuming and often needs overnight incubation of proteins and enzymes like trypsin. To accelerate enzymatic protein digestion, a variety of novel methods have been reported, including increasing the digestion

temperature, adding organic solvents, applying microwave energy, using high intensity focused ultrasound or employing microchip reactor.[38, 40, 43, 46, 47, 138-141] Microdroplet digestion appears to be an ultrafast approach in this regard. However, detailed investigation of microdroplet protein digestion has not been done, including the examination of peptide miscleavage, cleavage specificity, and chemical modification involved in digestion.

Monoclonal antibodies (mAbs) and related products are the fastest growing class of human therapeutics in the pharmaceutical industry,[142] and many mAb products have been approved for treatment of different pathologies including cancers, and immunological disorders.[142-146] Most therapeutic mAbs are a class of recombinant proteins that are susceptible to a variety of enzymatic or chemical modifications, also called post-translational modifications (PTMs), during cell culture, purification, formulation and long-term storage.[147-150] Common PTMs previously identified include glycosylation, deamidation, isomerization, and oxidation, incomplete disulfide bond formation, glycation, N-terminal glutamine cyclization, and C-terminal lysine processing.[149, 151-154] Deamidation is one of the most common chemical modifications observed during the degradation processes of mAbs, which may result in changes in physiochemical properties, such as hydrophobicity, charge, and secondary or tertiary structure, and may lower the thermodynamic or kinetic barrier to unfold.[150] This may affect the stability, binding affinity, half-life, and efficacy of mAb products, potentially causing immunogenicity.[155] Therefore, characterization and control of such modifications is important for the quality control of antibody drugs throughout the product life cycle. Currently, peptide mapping, a bottom-up strategy, via reversed-phase liquid chromatography coupled with mass spectrometry (LC-MS) is considered as a gold standard for monitoring and characterization of site-specific modifications including deamidation that may arise during production, processing, or storage.[156] However, to generate a peptide map, the therapeutic protein must

first be digested into its constituent peptides through enzymatic reaction in which the sample needs to be exposed to various buffers, even elevated temperatures for up to 24 h to reach the maximum digestion efficiency. Unfortunately, the conditions that are amenable for effective digestion are often similar to conditions that promote unwanted modifications. For example, it has been reported that asparagine deamidation is promoted by conditions such as elevated temperatures or high pH and are further exacerbated by exposure to these extreme conditions for extended incubation time.[147, 157, 158] Thus, it is often challenging to find a balance between maximum digestion efficiency and minimizing artificial modifications. Considering the ultrafast speed of microdroplet protein digestion,[134] we reason that chemical modifications on antibody peptides could be reduced if microdroplet digestion is used to replace traditional digestion protocols.

In this study, we evaluated the performance of microdroplet protein digestion including digestion efficiency, sequence coverage, peptide cleavage specificity and deamidation resulted from digestion. Both model protein β-lactoglobulin B and antibody mAb were tested. In general, in comparison to bulk solution digestion, long peptides tend to be well preserved in microdroplet digest probably due to the much shorter digestion time and room temperature used. Equally importantly, deamidation is reduced. Our results suggest that microdroplet-assisted enzymatic reactions could serve as an alternative to traditional digestion method commonly used in bottom-up proteomic studies, as well as for the biotherapeutic protein characterization.

2.2 Experimental

2.2.1 Reagents and materials

Monoclonal antibody reference material 8671 (NIST 8671 mAb) was obtained from the National Institute of Standards and Technology (NIST, Gaithersburg, MD). Phospholipase

B-like 2 protein (PLBL2, CHO-S-purified) was purchased from Immunology Consultants Laboratory (Portland, OR). *β*-Lactoglobulin B from bovine milk, trypsin (sequencing grade), urea (electrophoresis grade), ammonium bicarbonate (bioultra grade), dithiothreitol (DTT, bioultra grade), and iodoacetamide (IAM, bioultra grade) were all sourced from Sigma-Aldrich (St. Louis, MO). Peptide gp 100 (25−33) human (KVPRNQDWL, HPLC grade) was purchased from AnaSpec (Fremont, CA). Tuftsin (TKPR, HPLC grade) were obtained from Genscript Biotech (Piscataway, NJ). Acetonitrile (ACN, HPLC grade), acetic acid (LCMS grade) and formic acid (FA, LCMS grade) were purchased from Fisher Scientific (Fair Lawn, NJ). A Millipore Direct-Q5 purification system (Burlington, MA) was used to obtain purified water for sample preparation.

2.2.2 Microdroplet and bulk digestion of *β*-lactoglobulin B

β-lactoglobulin B (400 μg) from bovine milk was dissolved in 50 mM ammonium bicarbonate (ABC, NH_4HCO_3, pH 8.0) containing 8 M urea. The denatured protein solution (1 μg/ μL) was reduced with 20 mM DTT at 37 °C for 1 h and alkylated with 40 mM IAM at room temperature in the dark for 30 min. A second aliquot of DTT (20 mM) was added again to quench extra amount of IAM. The alkylated protein sample was loaded into Amicon Ultra-0.5, 3 kDa filters (Millipore Sigma), then centrifuged at 14 000g for buffer exchange to remove small molecule reagents like urea, DTT and IAM. The concentrated protein solution was diluted with 100 mM ABC buffer to 1 μg/μL for digestion. As shown in Scheme 2.1, for microdroplet digestion of *β*-lactoglobulin B, 200 μL of 1 μg/μL protein in ABC buffer was added into one syringe, and 200 μL of 0.05 μg/μL trypsin in 0.1% acetic acid was loaded into the other syringe. The injection flow rate of both syringes was 5 μL/min. The protein and enzyme were mixed via a T-mixer and then delivered to a homemade sonic spray ionization (SSI)[159] emitter for generating

microdroplets of the reaction mixture. The connection capillary between T mixer and emitter was 8 cm long with 98 μm ID (the dead volume = 0.6 μL). A 1.5 mL Eppendorf tube vial containing a quenching solvent of 50 μL of H_2O/ACN/FA (50:50:1, v/v) was used to collect the sprayed microdroplets (the distance between the emitter tip and the quenching solution in the vial was about 2 cm). The SSI emitter was composed of an inner fused-silica capillary (98 μm ID, 200 μm OD) and a coaxial outer fused-silica capillary (250 μm ID and 355 μm OD) and N_2 gas of 120 psi was used as the spray sheath gas to assist formation of microdroplets (no high voltage was applied). The coaxial capillary outlets were flush to reach the optimum spray geometry with smallest droplet sizes previously measured.[160] On the basis of the previous report[135] of microdroplet digestion employing an emitter with the same capillary dimensions, the same nebulizing gas pressure and the same spray distance as used in this work, the microdroplet digestion time of this experiment (i.e., the flight time of the sprayed microdroplets between the sprayer and the quenching solution) was estimated to be 250 μs (the same as previously reported[135]). The sprayed microdroplet was collected for 5 min for subsequent nanoESI-MS analysis.

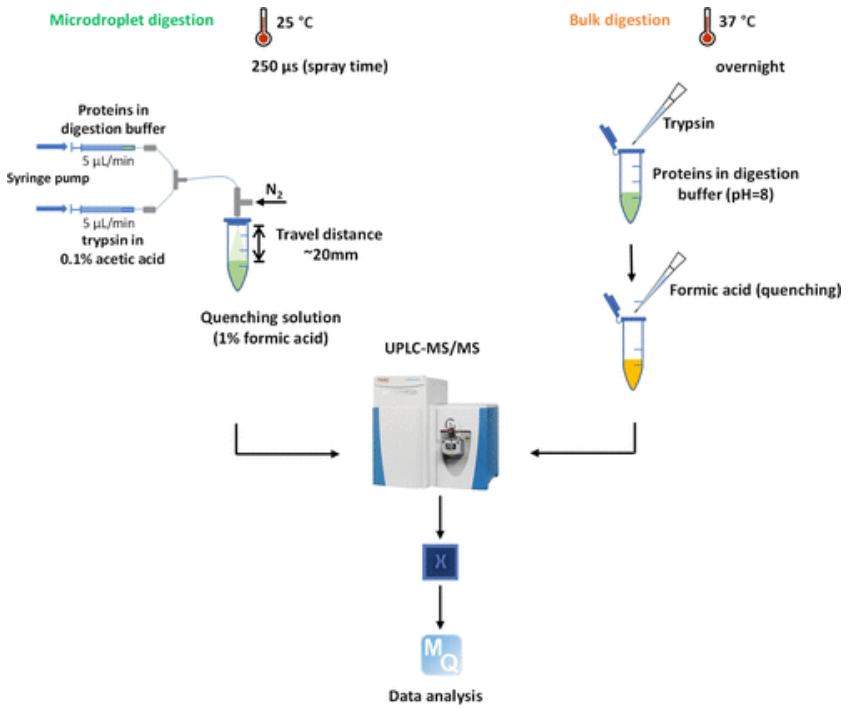

Scheme 2.1 Workflow of microdroplet and bulk digestions in this work.

During the microdroplet digestion experiment, as a control experiment to assess the contribution of bulk digestion inside the short connection capillary after mixing of protein and trypsin via the Tee, the outlet end of the connection capillary was directly immersed in the quenching buffer of H_2O/ACN/ FA (50:50:1, v/v) contained in a vial (setup shown in Scheme 2.2). Fifty microliters of 1 µg/µL protein in ABC buffer was loaded into one syringe. Then, 50 µL of 0.05 µg/µL trypsin in 0.1% acetic acid was loaded into the other syringe. The flow rate of both syringes was 5 µL/min. The protein and enzyme were mixed via a Tee and collected for 5 min for nanoESI-MS analysis.

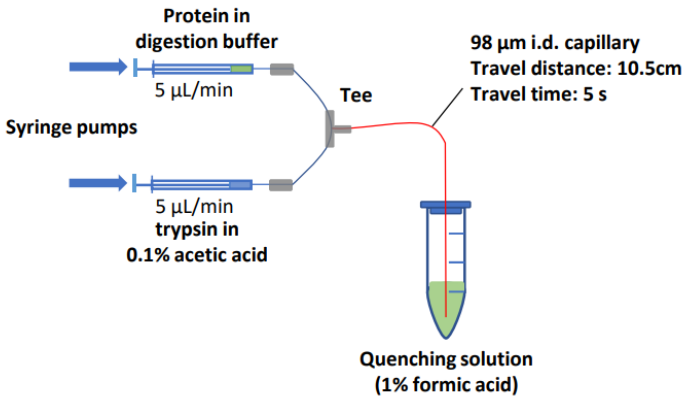

Scheme 2.2 Experimental setup of the control experiment in which protein and enzyme solutions were mixed online and delivered via a piece of transfer capillary to a quenching buffer.

For bulk digestion, an equal amount of protein and enzyme was mixed (25 µL of 1 µg/µL β-lactoglobulin B and 25 µL of 0.05 µg/µL trypsin) and incubated at 37 °C overnight (14 h). FA was added to 1% (v/v) to quench the digestion. The collected digests from both microdroplet and bulk digestions were vacuum-dried and reconstituted with 60 µL of H_2O/ACN/FA (50:50:1, v/v). Fifteen microliters of peptide TKPR (355.9 µM) was added as the internal standard for nanoESI-MS analysis. The injection flow rate was 2 µL/min, and +3.5 kV was applied for nanoESI ionization. The temperature of the MS inlet was 250 °C. A Thermo Scientific Q Exactive mass spectrometer (San Jose, CA) was used with resolution set to 140 000 for the MS analysis.

2.2.3 Microdroplet and bulk digestion of a mixture of mAb and PBL2

One milligram of NIST 8671 mAb was spiked with 10 µg of $PLBL_2$ to mimic an antibody sample containing an impurity protein. The sample was, then, diluted to 1 mg/mL mAb and 0.01 mg/mL $PLBL_2$ with 50 mM ABC buffer (pH 8.0) containing 8 M urea. The denatured protein mixture was reduced with 20 mM DTT at 37 °C for 1 h and alkylated with 40 mM IAM at room temperature in the dark for 30 min. A second aliquot of DTT (20 mM) was added again to quench excess amount of IAM. The alkylated protein sample

was loaded into Amicon Ultra-0.5, 10 kDa filters (Millipore Sigma), then centrifuged at 14 000g for buffer exchange. The concentrated protein solution was diluted with 100 mM ABC to 250 µL. The final concentration of mAb and PLBL2 were 4 and 0.04 µg/µL, respectively. For microdroplet digestion, digestion was performed in triplicates using the setup as described in Scheme 2.1. Two hundred microliters of mAb (4 µg/µL) and PLBL2 (0.04 µg/µL) was loaded in one syringe and 200 µL of trypsin (0.1 µg/µL) in 0.1% acetic acid was loaded in the other syringe. The flow rate of both syringes was set at 5 µL/min. A 1.5 mL tube containing a quenching solvent of 50 µL of H_2O/ACN/FA (50:50:1, v/v) was used to collect the digest for 10 min. Nitrogen sheath gas was applied at 120 psi to assist the spray. For bulk solution digestion, 50 µL of 4 µg/µL mAb and 0.04 µg/µL $PLBL_2$ was mixed with 50 µL of 0.1 µg/µL trypsin and then incubated at 37 °C for overnight (14 h). FA was added to 1% (v/v) to quench the digestion. The collected digests from both microdroplet and bulk digestions were vacuum-dried and reconstituted with 60 µL H_2O/ACN/FA (95:5:0.1, v/v) followed by centrifuge at 14000 g for 5 min. The supernatant was transferred for LC/ MS analysis.

2.2.4 Peptide recovery test

For the peptide recovery test experiment, 100 µL of 20 µM KVPRNQDWL in 0.1% FA was loaded in one syringe and 100 µL H2O was loaded in the other syringe to undergo spray and collection in a vial containing a quenching solution of 50 µL H2O/ACN/FA (50:50:1, v/v) (using the apparatus shown in Scheme 1). The flow rate of both syringes was 5 µL/min. N2 was set at 120 psi. The peptide sample was collected for 5 min. For control (no spray), 25 µL KVPRNQDWL (20 µM) was directly mixed with 25 µL H2O. Both the sprayed sample and control were vacuum dried and reconstituted in 100 µL H2O/ACN/FA

(50:50:1, v/v) followed by adding 2 μL TKPR (355.9 μM) as IS. Both the sprayed and control samples were analyzed with nano-ESI MS.

2.2.5 UPLC-MS/MS analysis of tryptic digests

The prepared tryptic peptides were analyzed using UPLC-MS/MS. Samples were directly separated using a Waters Acquity UPLC equipped with a BEH C18 column (2.1 × 150 mm, 1.7 μm particle size; Milford, MA, U.S.A) at an injection volume of 5 μL. Separation was performed with mobile phase A consisting of 0.1% formic acid in water and mobile phase B consisting of 0.1% formic acid in acetonitrile. The mobile phase flow rate was kept at 200 μL/min. The gradient conditions were as follows: 0−65 min, increased from 5% to 35% B; 65−75 min, linear ramp from 35% to 40% B; 75−80 min, climbed to 90% B and remained at 90% for 5 min before returning to 5% B. Total run time per sample was 90 min. Mass spectrometric analysis was performed on the Thermo Scientific Q Exactive mass spectrometer (San Jose, CA). Data-dependent MS/MS was performed as follows: the first event was the survey positive mass scan (m/z range of 250−1800), followed by 20 HCD events (30% NCE) on the 20 most abundant ions detected from the first event. Ions were generated using a sheath gas flow rate of 35, an auxiliary gas flow rate of 10, a spray voltage of 4.0 kV, a capillary temperature of 300 °C, an auxiliary gas temperature of 100 °C and an S-Lens RF level of 50. Resolution was set at 70 000 (AGC target of 3E6) and 17 500 (AGC target of 5E4) for survey scans and MS/MS events, respectively. The maximum ion injection time was 100 ms for survey scan, and 100 ms for the other scans. The dynamic exclusion duration of 8 s was used with a single repeat count.

2.2.6 Data analysis

Raw files were searched using MaxQuant software (version 2.0.3.1) equipped with the Andromeda search engine (Max Planck Institute, Martinsreed, Germany). The first search

peptide mass tolerance was set to 20 ppm, and the main search peptide mass tolerance was 4.5 ppm. Trypsin was set as the digestion enzyme with a maximum of two miscleavages. Carbamidomethylation was set as a fixed modification, while oxidation (on methionine M), acetylation (protein N-term), and deamidation (occurring to either asparagine N or glutamine Q) were set as variable modifications. Spectra were searched against the sequence of NIST 8671 mAb light chain and heavy chain plus the sequence of PLBL2. The "match between runs" feature was used with a matching time window of 0.7 min and an alignment time window of 20 min. Target decoy analysis was performed by searching a reverse database with a PSM FDR of 1% and protein FDR of 5%. Label-free quantification (LFQ) was performed using the MaxLFQ algorithm in MaxQuant software (MaxPlanck) according to default LFQ parameters with minimum ratio count set as 2, normalization type as classic, minimum number of neighbors equal to 3 and average number of neighbors equal to 6. A separate database search was performed with digest mode set to semispecific and unspecific, respectively. The MaxQuant output tables were used for further analysis and visualization of data.

2.3 Results and Discussion

2.3.1 Comparison of the tryptic digestion of *β*-lactoglobulin B in microdroplet and bulk solution

To evaluate the performance of microdroplet protein digestion, we started with trypsin digestion of a single protein first and *β*-lactoglobulin B was chosen as the test sample. We used an online mixing setup as shown in Scheme 2.1 for microdroplet digestion, for the reason that the online mixing would minimize the contribution of protein digestion in bulk phase before performing microdroplet digestion. As shown in the microdroplet digestion setup (Scheme 2.1), the residence time of protein and trypsin in the connection capillary before spray was estimated to be 4 s, based on the capillary dead volume of 0.6 μL and the

mixed solution flow rate of 10 µL/min. In the control experiment (Scheme 2.2 and Figure 2.1), online mixing of β-lactoglobulin B and trypsin for 5 s led to little digestion of the protein and the acquired MS spectrum (Figure 2.1b) showed intact protein ions (+10 to + 21 ions) along with two peptide ions at *m/z* 419 and *m/z* 858 were detected. *m/z* 419 and 858 corresponded to +2 ions of ALPMHIR and LSFNPTQLEEQCHI, respectively, two peptides from the C terminal of *β*-lactoglobulin B, which were also observed in the MS spectrum of intact protein (Figure 2.1a).

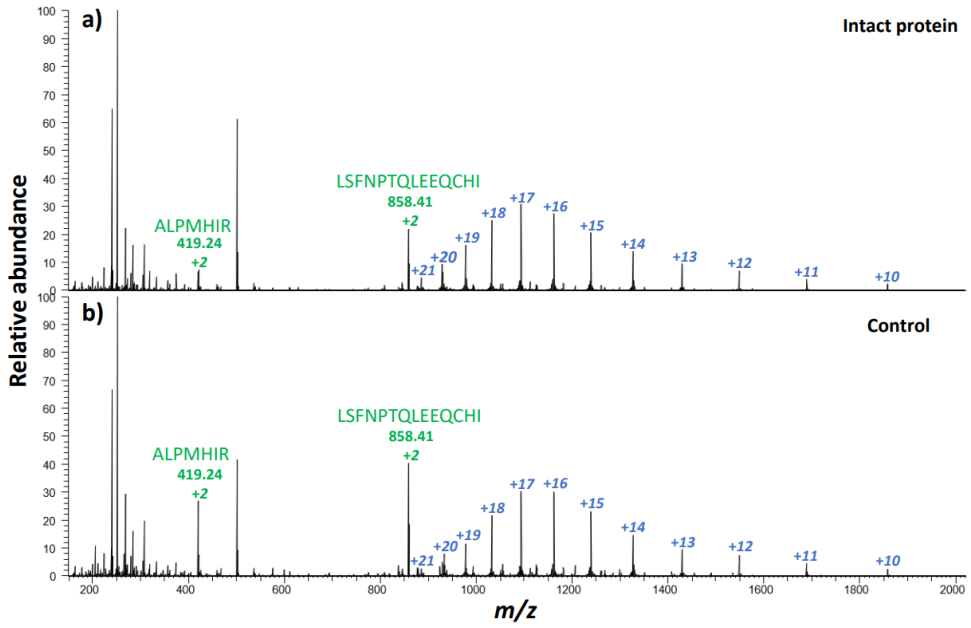

Figure 2.1 NanoESI mass spectra of (a) intact β-lactoglobulin B and (b) the *β*-lactoglobulin B after mixing with trypsin for 5 s before quenching.

Using the Scheme 2.1 setup for microdroplet digestion of *β*-lactoglobulin B, we used two syringe pumps to deliver protein and enzyme solution separately at 5 µL/min flow rate. The reactants were mixed online via a Tee before spray. Microdroplet digestion was quenched immediately by the quenching solution after reaching the collection vial. Overnight bulk digestion (at 37 °C) of β-lactoglobulin B was conducted for comparison. After digestion, both digests were vacuum dried and reconstituted in solvent with peptide TKPR being spiked as an internal standard (IS) for nanoESI-MS analysis. As shown in

Figure 2.2a, after digestion, numerous peptide fragments were observed while signals corresponding to the intact protein could no longer be seen in both microdroplet and bulk digests, indicating the tryptic digestion in both conditions was complete. Moreover, by manually searching fully cleaved peptides (Figure 2.2a inset) based on the sequence of β-lactoglobulin B, the same number of fully cleaved peptides were identified both in microdroplet and bulk digestion, leading to the same sequence coverage (Figure 2.2b). Interestingly, there were some peptides (highlighted in red, Figure 2.2a inset) showing higher abundance in microdroplet than bulk digestion. For example, top two long peptide VAGTWYSLAMAASDISLLDAQSAPLR and YLLFCMENSAEPEQSLACQCLVR were detected with much lower intensities in overnight bulk digest (2.64×10^5 and 5.63×10^5) than in microdroplet digest (5.18×10^6 and 2.51×10^6). This result indicates that long peptides might suffer hydrolysis in solution with long incubation time and elevated temperature at 37 °C, while they could be well preserved during short microdroplet digestion period. This finding is consistent with the previously reported proteomic studies in which long digestion time resulted in reduced number of identified peptides and low protein sequence coverage.[34, 161, 162]

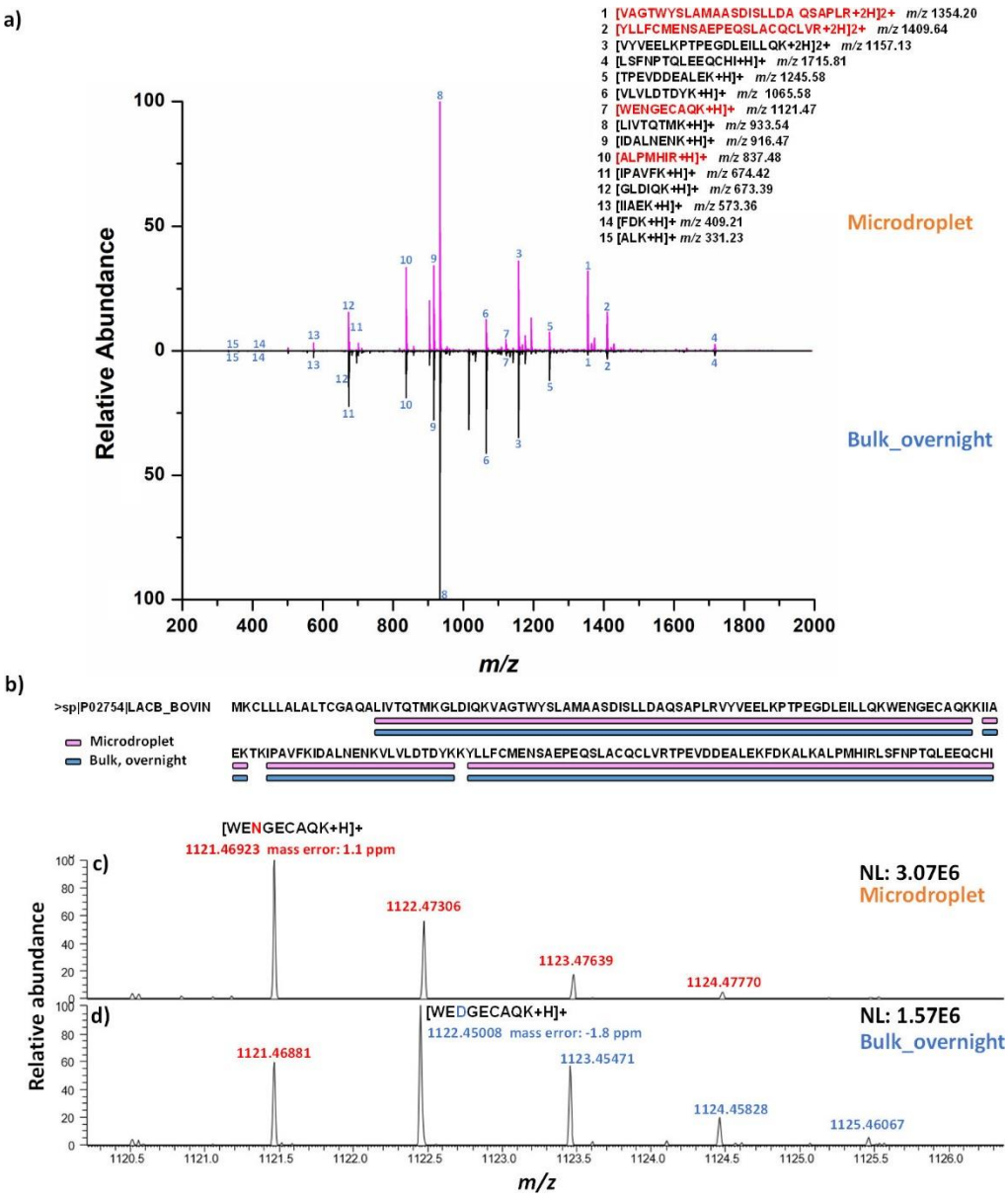

Figure 2.2 (a) Positive ion mode nanoESI mass spectra showing the microdroplet digestion (top panel) and bulk digestion (bottom panel) of *β*-lactoglobulin B. Inset: Fully cleaved tryptic peptides from β-lactoglobulin B (peptides highlighted in red showing higher abundance from microdroplet digestion). (b) Sequence coverage plot of *β*-Lactoglobulin B obtained from microdroplet digestion and bulk digestion based on fully cleaved peptides. Mass spectra of unmodified WENGECAQK from microdroplet digestion (c) and deamidated WENGECAQK from bulk overnight digestion (i.e., the deamidation product peptide WEDGECAQK) (d), respectively; NL indicates normalized level (NL) intensity.

In addition, we also examined the digestion-induced chemical modification of asparagine deamidation of our detected peptides (Figure 2.2a) in microdroplet and bulk digests. Deamidation as an important PTM during protein degradation, has been widely studied and known to be accelerated at high temperatures and high pH values.[163] Indeed,

one peptide from *β*-lactoglobulin B, WENGECAQK, had much higher deamidation level observed in the bulk overnight digest. As shown in Figure 2.2c, only native form of WENGECAQK was detected at *m/z* 1121 from MD (theoretical mass *m/z* 1121.46803, mass error: 1.1 ppm); in contrast, the deamidated form, WEDGECAQK with 1 Da shift (*m/z* 1122.45008, theoretical mass *m/z* 1122.45205, mass error = 1.8 ppm), was observed in bulk digest (Figure 2.2d). This result indicated that the ultrafast microdroplet digestion (∼250 μs) at room temperature also tends to prevent the digested peptides from deamidation, besides preserving long peptides.

Because reproducibility is important for protein digestion, in this study, we repeated the microdroplet digestion with three individual runs using the online mixing setup described above (Scheme 2.1). The nanoESI MS spectra for triplicate microdroplet digestions (a−c) and triplicate bulk overnight digestions (d−f) are shown in Figure 2.3. Similar profile across digestion replicates were observed for each digestion condition. In general, microdroplet digestion showed high reproducibility between three individual runs in terms of the sequence coverage. For most of the fully cleaved peptides, the standard deviation among three digestion replicates is acceptable (Figure 2.4).

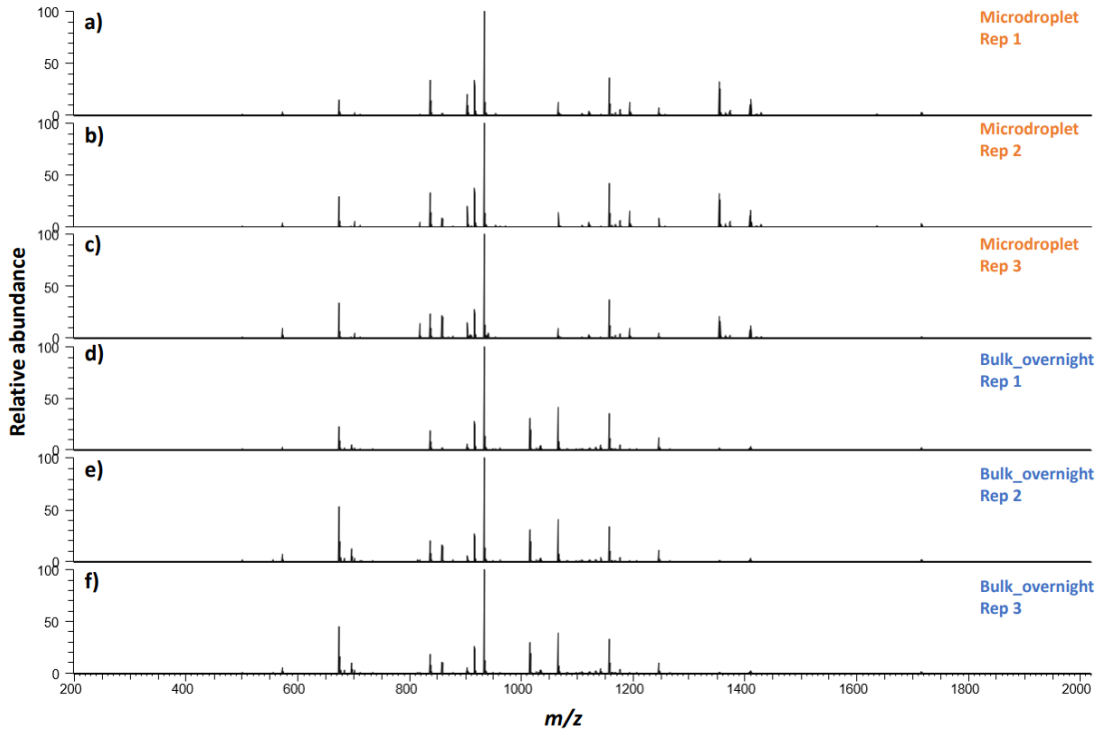

Figure 2.3 (a) NanoESI mass spectra of β-lactoglobulin B by triplicate microdroplet digestions (a-c) and triplicate bulk overnight digestions (d-f). Experimental condition was kept the same for each condition as described in Experimental Section. No remaining intact β-lactoglobulin B was detected.

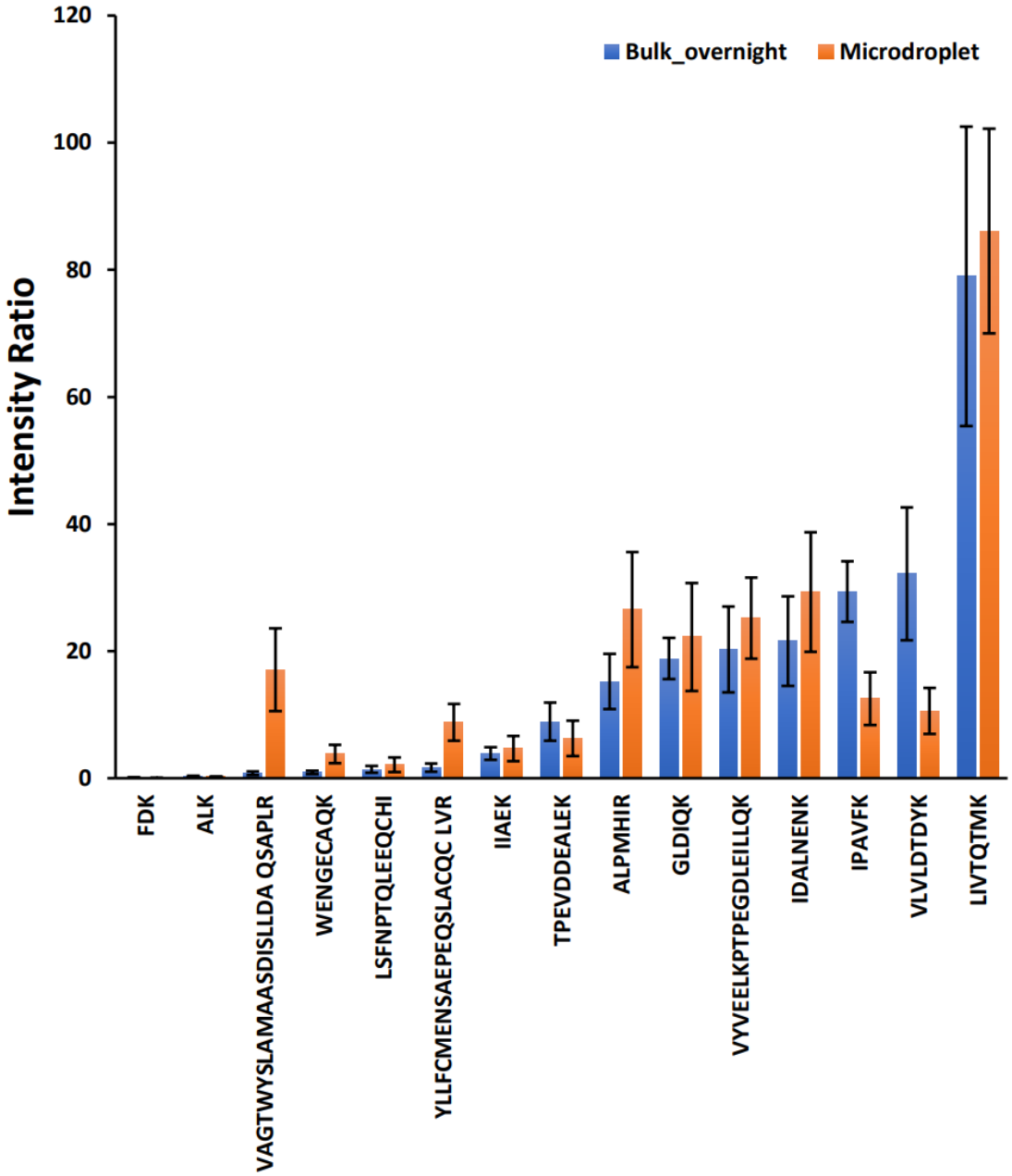

Figure 2.4 Intensities of fully cleaved peptides from β-lactoglobulin B (relative to internal standard peptide TKPR) under bulk overnight and microdroplet digestion conditions. Standard deviations from the reported mean shown are for n = 3 digestion replicates.

In our microdroplet digestion setup (Scheme 2.1), to reduce the loss of peptides from collection of the sprayed microdroplets, the collection vial was covered with a lid and the emitter tip was inserted into the vial through the lid via a predrilled hole. As a test, standard peptide KVPRNQDWL solution was sprayed and collected using the setup shown in Scheme 2.1. By comparing the sprayed peptide signals before and after the spray, we

measured the collection recovery to be 105% (details shown in Table 2.1), indicating that there was no notable peptide loss during microdroplet spray collection process.

Table 2.1 Peptide Recovery of KVPRNQDWL (gp-100) after Spray Compared with Control (no spray)

	Control				Microdroplet				
	IS (m/z 251.16)	gp-100 (m/z 578.32)	Intensity ratio	Average ratio	IS (m/z 251.16)	gp-100 (m/z 578.32)	Intensity ratio	Average ratio	Recovery%
Rep 1	9.79E+07	1.30E+08	1.32788 5598	1.33099 3	1.31E+08	1.79E+08	1.366412214	1.40338 7405	105.44
Rep 2	9.92E+07	1.34E+08	1.35080 6452	1.31E+0 8	1.6E+08	2.16E+08	1.35		
Rep 3	1.05E+08	1.38E+08	1.31428 5714		1.6E+08	2.39E+08	1.49375		

2.3.2 Comparison of the tryptic digestion of mAb and PLBL2 in microdroplet and bulk solution

After examining microdroplet digestion with β-lactoglobulin B as an example, we moved forward to investigate the microdroplet digestion of proteins in mixture. No digestion of multiple proteins in microdroplet was examined before. In our experiment, NIST 8671 mAb was mixed with HCP protein PLBL2 at 100:1 ratio to mimic a protein mixture where one protein is dominant, and the other one is a minor species. PLBL2 is a 66KDa catalytic HCP protein that copurifies frequently in mAb preparations produced in Chinese hamster ovary (CHO) cells, which might cause the unwanted immunogenic effects in patients and affect the drug stability due to its enzymatic degradation of polysorbates 20 and 80, common adjuvants present in formulated drug substance (DS).[164, 165] Therefore, PLBL2 needs to be removed from mAb preparations down to acceptable levels, and therefore, it is necessary to monitor the presence of PLBL2 in IgG antibodies. In this study, we attempted to examine how the microdroplet digestion would occur to a low-level PLBL2 protein and a high-level concentration of large mAb antibody. On the other hand, we evaluated if

chemical modifications to antibody like asparagine/glutamine deamidation could be reduced during the short digestion time of MD.

Microdroplet digestion and bulk digestion of the mixture of NIST 8671 mAb and PLBL2 were conducted as described in Experimental Section. Both microdroplet digest and bulk overnight digest were prepared as 3 digestion replicates and then subject to LC/MS analysis. Following LC/MS/MS analysis, peptide identification and quantification were performed to evaluate the quality of the digested samples between the two different digestion conditions. The digestion efficiency was studied in terms of the determination of sequence coverage, missed cleavage, semi-specific cleavage, and nonspecific cleavage as the metrics. As shown in Figure 2.5, comparable sequence coverage of antibody heavy chain was attained for both microdroplet and bulk digestions. A slightly higher sequence coverage of antibody light chain and lower abundance protein PLBL2 in microdroplet was observed compared with bulk digestion. Upon further investigating the identified peptides containing zero, one, or two missed tryptic cleavages (Figure 2.5b−d), microdroplet and bulk overnight digestion showed comparable trypsin digestion efficiency for mAb heavy chain. However, for mAb light chain and low abundance PLBL2, microdroplet showed less miss cleaved peptides than bulk.

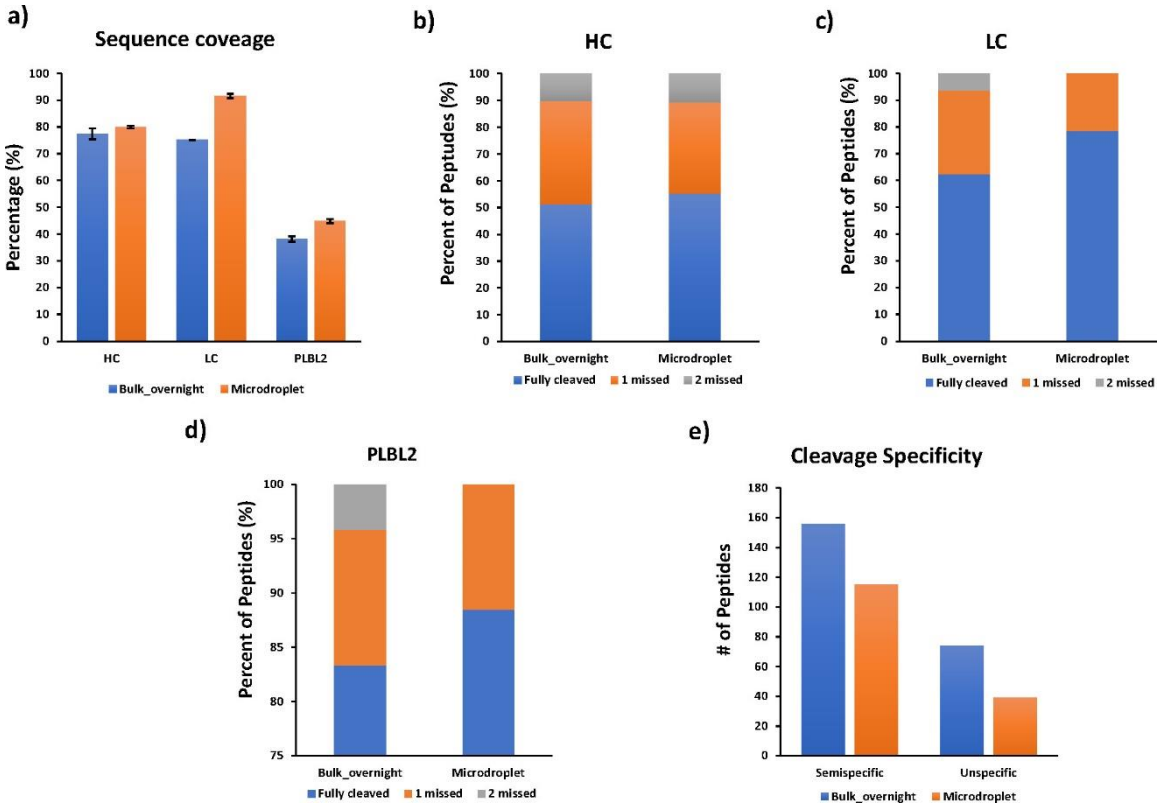

Figure 2.5 (a) Sequence coverages of mAb heavy chain, light chain and PLBL2. The percentages of identified peptides containing 0, 1, or 2 missed tryptic cleavages from mAb heavy chain (HC, b), mAb light chain (LC, c) and PLBL2 (d). Numbers of semispecific cleaved peptides and unspecific cleaved peptides identified under different digestion conditions.

Aside from the missed cleavages, we also checked the semispecific cleavage (a specific cleavage at one terminus and a nontryptic cleavage site at the other end) and nonspecific cleavage (enzymatic cleavage of C-terminal to a residue other than Lys or Arg for both termini), since microdroplet digestion was conducted in a new reaction environment with unknown reaction mechanism which may affect the enzyme specificity. As shown in Figure 2.5e, bulk overnight digestion showed higher level of semispecific cleavages with 156 peptides identified, whereas the number of identified semispecific peptides from microdroplet digest was 115. This trend continued when comparing nonspecific cleavage in Figure 2.5e, a lower-level nonspecific cleavage was observed in microdroplet digestion with 39 peptides identified, whereas 74 nonspecific cleaved peptides were found from bulk overnight digestion. All these results suggested that

microdroplet digestion has comparable digestion efficiency with bulk and no significant increment of semi-specific cleavage, as well as nonspecific cleavage, was observed.

It is noteworthy that a significant number of semi-specific and nonspecific tryptic peptides were identified in the case of antibody sample digestion. However, most of these peptides were of relatively low-abundance compared to fully tryptic peptides. For example, as shown in Figure 2.6a, four semitryptic peptides were detected corresponding to fully tryptic peptides VYACEVTHQGLSSPVTK (amino acid 190−206) from light chain. However, the relative abundance of those semitryptides were lower than 1%. Similar result was observed for another peptide TPEVTCVVVDVSHEDPEVK (amino acid 259−277) from heavy chain (Figure 2.6b). Although increased number of semitryptic peptides were detected, the overall relative abundance corresponding to the fully tryptic peptides were low. The intensity distributions of semispecific and unspecific peptides are shown in Figure 2.6c and d, whereby the major peptides were detected at low abundance (lower than 1 × 106). Indeed, in previous studies, nonspecific trypsin cleavages have been frequently reported and showed a high percentage especially in standard protein digest.[166, 167] Several potential sources for generating partially tryptic peptides has been reported, including possible chymotrypsin contamination in trypsin, pseudotrypsin activity due to partial autolysis of trypsin, proteolytic products due to endogenous proteases, and in-source fragmentation of fully tryptic peptides.[167] Besides, it has been shown to be related to a number of digestion conditions and predigestion treatment.[168-170] In this work, to prevent the autolysis of trypsin before spray, trypsin was reconstituted in 0.1% acetic acid. Although mildly acidic environment was often recommended by the manufacturer to prevent trypsin autolysis, a significantly increased level of nonspecific cleavages during the trypsin digestion process has been reported before.[171]

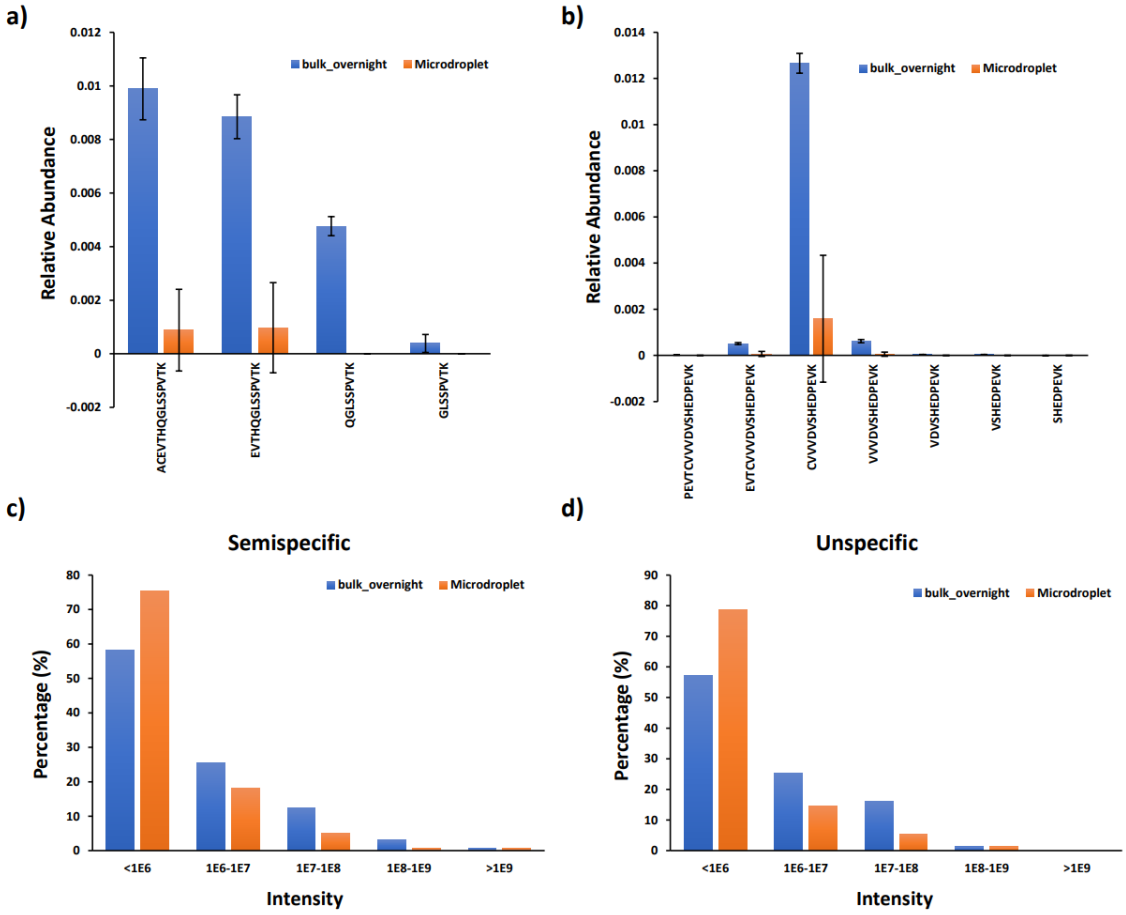

Figure 2.6 Abundances of semi-specific peptides relative to their corresponding fully tryptic peptide VYACEVTHQGLSSPVTK (amino acid 190-206) from light chain (a) and TPEVTCVVVDVSHEDPEVK (amino acid 259-277) from heavy chain (b) under different digestion conditions. Intensity distribution of semi-specific peptides (c) and unspecific peptides (d).

In addition, we quantitatively compared each fully cleaved peptide based on the peak intensities reported from Maxquant. Interestingly, the abundance of different fully cleaved tryptic peptides was found to be quite distinct under the two digestion conditions. For example, as shown in Figure 2.7a and b, several long peptides showed much lower intensities in bulk overnight digest than in microdroplet digest, such as VTNMDPADTATYYCAR, WQQGNVFSCSVMHEALHNHYTQK, ESGPALVKPTQ-TLTLTCTFSGFSLSTAGMSVGWIR, TPEVTCVVVDVSHEDPEVK, and THTCPPCP-APELLGGPSVFLFPPKPK. It is likely that these peptides are long and more susceptible to hydrolysis during bulk overnight digestion at 37 °C, whereas microdroplet digestion

could significantly minimize the hydrolysis because of the fast digestion speed at room temperature. However, the other long peptides from the mAb heavy chain, such as DMIFNFY FDVWGQGTTVTVSSASTK and GFYPSDIAVEWESNGQPENNYK, showed higher abundance in bulk overnight digest than microdroplet.

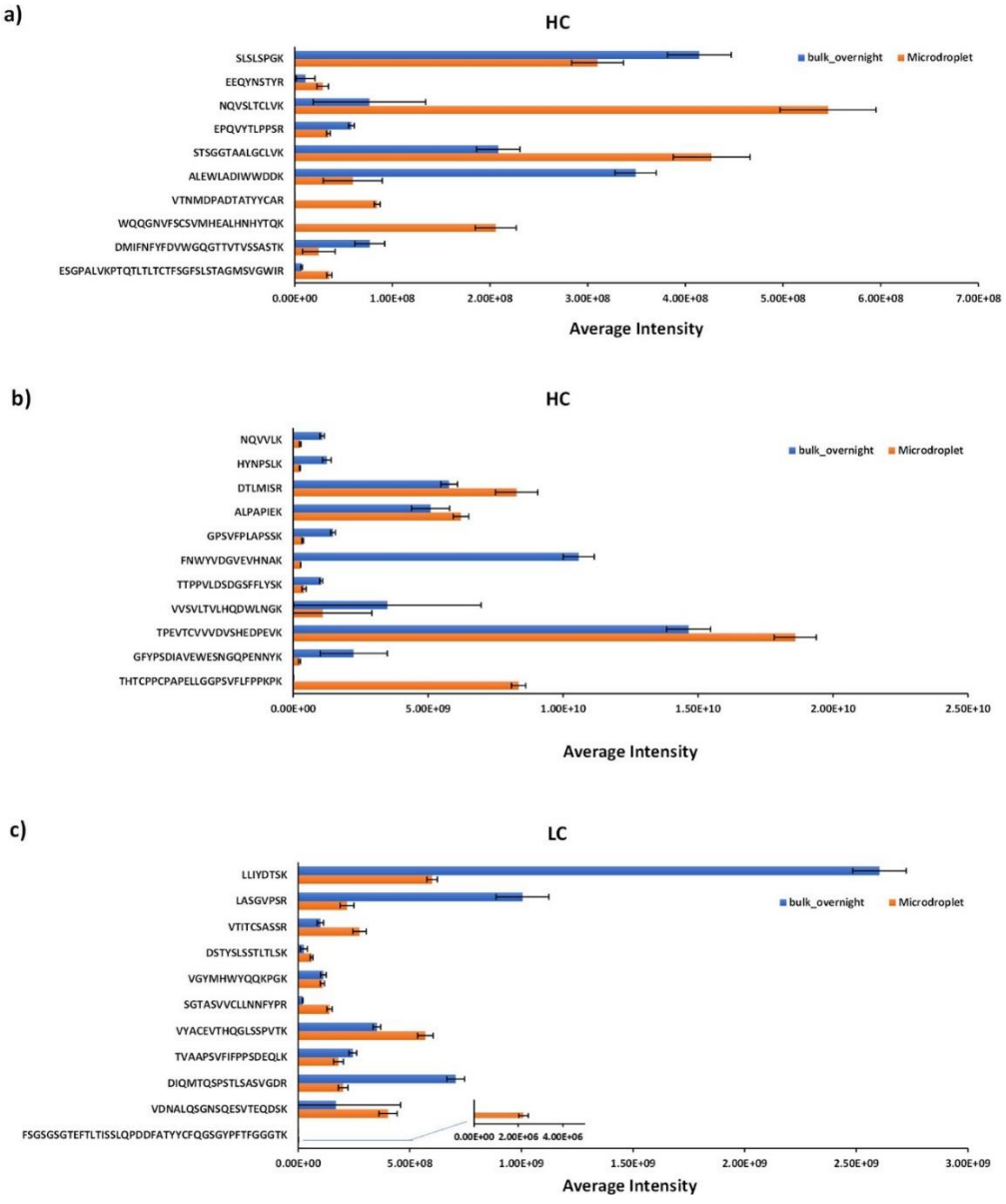

Figure 2.7 Averaged intensities of fully cleaved peptides identified from mAb heavy chain (a and b) and light chI (c) under different digestion conditions (the fully cleaved peptides identified from mAb heavy chain were grouped in panels a and b those due to the large difference in scale of the averaged intensities across different peptides). Standard deviations from the reported mean shown are for n = 3 digestion replicates.

The same trend was observed for mAb light chain (Figure 2.7c) wherein long peptides like SGTASVVCLLNNFYPR, VYACEVTHQGLSSPVTK, VDNALQSGNSQ-ESVTEQDSK, and FSGSGSGTEFTLTISSLQPDDFATYYCFQGSGYPFTFGGGTK, were detected with lower intensities in bulk overnight digest than microdroplet digest. For low abundance protein PLBL2 (Figure 2.8), most of the fully cleaved peptides showed a relatively higher intensity in microdroplet than bulk, indicating that microdroplet might have a slightly higher digestion efficiency of low abundance proteins. It has been reported that the digestion bias exists between low and high abundance proteins due to the fact that the rate of trypsin digestion is dependent on the concentration of each individual protein in a mixture.[172] Common strategies to address the abundance challenge include affinity depletion and enrichment of proteins with antibody arrays or ligand libraries and prefractionation of proteins.[173] In our microdroplet and bulk digestions of PLBL2, the sequence coverage was about 40% (Figure 2.5). To further improve the sequence coverage of spiked PLBL2, the prefractionation or affinity enrichment could be the solution.

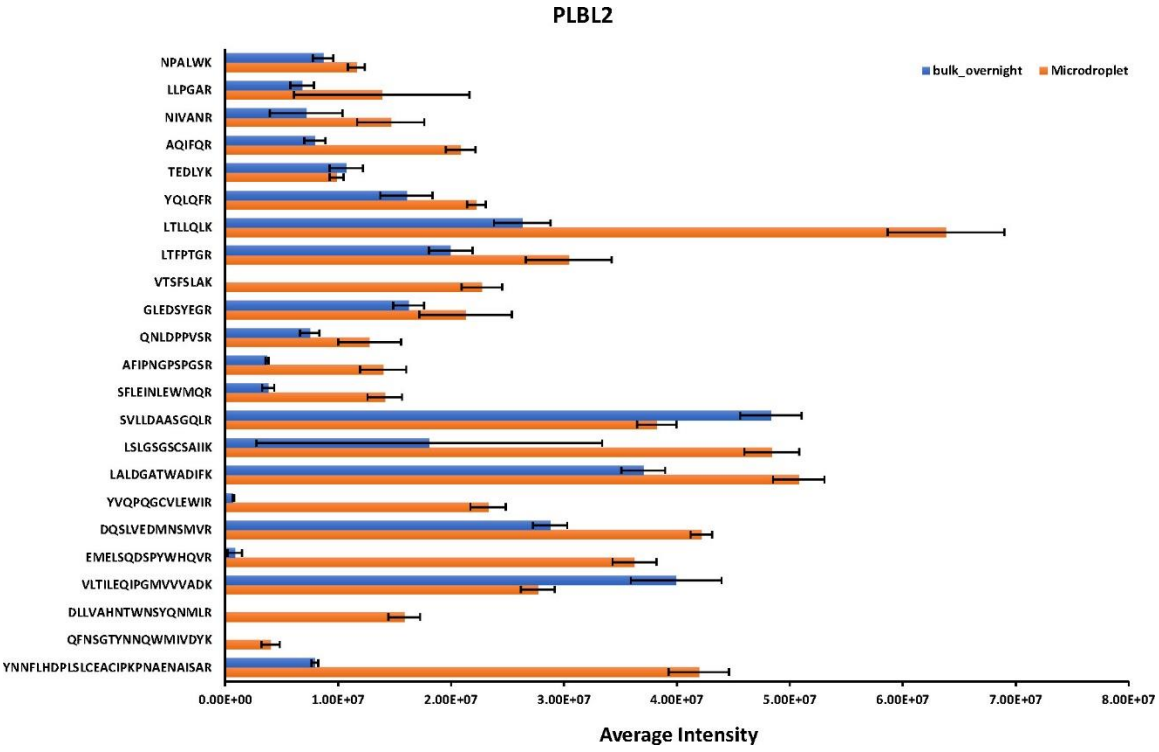

Figure 2.8 Averaged intensities of fully cleaved peptides identified from PLBL2 under different digestion conditions. Standard deviations from the reported mean shown are for n = 3 digestion replicates.

Peptides that contain asparagine deamidation site as shown in Figure 2.9 were investigated. For example, deamidation sites, such as N385 and N469 from PLBL2 and N136 and N151 from the light chain, as well as N300, N289 (279), N387, N364, N78(Q79), and N318 from the heavy chain, were identified and relative levels are quantified, as shown in Figure 5a (denotation of N289(279) means either N289 or N279 underwent deamidation, the same for N78(Q79)). Overall, a much higher level of deamidation was observed in bulk overnight digest than microdroplet. As the rate of deamidation also depends on the adjacent amino acid residue's size (smaller size reduces steric hindrance for the initial cyclization reaction of the deamidation process),[150] the level of deamidation varies among different peptides. For instance, Gly is considered as the most favorable amino acid promoting deamidation, followed by Ser, Thr, and Asn,[174, 175] whIch is in line with the detected deamidation rate diIplayed in Figure 2.9a in which high deamidation level site like N385

from PLBL2, N387, and N318 from heavy chain are followed by Gly, whereas N136 from light chain is adjacent to Asn. All these results indicated that reducing the digestion time without reducing digestion efficiency is preferable to minimize the digestion-induced deamidation.

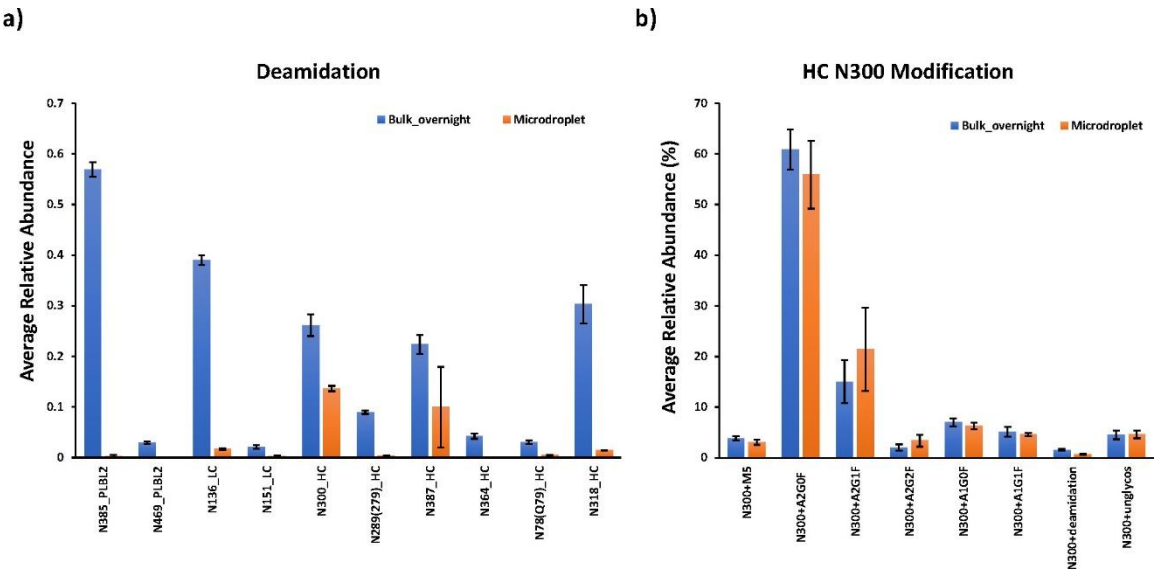

Figure 2.9 Averaged relative abundances of (a) deamidation for mAb and PLBL2 and (b) glycosylation for mAb heavy chain N300 under different digestion conditions. Averaged relative abundance was calculated as the intensity ratio of one modified peptide to the intensity sum of modified and native peptides. Peak intensities of native and modified peptides were recorded after manually searching of +2 charge forms of each peptide from MS1 spectra with 5 ppm mass accuracy tolerance. Standard deviations from the reported mean shown are for n = 3 digestion replicates.

Interestingly, EEQY300NSTYR containing one glycan site at N300 was detected with slightly higher deamidation rate in bulk overnight than microdroplet (Figure 2.9). Upon further investigation of glycans, deamidated and unmodified peptides of EEQY300NSTYR in Figure 2.9b, we found that the relative abundance of unmodified peptides in microdroplet and bulk were similar, indicating deamidation rate is relevant to the glycan loss. Indeed, this result is consistent with the previous report that glycan loss in solution is accompanied by the conversion of Asn to Asp.[176] Thus, a lower level of

deamidation rate observed in microdroplet digestion might prevent glycan shedding that occurs during overnight digestion.

Finally, glycosylation was also assessed for the glycan profiles on heavy chain N300 site, as shown in Figure 2.9b. Most abundant glycan forms including complex biantennary oligosaccharides containing from 0 to 2 nonreducing galactoses with fucose attached to the reducing end of N-acetylglucosamine (A2G0F, A2G1F, A2G2F, A1G0F, A1G1F), along with high mannose structures (M5), were searched. The ratio of the relative abundances of most glycan forms was consistent between bulk and microdroplet digestions, suggesting that microdroplet digestion could be applied to monitor PTMs for mAb.

In addition, in the microdroplet digestion experiments described above, the flow rate for protein injection was low. We further explored the possibility of using a high flow injection rate like 100 μL/min for each pump. In our test, 100 μL of 1 μg/μL β-lactoglobulin B in ABC buffer was loaded in one syringe and 100 μL of 0.05 μg/μL trypsin in 0.1% acetic acid was loaded in the other syringe for microdroplet spray (using the apparatus shown in Scheme 2.1). The flow rate of both syringes was 100 μL/min and N2 was set at 120 psi. The microdroplet was collected into a vial containing a quenching solution of 50 μIf H_2O/ACN/FA (50:50:1, v/v) for just 10 s MS spectrum (Figure 2.10) showed *β*-lactoglobulin B was still well digested under such a high flow rate. The tolerance of high sample flow rate for microdroplet digestion would further speed up the total collection procedure. Overall, the data presented in this study demonstrate that microdroplet digestion has the potential to significantly speed up the bottom-up LC/MS analysis of mAb, stemming from the efficient digestion, even for the low abundant proteins. Moreover, ultrafast digestion performed at room temperature allows to minimize artificial modification like asparagine/ glutamine deamidation.

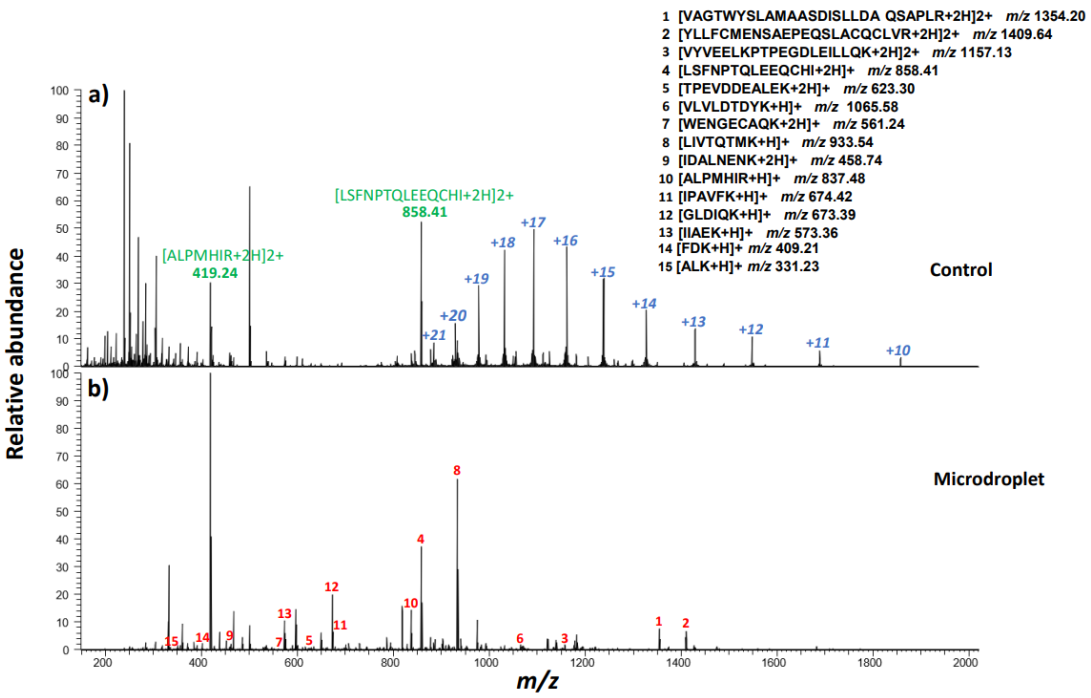

Figure 2.10 NanoESI mass spectra of β-lactoglobulin B from online mixing without microdroplet spray (control experiment, a) and from microdroplet digestion at a high injection flow rate of 100 µL/min (b). Inset: list of fully cleaved tryptic peptides from *β*-lactoglobulin B.

2.4 Conclusions

Fast enzymatic reactions of proteins and antibodies in microdroplet were investigated with detailed peptide analysis in this study. Some interesting features of MD were found. First, MD is fast, resulting in the preservation of long peptides in digest. Second, fast microdroplet digest could reduce deamidation of asparagine or glutamine residues, in comparison to bulk digestion. Third, MD is applicable to digest both high- and low-abundance proteins in a mixture. Fourth, no significant difference between MD and bulk digestion was observed for trypsin digestion specificity based on examination of semi- and unspecific-cleaved peptides. Fifth, similar glycan profiles on heavy chain N300 site were observed in both microdroplet and bulk digestions. A lower level of deamidation degradation was found in microdroplet than in bulk. Sixth, microdroplet digestion tolerates

a high sample injection flow rate, which could reduce the digest collection time. Our study demonstrates that microdroplet could be considered as an emerging, fast and simple protein digestion approach and has the potential for the routine usage in bottom-up protein characterization such as peptide mapping for mAbs.

CHAPTER 3

STANDARD-FREE ABSOLUTE QUANTITATION OF TRYPTOPHAN-CONTAINING PEPTIDES AND AMYLOID *β*-PEPTIDE FRAGMENTS BY COULOMETRIC MASS SPECTROMETRY

A version of this work has been published in the *Journal of the American Society for Mass Spectrometry* as the article: Ai, Y.; Zhao, P.; Fnu, P. I. J.; Chen, H., Absolute Quantitation of Tryptophan-Containing Peptides and Amyloid *β*-peptide Fragments by Coulometric Mass Spectrometry. *Journal of the American Society for Mass Spectrometry* **2021,** *32* (7), 1771-1779.

3.1 Introduction

Quantitative mass spectrometry reporting the relative or absolute quantities of target peptides and proteins is very important for biological research.[61, 82, 177-182] Although relative quantification is now routinely used to provide valuable information on alteration of protein abundance in a proteome wide scale,[183-186] the absolute quantitation determines the absolute concentration of target peptides and proteins within a sample, providing a far more precise description of molecular events in the biological processes.[187] Moreover, absolute quantitation is crucial for the evaluation of clinical biomarker candidates and enables the data integration and comparison among different laboratories.[53, 79, 188] For the MS-based absolute quantitation of peptides and proteins, the isotope-labeled internal standards and the calibration curve are often needed.[79] However, there are some challenges for employing those isotope-labeling absolute quantitation strategies. First, the most suitable standard needs to be selected and synthesized in advance, which is time-consuming, expensive, and sometimes unavailable. Second, using this costly technique, the concentration of only a few peptides of interest can be determined and it unsuits large-scale proteomic studies.[177] To address this, we recently developed a novel MS-based absolute quantitation method, named coulometric mass spectrometry (CMS), which combines electrochemistry (EC) with MS for absolute quantitation without the need of using any standards or calibration curves.[109, 114, 115, 189]

As illustrated in Scheme 3.1, the basic workflow of CMS involves two steps. First, an electrochemically active substance that elutes from the LC column undergoes an electrochemical reaction (oxidation or reduction). Electrons are transferred, resulting in an electrical current peak that then can be integrated over time to obtain the total charge Q. According to the Faraday's Law, the total electric charge (Q) involved in the electrochemical reaction is proportional to the quantity of the oxidized/reduced substance: Q = nzF, where n denotes the moles of the oxidized/reduced analyte, z is the number of electrons transferred per molecule during the redox reaction, and F is the Faraday constant taken to be 9.65 × 104 C/mol. Second, from the acquired MS spectra before and after electrolysis, the redox conversion yield Δi can be determined by measuring the relative change of the target analyte peak area in the extracted ion chromatogram (EIC). Thus, the total amount of the analyte can be calculated as the quotient of the amount of the oxidized analyte n and the oxidation yield Δi (i.e., Q/(zFΔi)).

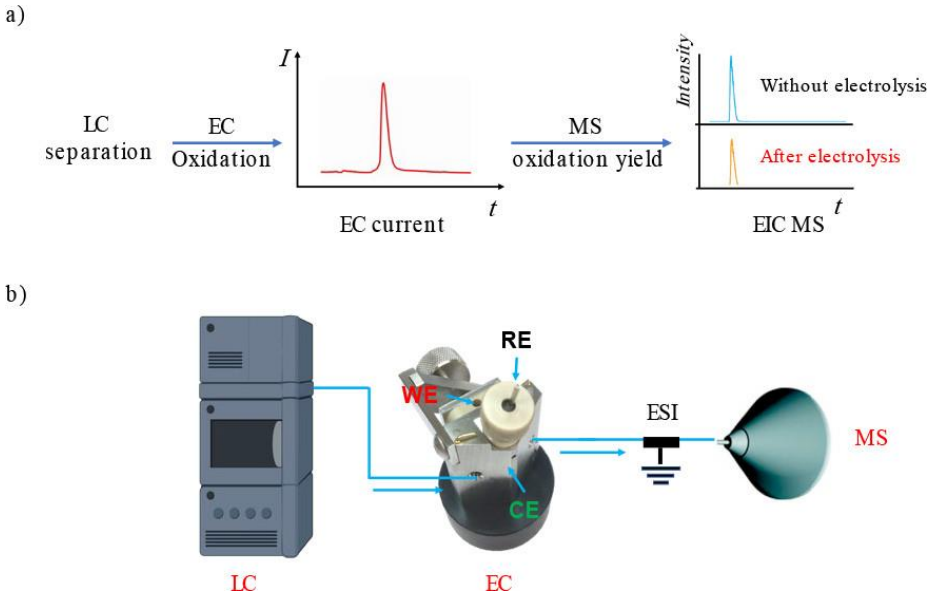

Scheme 3.1 (a) CMS workflow and (b) schematic illustration of our LC/EC/MS apparatus for CMS quantitation.

Previously, we have demonstrated that CMS can be used for accurately quantifying tyrosine- or cysteine-containing peptides[109, 115] as well as proteins.[122] However, mainly

relatively short peptides were examined, and long peptides were not investigated. Additionally, peptide quantitation based on tryptophan oxidation were not studied. Among the 20 naturally occurring amino acids, tryptophan (W) is another oxidizable amino acid with a relatively low oxidation potential (1.01 V vs NHE) compared to other oxidizable residues (others aIcysteine (C), tyrosine (Y), and methionine (M)).[115] In our trials, we also found that tryptophan-containing peptides often exhibit a higher electric current signal than tyrosine-containing peptides, indicating that CMS would have a better sensitivity, if it could be built on tryptophan oxidation. Therefore, in this study, we attempted to explore the feasibility of CMS quantitation based on tryptophan residue oxidation in the purpose of expanding CMS applications for absolute peptide/ protein quantitation. We successfully quantified a set of tryptophan-containing peptides as well as one surrogate peptide GITWK digested from cytochrome c with good quantitation accuracy. In addition, we successfully quantified two long tyrosine-containing peptides, Aβ peptide fragment Aβ1−16 and Aβ1−28, using CMS based on tyrosine oxidation.

3.2 Experimental

3.2.1 Reagents and materials

[Glu11]-amyloid β 1−16 (Aβ1−16, DAEFRHDSGYEVHHQK, HPLC grade), [Gln11]-amyloid β 1−28 human (Aβ1−28, DAEFRHDSGYQVHHQKLVFFAEDVGSNK, HPLC grade), fibronectin adhesion-promoting peptide (WQPPRARI, HPLC grade), delta sleep inducing peptide (WAGGDASGE, HPLC grade) and cytochrome c from equine heart (99% purity) were bought from Sigma-Aldrich (St. Louis, MO). Trp-Gly-Gly-OH (WGG, HPLC grade) were obtained from Chem-Impex (Wood Dale, IL). BDC2.5 Mimotope (RTRPLWVRME, HPLC grade) and gp 100 (25−33) human (KVPRNQDWL, HPLC grade) were purchased from AnaSpec (Fremont, CA). Stable isotope-labeled peptide

standards GITWK^ (labeled at lysine, $^{13}C6$, $^{15}N2$) was purchased from Vivitide (Gardner, MA). Trypsin/Lys-C mix (mass spec grade) was purchased from Promega (Madison, WI).Ietonitrile (ACN, HPLC grade) and Formic acid (HPLC grade) were bought from Fisher Scientific (Fair Lawn, NJ). Ammonium bicarbonate (bioultra grade) were bought from Sigma-Aldrich (St. Louis, MO). A Millipore Direct-Q5 purification system (Burlington, MA) was used to obtain purified water for sample preparation.

3.2.2 Instrumentation

As shown in Scheme 3.1b, the experimental setup used for CMS consisted of a ultraperformance liquid chromatography (UPLC, Waters, Milford, MA) coupled with an electrochemical thin-layer flow cell (BASi, West Lafayette, IN; cell dead volume: ca. 1 μL) and a high resolution Orbitrap Q Exactive mass spectrometer (Thermo Scientific, San Jose, CA). The electrochemical cell equipped with a glassy carbon disc (i.d., 3 mm and 6 mm, catalog nos. MF-1095 and MF-1015, respectively) as the working electrode (WE). An Ag/AgCl (3 M NaCl) electrode was used as the reference electrode (RE, catalog no. MW-2021) and the cell stainless steel body served as a counter electrode (CE, catalog no. MF1092). The working electrode was cleaned by polishing with alumina slurry before and after use.

A reversed-phase column (BEH C18, 2.1 mm × 50 mm, 1.7 μm) was used for separation. A potential of +1.00 V or +1.05 V (vs Ag/AgCl) was applied to WE to trigger the oxidation of peptides. An Epsilon Eclipse potentiostat (BASi, West Lafayette, IN) was used to monitor and record the oxidation current. OriginPro 2018b was used to import and integrate the electric current peak to calculate the total electric charge of Q. The peptide flowing out of electrochemical cell was online analyzed using the Orbitrap mass spectrometer equipped with a heated electrospray ionization (HESI) source with the

following parameters: sheath gas flow rate, 35; auxiliary gas flow rate, 10; spray voltage, 4.0 kV; sweep gas flow rate, 0; capillary temperature, 300 °C; auxiliary gas heater temperature, 100 °C; S-lens RF level, 50. Mass spectra were acquired by Thermo Xcalibur (3.0.63).

3.2.3 Proteolytic digestion of cytochrome c

Cytochrome c (100 μg) was dissolved in 50 mM ammonium bicarbonate (NH4HCO3, pH 8.0) followed by addition of 50 μL of 0.2 μg/μL trypsin/ lys-c mix solution. The protein sample was incubated at 37 °C for overnight. The digested cytochrome c sample was then diluted to the final concentration of 10 μM by adding mobile phase A (water with 0.1% formic acid).

3.2.4 LC/EC/MS analysis

For LC/EC/MS analysis of Aβ1−16 (DAEFRHDSGYEVHHQK), the mobile phase flow rate was 200 μL/min. In an 8 min linear gradient elution (mobile phase A: water with 0.1% formic acid), the mobile phase B (acetonitrile with 0.1% formic acid) increased from 5% to 10% in 3 min, and reached 40% in 1 min. Then, mobile phase B was kept at 40% for 1 min before returning to 5%. The concentration of Aβ1−16 used was 20.02 μM. The injection volume was 3 μL per analysis.

For LC/EC/MS analysis of Aβ1−28 (DAEFRHDSGYQVHHQKLVFFAED-VGSNK), fibronectin adhesion-promoting peptide (WQPPRARI), and delta sleep inducing peptide (WAGGDASGE), the mobile phase flow rate was 200 μL/min. In an 8 min linear gradient elution, the mobile phase B (acetonitrile with 0.1% formic acid) increased from 5% to 20% in 3 min and reached 40% in 1 min. Then mobile phase B was kept at 40% for 1 min before returning to 5%. The concentrations of Aβ1−28, WQPPRARI, and

WAGGDASGE were 20.87, 20.07, and 20.13 μM, respectively. The injection volume was 3 μL per analysis.

For LC/EC/MS analysis of WGG, the mobile phase flow rate was set as 200 μL/min. An isocratic elution program using 90% A (mobile phase A: water with 0.1% formic acid and mobile phase B: acetonitrile with 0.1% formic acid) for 6 min was used. The concentration of WGG used was 29.65 μM and the injection volume was 3 μL per analysis.

For LC/EC/MS analysis of BDC2.5 Mimotope (RTRPLWVRME) and gp 100 (25−33) human (KVPRNQDWL), the mobile phase flow rate was 200 μL/min. In an 8 min gradient elution, the mobile phase B (acetonitrile with 0.1% formic acid) increased from 5% to 30% in 3 min, and reached 50% in 1 min. Then, mobile phase B was kept at 50% for 1 min before returning to 5%. The concentrations of RTRPLWVRME and KVPRNQDWL were 20.03 and 20.05 μM, respectively. The injection volume was 3 μL per analysis.

For LC/EC/MS setup of digested cytochrome c, the mobile phase flow rate was 250 μL/min. The mobile phase B (acetonitrile with 0.1% formic acid) increased from 5% to 10% in 1 min, and then reached to 14% from 1 to 16 min. Then the mobile phase B climbed to 70% in 1 min and remained at 70% for 3 min before returning to 5%. The injection concentration of digested cytochrome c was 10 μM. The injection volume was 6 μL per analysis.

3.2.5 The isotope dilution MS measurement of GITWK

The isotope-labelled peptide GITWK^ (labeled at lysine, 13C6, 15N2) was spiked into the digested cytochrome c sample at the final concentrations of 0.99, 4.97, 9.94, 14.91, and 24.86 μM, respectively. The LC/MS was set at the mobile phase flow rate of 250 μL/min.

The mobile phase B (acetonitrile with 0.1% formic acid) increased from 5% to 10% in 1 min, and then reached to 14% from 1-16 min. Then the mobile phase B climbed to 70% in 1 min and remained at 70% for 3 min before returned to 5%. The concentration of diluted digested cytochrome c was 10 μM. The injection volume was 6 μL per analysis.

3.3 Results and Discussion

3.3.1 Absolute quantitation of amyloid beta peptide fragments by coulometric mass spectrometry

Alzheimer's disease (AD) is becoming a major public health problem worldwide.24,25 Amyloid beta (Aβ) peptide and its peptide fragments, derived from the proteolytic processing of amyloid precursor protein (APP),[190, 191] have been considered as the diagnostic biomarker and therapeutic target of Alzheimer's disease (AD).[192-194] Therefore, quantification of those different Aβ isoforms and their fragments is significant for early diagnosis of AD[193, 195] as well as facilitating the investigation of disease mechanism and thus benefiting drug discovery. MS is widely used and represents an important tool in the field of AD due to their capability of providing both qualitative and quantitative information on the Aβ involved in AD.[196, 197] However, for traditional MS-based absolute quantitation of Aβ peptides,[198, 199] isotopically labeled Aβ peptides are often needed as internal standards, which are time-consuming and expensive. In this study, we first conducted quantifications of two long Aβ peptide fragments Aβ1−16 and Aβ1−28 using CMS based on the electrochemical oxidation of tyrosine residue without adding isotope labeling standards.

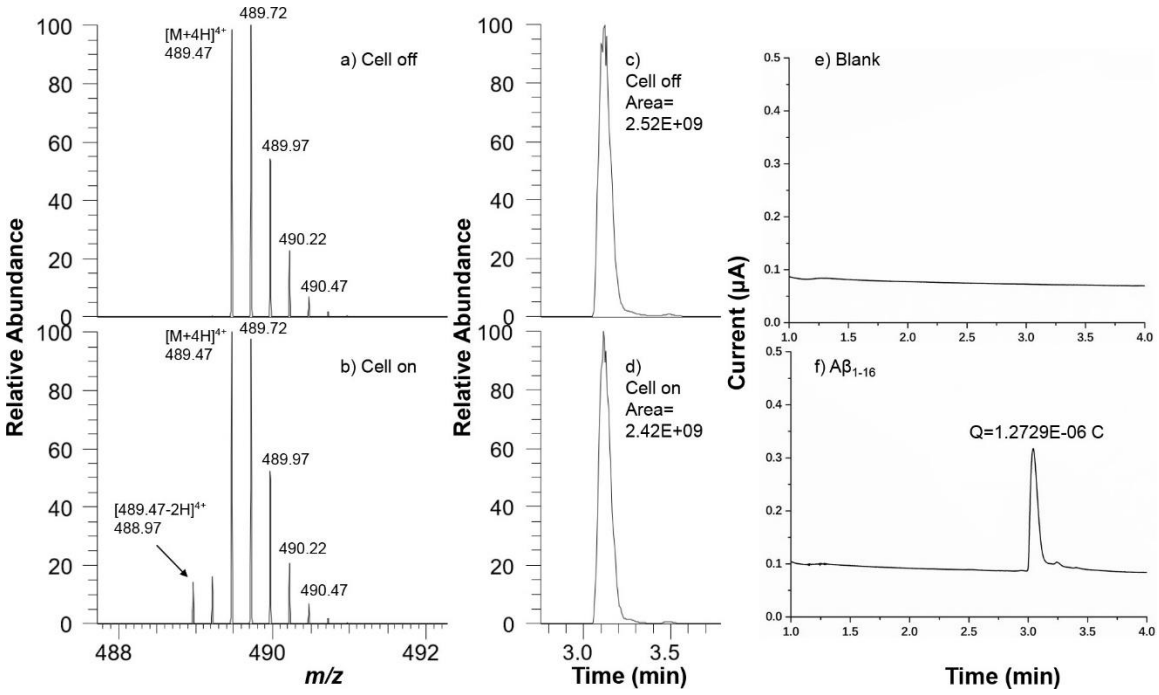

Figure 3.1 MS spectra of Aβ1−16 (a) when the cell was off and (b) when the cell was turned on (applied potential: + 1.05 V). The oxidation product of Aβ1−16 was detected at *m/z* 488.97. EICs of Aβ1−16 were acquired (c) when the cell was off and (d) when the cell was turned on (applied potential: + 1.05 V). Electric current diagrams were collected from (e) blank solvent and (f) the oxidation of Aβ1−16.

Aβ peptide fragments, Aβ1−16, was first chosen for CMS test, which is a Tyr-containing peptide (sequence: DAEFRHDSGYEVHHQK). On the basis of our previous studies, tyrosine residue can be oxidized into semiquinone by losing two electrons and two protons.[115, 122] A blank sample (solvent only) was first injected and no electric current peak was observed when the oxidation potential +1.05 V was applied (Figure 3.1). In contrast, after the injection of Aβ1−16 sample, a sharp electric current peak was observed under the same oxidation potential of +1.05 V (Figure 3.1f), indicating that the current peak observed in Figure 3.1f was derived from electrochemical oxidation of Aβ1−16. Indeed, it was further confirmed by the corresponding pair of MS spectra recorded upon the electrochemical oxidation. Compared to the mass spectrum (Figure 3.1a) without electrolysis in which the +4 ion of DAEFRHDSGYEVHHQK was observed at m/z 489.47, a new peak at m/z 488.97 arose (Figure 3.1b), corresponding to +4 ion of the oxidized

peptide product, when +1.05 V was applied to the cell for oxidation. The integrated EIC peak area of m/z 489.47 shown in Figure 3.1d was reduced by 11.3% compared to the same peak in Figure 3.1c, suggesting that the oxidation yield for DAEFRHDSGYEVHHQK was 11.3% (see detailed data in Table 3.1). The amount of the oxidized Aβ1−16 was calculated to be 6.6 pmol, based on the integration of the current peak area shown in Figure 1f and the Faraday's Law. Therefore, the measured amount of Aβ1−16 was 58.3 pmol (Table 3.1). A triplicate measurement gave the average amount of Aβ1−16 to be 58.3 pmol, which turned out to be very close to the theoretical amount of 60.1 pmol, with the measurement error of −3.0% (Table 3.1). Aβ1−28, another long amyloid peptide that contains Tyr (sequence: DAEFRHDSGYQVHHQKLVFFAEDVGSNK), was also analyzed by CMS (Figure 3.2). The average amount of Aβ1−28 was measured at 60.6 pmol with the quantitation error of −3.2% (Table 3.2).

Table 3.1 Electric Current and MS Data for Aβ1-16

	Q (A*s)	Amount of the oxidized analyte (mol)	Oxidation yield	Measured amount (mol)	Averaged amount (pmol)	Theoretical amount (pmol)	Measurement error
	1.1577E-06	5.9982E-12	0.10058525	5.9633E-11			
$A\beta_{1-16}$	1.2729E-06	6.5951E-12	0.11313182	5.8296E-11	58.3	60.1	-3.0%
	1.3882E-06	7.1929E-12	0.1262624	5.6968E-11			

	EIC peak area of *m/z* 489.47 before electrolysis	EIC peak area of *m/z* 489.47 after electrolysis	Corrected EIC peak area* of *m/z* 489.47	Oxidation yield
	2467591174	2373714593	2219387898	0.10058525
$A\beta_{1-16}$	2524900787	2419052383	2239254162	0.11313182
	2523288257	2382492714	2204691828	0.1262624

*Note that, after oxidation, the third isotopic peak of the oxidized peptide ion at *m/z* 488.97 overlaps with the peak of the remaining intact peptide ion at *m/z* 489.47 (Figure 3.1). The contribution to the EIC peak area of *m/z* 489.47 after oxidation from the third isotopic peak of *m/z* 488.97 was calculated, based on the EIC peak area of *m/z* 488.97 and α that is the theoretical ratio of the third isotopic peak and the first isotopic peak of *m/z* 488.97. Approximately, α equals to the ratio of the third isotopic peak and the first isotopic peak of *m/z* 489.47 before oxidation (that is 0.56 as shown in Figure 3.1a). Thus, the corrected EIC peak area of *m/z*

489.47 after oxidation = EIC peak area of *m/z* 489.47 after oxidation- α × EIC peak area of *m/z* 488.97 after oxidation.

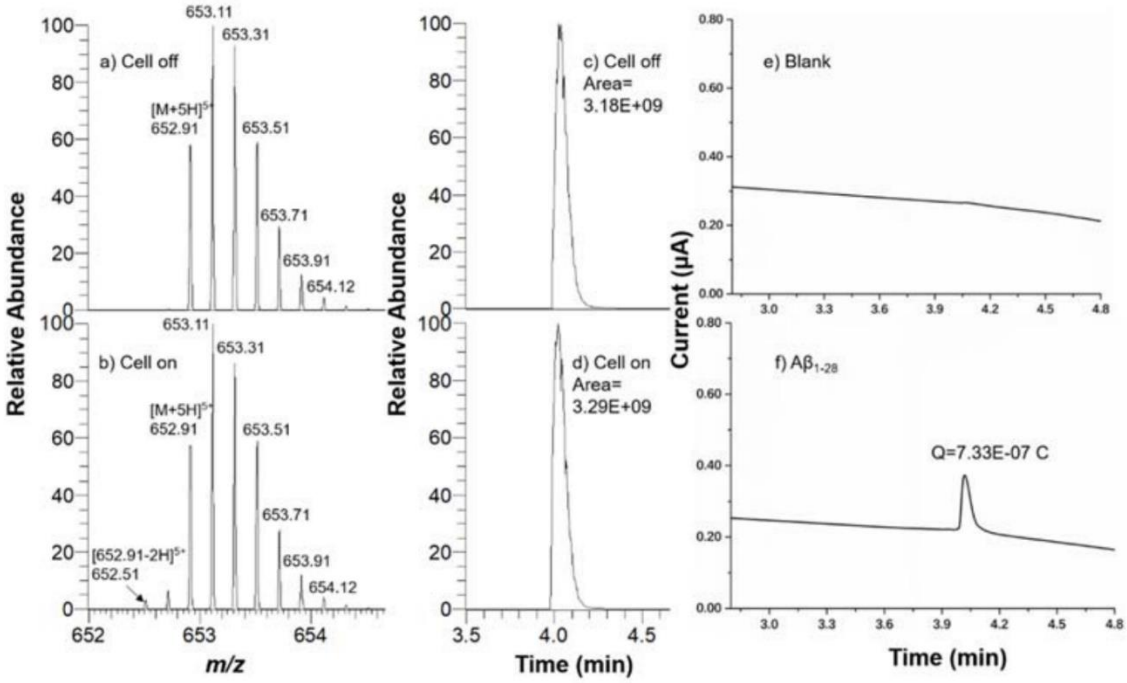

Figure 3.2 MS spectra of Aβ1-28 (a) when the cell was off and (b) when the cell was turned on (applied potential: + 1.05 V). The oxidation product of Aβ1-28 was detected at *m/z* 652.51. EICs of Aβ1-28 were acquired (c) when the cell was off and (d) when the cell was turned on (applied potential: + 1.05 V). Electric current diagrams were collected from (e) blank solvent and (f) the oxidation of Aβ1-28.

Table 3.2 Electric Current and MS Data for [Gln11]-amyloid Beta 1-28

	Q (A*s)	Amount of the oxidized analyte (mol)	Oxidation yield	Measured amount (mol)	Averaged amount (pmol)	Theoretical amount (pmol)	Measurement error
	7.3286E-07	3.7972E-12	0.06335253	5.9937E-11			
$A\beta_{1-28}$	7.7561E-07	4.0187E-12	0.06683309	6.0131E-11	60.6	62.6	-3.2%
	8.3681E-07	4.3358E-12	0.07031522	6.1662E-11			

	EIC peak area of *m/z* 652.91 before electrolysis	EIC peak area of *m/z* 652.91 after electrolysis	Corrected EIC peak area* of *m/z* 652.91	Oxidation yield
	3177981472	3285156348	2976648307	0.06335253
$A\beta_{1-28}$	3134403969	3234075893	2924922082	0.06683309
	3256019749	3386068094	3027072003	0.07031522

*Note that, after oxidation, the third isotopic peak of the oxidized peptide ion at *m/z* 652.51 overlaps with the peak of the remaining intact peptide ion at *m/z* 652.91(Figure 3.2). The contribution to the EIC peak area of *m/z* 652.91 after oxidation from the third isotopic peak of *m/z* 652.51 was calculated, based on the EIC peak

area of *m/z* 652.51 and α that is the theoretical ratio of the third isotopic peak and the first isotopic peak of *m/z* 652.51. Approximately, α equals to the ratio of the third isotopic peak and the first isotopic peak of *m/z* 652.91 before oxidation (that is 1.61 as shown in Figure 3.2). Thus, the corrected EIC peak area of *m/z* 652.91 after oxidation = EIC peak area of *m/z* 652.91 after oxidation- α × EIC peak area of *m/z* 652.51 after oxidation.

3.3.2 Absolute quantitation of tryptophan-containing peptides by coulometric mass spectrometry

The result above reveals that our CMS method is applicable to absolute quantitation of quite long tyrosine containing peptides, in addition to short peptides that we demonstrated before. To further extend the CMS application, we investigated the possibility of using it for absolute quantitation of tryptophan-containing peptides in this study. Tryptophan is known to be electroactive and has a relatively low oxidation potential (+1.01 V, vs NHE21). The major oxidation products and pathways of Trp-containing peptides have been reported in the literature using combined EC/MS systems.[200, 201] As illustrated in Scheme 3.2, in general, the major oxidation products are observed as the singly hydroxylated M + 16 ($2e^-$ oxidation product) and the ketone product M + 14 ($4e^-$ oxidation product) and minor products include the doubly hydroxylated M + 32 ($4e^-$ oxidation product) and cleavage product R1W + 14 ($4e^-$ oxidation product, cleavage products were observed in oxidation of some peptides such as KVPRNQDWL and GITWK in this study). The various oxidation products can be readily monitored by our online LC/EC/MS system. Based on the similar structures of those oxidation products, we assume that the intensity ratios of the different mass peaks of the oxidized products are approximately equal to ratios of moles of the different oxidized products, as shown in eq 1−3. For calculation, we assume that moles of products M + 16, M + 14, M + 32, and R1W + 14 are n1, n2, n3, and n4, respectively, and the total mole of the oxidized peptide is n = n1 + n2 + n3 + n4. On the basis of Faraday's Law, the electricity Q is obtained from all four oxidation pathways (eq 4). From eqs 1−4, the total amount of oxidized peptide n can be calculated as denoted in eq 5, where the Q is experimentally obtained by integrating the Faradaic current over time and F is the Faraday

constant (9.65 × 104 C/ mol). Once we obtain n and the oxidation yield, the total amount of the peptide could be calculated as the quotient of the amount of the oxidized peptide n and the oxidation yield Δi (i.e., n/Δi).

$$\frac{n2}{n1} = \frac{[M+14]}{[M+16]} \quad (1)$$

$$\frac{n3}{n1} = \frac{[M+32]}{[M+16]} \quad (2)$$

$$\frac{n4}{n1} = \frac{[R1W+14]}{[M+16]} \quad (3)$$

$$Q = 2n1F + 4n2F + 4n3F + 4n4F \quad (4)$$

$$n = n1 + n2 + n3 + n4 = \frac{Q}{2F} \times \frac{1 + ([M+14] + [M+32] + [R1W+14)/[M+16]}{1 + 2 \times ([M+14] + [M+32] + [R1W+14])/[M+16]} \quad (5)$$

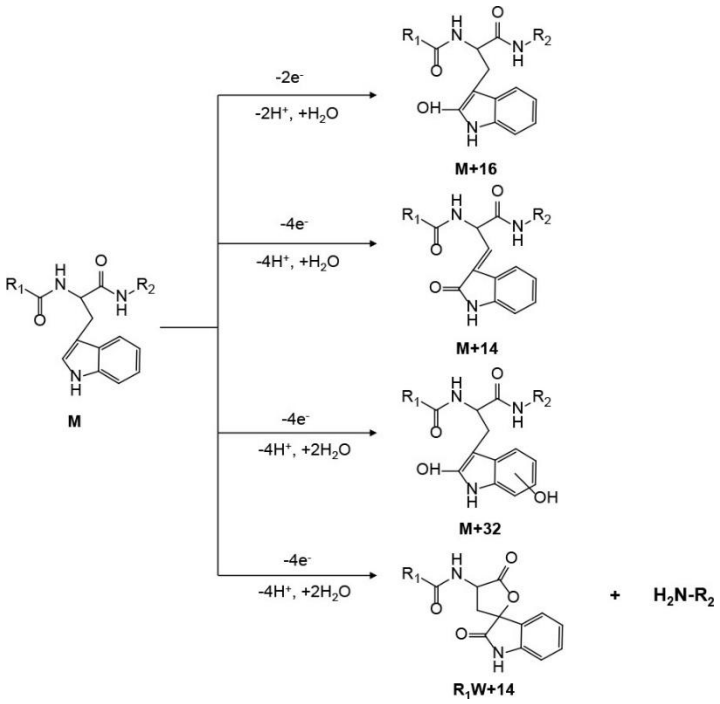

Scheme 3.2 Equation showing electrochemical oxidation of a trp-containing peptide[a]

[a] R_1 and R_2 denote the peptide N-terminal and C-terminal moieties, respectively.

To explore the feasibility of CMS peptide quantitation based on tryptophan oxidation, a tripeptide WGG was first tested. A blank solvent sample was first injected and no electric current peak was observed when the oxidation potential +1.00 V was applied

(Figure 3.3). In contrast, after the injection of WGG sample, a sharp electric current peak was observed under the same oxidation potential of +1.00 V (Figure 3.3f), indicating that the current peak observed in Figure 3.3f originated from electrochemical oxidation of WGG. Before electrolysis (Figure 3.3a), the protonated WGG was detected at *m/z* 319.14. After electrolysis (Figure 3.3b), the oxidation products WGG + 14, WGG + 16, and WGG + 32 were observed at *m/z* 333.12, 335.13, and 351.13, respectively. In particular, the ion intensities of M + 14 and M + 16 were much higher than the M + 32 (the ion intensities and intensity ratios are shown in Table 3.3). The integrated EIC peak area of *m/z* 319.14 shown in Figure 3.3d was smaller by 4.4% compared to the same peak in Figure 3.3c, suggesting that the oxidation yield for WGG was 4.4% (see detailed data in Table 3.3). On the basis of eq 5 using the integration of the current peak area (i.e., total electric charge Q, Figure 3.2f) as well as the intensity ratios of M + 14/ M + 16 and M + 32/M + 16, we calculate the oxidized amount of WGG to be 3.8 pmol. In combination of the oxidation yield 4.4%, the measured amount of WGG was 87.1 pmol. The average amount of a triplicate measurement was to be 87.1 pmol, which is quite close to the injection amount of 89.0 pmol with the measurement error of −2.1%.

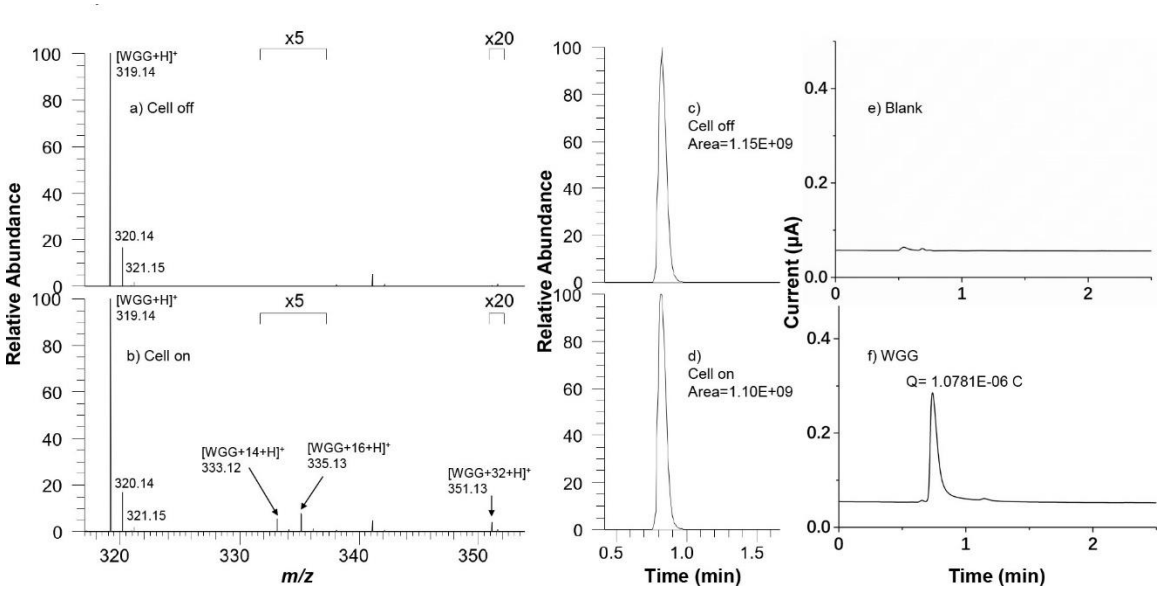

Figure 3.3 MS spectra of WGG (a) when the cell was off and (b) when the cell was turned on (applied potential: +1.00 V). The oxidation products of WGG were detected at *m/z* 333.12, 335.13, and 351.13. EICs of WGG were acquired (c) when the cell was off and (d) when the cell was turned on (applied potential: +1.00 V). Electric current diagrams were collected from (e) blank solvent and (f) the oxidation of WGG.

Table 3.3 Electric Current and MS Data for WGG.

	Q (A*s)	Amount of the oxidized analyte (mol)	Oxidation yield	Measured amount (mol)	Averaged amount (pmol)	Theoretical amount (pmol)	Measurement error
	1.0781E-06	3.8051E-12	0.043686438	8.7101E-11			
WGG	9.9626E-07	3.5435E-12	0.03959959	8.9482E-11	87.1	89.0	-2.1%
	1.0829E-06	3.8723E-12	0.045693375	8.4745E-11			

	EIC peak area of *m/z* 319.14 before electrolysis	EIC peak area of *m/z* 319.14 after electrolysis	Oxidation yield
	1148187168	1098026961	0.043686438
WGG	1147974939	1102515602	0.03959959
	1179430699	1125538530	0.045693375

Table 3.3 Electric Current and MS Data for WGG (Continued).

	Intensity for oxidized peptide ions			Intensity ratio	
	[M+14] *m/z* 333.12	[M+16] *m/z* 335.13	[M+32] *m/z* 351.13	[M+14]/[M+16] *m/z* 333.12 to *m/z* 335.13	[M+32]/[M+16] *m/z* 351.13 to *m/z* 335.13
	1.35E+06	1.81E+06	2.42E+05	0.75	0.13
WGG	1.27E+06	1.79E+06	2.35E+05	0.71	0.13
	1.45E+06	2.14E+06	2.94E+05	0.68	0.14

To confirm that the oxidized products M + 14, M + 16, and M + 32 were truly produced from electrochemical oxidation of tryptophan in the WGG as shown in Scheme 3.2, MS/MS analysis of *m/z* 319.14, 333.12, 335.13, and 351.13 were conducted. In this experiment, the WGG sample was directly injected into the electrochemical cell by a syringe pump for oxidation at +1.00 V potential. The resulted oxidation products and unoxidized peptide were analyzed using online EC/MS/MS. Collision-induced dissociation (CID) spectra of *m/z* 319.14, 333.12, 335.13, and 351.13 were recorded. As shown in Figure 3.4, upon CID, the unoxidized peptide ion (*m/z* 319.14) gave rise to fragment ion b2 (*m/z* 244.11, Figure 3.4a), while b2 + 14 (*m/z* 258.09, Figure 3.4b), b2 + 16 (*m/z* 260.10, Figure 3.4c), and b2 + 32 (*m/z* 276.10, Figure 3.4d) were observed for oxidation products WGG + 14, WGG + 16 and WGG + 32, respectively, in agreement with the fact that the observed m/z 333.12, 335.13, and 351.13 resulted from the oxidation of tryptophan residue in the peptide. Moreover, the b1 ion readily loses CO to form a1 ion (*m/z* 159.09) which was observed upon CID of the unoxidized peptide ion (*m/z* 319.14, Figure 3.4a). As shown in Figure 3.4b−d, the corresponding a1 ions were all observed from CID of WGG + 14, WGG + 16, and WGG + 32 ions with mass shift of +14, +16, and +32 Da, respectively, confirming that the oxidation occurred to the first tryptophan residue of WGG.

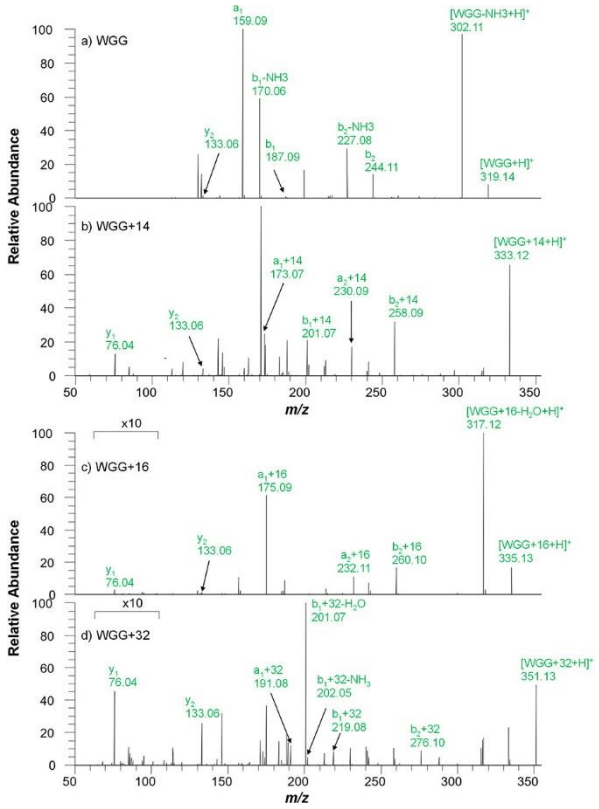

Figure 3.4 CID MS/MS spectra of (a) the unoxidized peptide ion $[WGG + H]^+$ (*m/z* 319.14), (b) the oxidized peptide ion $[WGG + 14 + H]^+$ (*m/z* 333.12), (c) [WGG + 16 + H]+ (*m/z* 335.13), and (d) $[WGG + 32 + H]^+$ (*m/z* 351.13).

WAGGDASGE, another Trp-containing peptide with nine amino acid residues, was also analyzed by the same approach. Without oxidation (Figure 3.5a), a +1 ion of WAGGDASGE was observed at *m/z* 849.34. As shown in Figure 3.5b, after electrolysis, the oxidation products at *m/z* 863.32 (M + 14 ion), *m/z* 865.33 (M + 16 ion) and *m/z* 881.33 (M + 32 ion) were observed. Based on EIC peak change for *m/z* 849.34 upon oxidation (Figure 3.5c,d), the oxidation yield for WAGGDASGE was measured as 19.0% (see detailed data in Table 3.4). Figure 3.5f shows the electric current peak from oxidation of WAGGDASGE (as a control, no oxidation current peak was observed in Figure 3.4e from solvent blank under the same oxidation potential). The amount of oxidized WAGGDASGE was calculated to be 11.1 pmol, on the basis of eq 5 using the integration of the current peak area (total electric charge Q) and the intensity ratios of *m/z* 863.32 and 881.33 to *m/z* 865.33. Therefore, the measured amount of WAGGDASGE was 58.4 pmol (Table 3.4). In

a triplicate measurement, the averaged quantity of this peptide measured by CMS was 57.7 pmol which is close to the initial amount of 60.4 pmol injected with a measurement error −4.5% (Table 3.4). WQPPRARI and RTRPLWVRME, another two peptides containing tryptophan either as the first residue or in the middle of the sequence, were also quantified using CMS. The measurement error was 4.3% (Table 3.5 and Figure 3.6) and −2.3% (Table 3.6 and Figure 3.7), respectively.

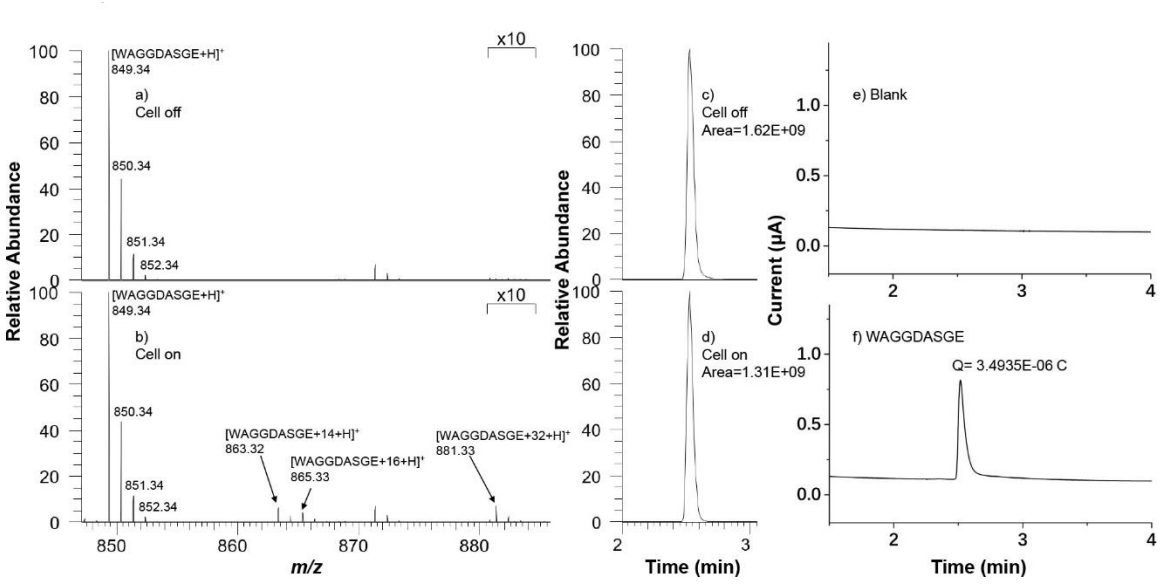

Figure 3.5 MS spectra of WAGGDASGE (a) when the cell was off and (b) when the cell was turned on (applied potential: + 1.00 V). The oxidation product of WAGGDASGE was detected at *m/z* 863.32, *m/z* 865.33 and *m/z* 881.33. EICs of WAGGDASGE were acquired (c) when the cell was off and (d) when the cell was turned on (applied potential: + 1.00 V). Electric current diagrams were collected from (e) blank solvent and (f) the oxidation of WAGGDASGE.

Table 3.4 Electric Current and MS Data for WAGGDASGE

	Q (A*s)	Amount of the oxidized analyte (mol)	Oxidation yield	Measured amount (mol)	Averaged amount (pmol)	Theoretical amount (pmol)	Measurement error
	3.4435E-06	1.0896E-11	0.18674237	5.8347E-11			
WAGGDASGE	3.3814E-06	1.0721E-11	0.18969197	5.6516E-11	57.7	60.4	-4.5%
	3.4935E-06	1.1109E-11	0.19037197	5.8356E-11			

Table 3.4 Electric Current and MS Data for WAGGDASGE (Continued)

	EIC peak area of *m/z* 849.34 before electrolysis	EIC peak area of *m/z* 849.34 after electrolysis	Oxidation yield
	1623125872	1320019500	0.18674237
WAGGDASGE	1619609558	1312382631	0.18969197
	1617508913	1309580555	0.19037197

	Intensity for oxidized peptide ions			Intensity ratio	
	[M+14] *m/z* 863.32	[M+16] *m/z* 865.33	[M+32] *m/z* 881.33	[M+14]/[M+16] *m/z* 863.32to *m/z* 865.33	[M+32]/[M+16] *m/z* 881.33 to *m/z* 865.33
	6.57E+06	4.06E+06	5.71E+05	1.62	0.14
WAGGDASGE	6.63E+06	4.19E+06	6.33E+05	1.58	0.15
	7.04E+06	4.58E+06	7.35E+05	1.54	0.16

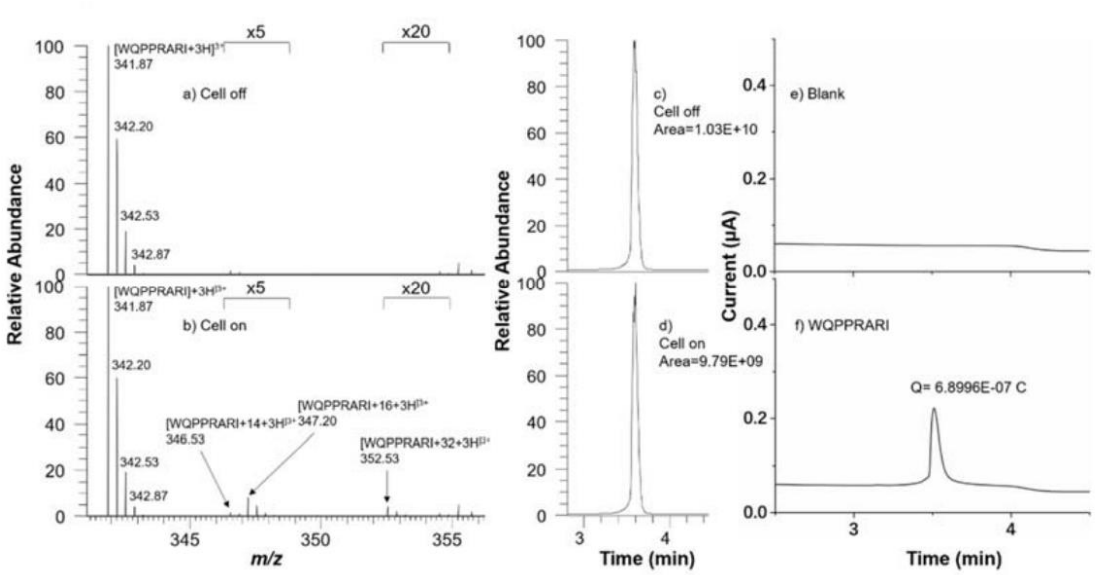

Figure 3.6 MS spectra of WQPPRARI (a) when the cell was off and (b) when the cell was turned on (applied potential: + 1.05 V). The oxidation product of WQPPRARI was detected at *m/z* 346.53, *m/z* 347.20 and *m/z* 352.53. EICs of WQPPRARI were acquired (c) when the cell was off and (d) when the cell was turned on (applied potential: + 1.05 V). Electric current diagrams were collected from (e) blank solvent and (f) the oxidation of WQPPRARI.

Table 3.5 Electric Current and MS data for WQPPRARI

	Q (A*s)	Amount of the oxidized analyte (mol)	Oxidation yield	Measured amount (mol)	Averaged amount (pmol)	Theoretical amount (pmol)	Measurement error
	6.5053E-07	2.7140E-12	0.043350531	6.2606E-11			
WQPPRARI	6.1197E-07	2.6148E-12	0.041609476	6.2842E-11	62.8	60.2	4.3%
	6.8996E-07	2.9278E-12	0.046601793	6.2826E-11			

	EIC peak area of *m/z* 341.87 before electrolysis	EIC peak area of *m/z* 341.87 after electrolysis	Oxidation yield
	10453112421	9999964452	0.043350531
WQPPRARI	10513938338	10076458872	0.041609476
	10272150196	9793449580	0.046601793

	Intensity for oxidized peptide ions			Intensity ratio	
	[M+14] *m/z* 346.53	[M+16] *m/z* 347.20	[M+32] *m/z* 352.53	[M+14]/[M+16] *m/z* 346.53 to *m/z* 347.20	[M+32]/[M+16] *m/z* 352.53 to *m/z* 347.20
	2.07E+06	1.02E+07	1.19E+06	0.20	0.12
WQPPRARI	1.75E+06	1.05E+07	1.08E+06	0.17	0.10
	1.84E+06	1.13E+07	1.37E+06	0.16	0.12

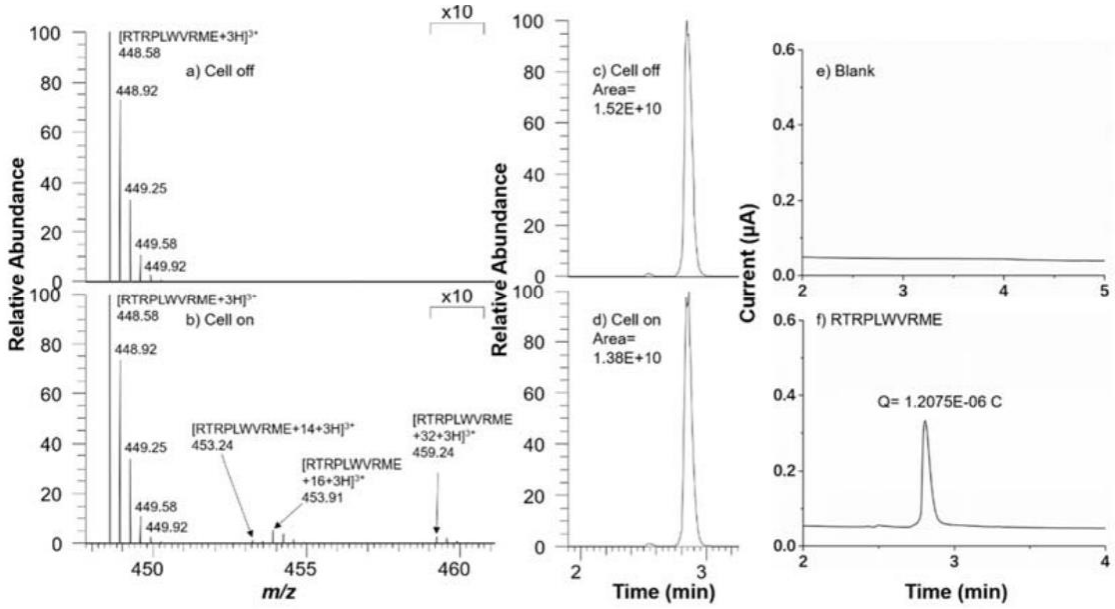

Figure 3.7 M S spectra of RTRPLWVRME (a) when the cell was off and (b) when the cell was turned on (applied potential: + 1.05 V). The oxidation product of RTRPLWVRME was detected at *m/z* 453.24, *m/z* 453.91, and *m/z* 459.24. EICs of RTRPLWVRME were acquired (c) when the cell was off and (d) when the cell was turned on (applied potential: + 1.05 V). Electric current diagrams were collected from (e) blank solvent and (f) the oxidation of RTRPLWVRME.

Table 3.6 Electric Current and MS Data for RTRPLWVRME

	Q (A*s)	Amount of the oxidized analyte (mol)	Oxidation yield	Measured amount (mol)	Averaged amount (pmol)	Theoretical amount (pmol)	Measurement error
	1.2266E-06	5.1279E-12	0.085896347	5.9698E-11			
RTRPLWVRME	1.2075E-06	5.0441E-12	0.090034863	5.6024E-11	58.7	60.1	-2.3%
	1.0879E-06	4.5555E-12	0.075631468	6.0232E-11			

	EIC peak area of *m/z* 448.58 before electrolysis	EIC peak area of *m/z* 448.58 after electrolysis	Oxidation yield
	15048679186	13756052614	0.085896347
RTRPLWVRME	15219502515	13849216696	0.090034863
	15366254043	14204081690	0.075631468

Table 3.6 Electric Current and MS Data for RTRPLWVRME (Continued)

	Intensity for oxidized peptide ions			Intensity ratio	
	[M+14] *m/z* 453.24	[M+16] *m/z* 453.91	[M+32] *m/z* 459.24	[M+14]/[M+16] *m/z* 453.24 to *m/z* 453.91	[M+32]/[M+16] *m/z* 459.24 to *m/z* 453.91
	1.34E+07	5.26E+07	3.15E+06	0.25	0.06
RTRPLWVRME	1.28E+07	4.89E+07	2.73E+06	0.26	0.06
	1.22E+07	4.77E+07	2.69E+06	0.25	0.06

In particular, upon electrochemical oxidation of another Trp-containing peptide KVPRNQDWL, besides M + 14, M + 16, and M + 32 products, the +3 ion of the cleavage product (KVPRNQDW+14, Figure 3.8b) with low intensity was observed at *m/z* 352.84. The oxidized amount of KVPRNQDWL was calculated as 5.9 pmol by eq 5 based on the integration of the current area (Figure 3.8f), and the intensity ratio of the oxidation products observed (Table 3.7). The integrated EIC peak area of unoxidized peptide ion at *m/z* 385.88 decreased by 9.6% after the cell was turned on, indicating the oxidation yield was 9.6%. Therefore, the total amount of KVPRNQDWL was measured to be 61.0 pmol. Triplicate measurements gave an averaged amount of KVPRNQDWL of 61.0 pmol, which is close to the injected amount of 60.1 pmol with a small quantitation error 1.5% (Table 3.7).

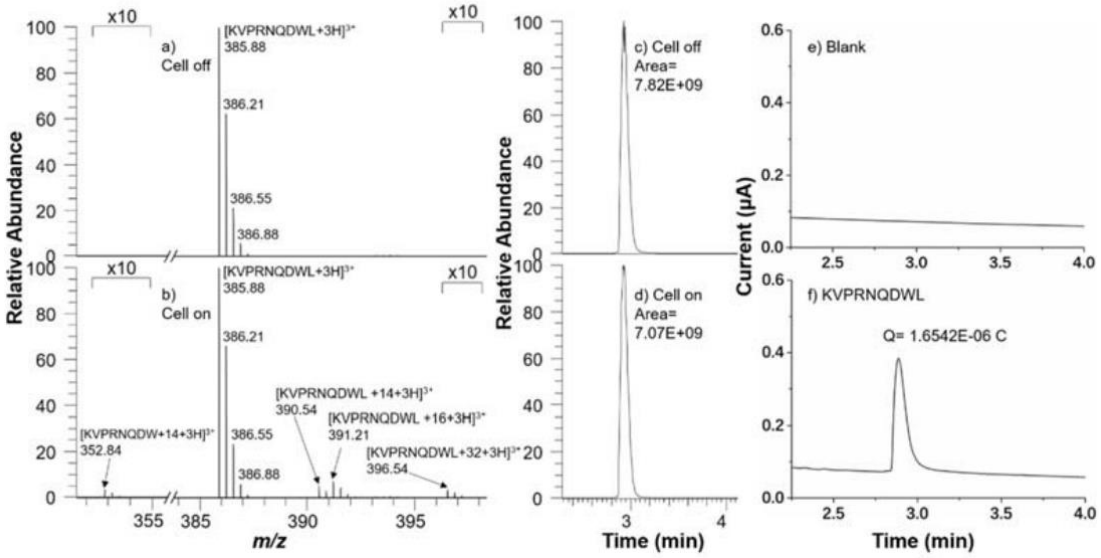

Figure 3.8 MS spectra of KVPRNQDWL (a) when the cell was off and (b) when the cell was turned on (applied potential: + 1.05 V). The oxidation product of KVPRNQDWL was detected at *m/z* 390.54, *m/z* 391.21, *m/z* 396.54 and *m/z* 352.84. EICs of KVPRNQDWL were acquired (c) when the cell was off and (d) when the cell was turned on (applied potential: + 1.05 V). Electric current diagrams were collected from (e) blank solvent and (f) the oxidation of KVPRNQDWL.

Table 3.7 Electric Current and MS Data for KVPRNQDWL

	Q (A*s)	Amount of the oxidized analyte (mol)	Oxidation yield	Measured amount (mol)	Averaged amount (pmol)	Theoretical amount (pmol)	Measurement error
	1.5797E-06	5.7446E-12	0.095801057	5.9964E-11			
KVPRNQDWL	1.5424E-06	5.5379E-12	0.088991616	6.2230E-11	61.0	60.1	1.5%
	1.6542E-06	5.8595E-12	0.096135336	6.0951E-11			

	EIC peak area of *m/z* 385.88 before electrolysis	EIC peak area of *m/z* 385.88 after electrolysis	Oxidation yield
	8280894952	7487576464	0.095801057
KVPRNQDWL	8413149270	7664449524	0.088991616
	7817957773	7066375778	0.096135336

Table 3.7 Electric Current and MS Data for KVPRNQDWL (Continued)

	Intensity for oxidized peptide ions				Intensity ratio		
	[M+14] *m/z* 390.54	[M+16] *m/z* 391.21	[M+32] *m/z* 396.54	[R_1W+14] *m/z* 352.84	[M+14]/[M+16] *m/z* 390.54 to *m/z* 391.21	[M+32]/[M+16] *m/z* 396.54 to *m/z* 391.21	[R_1W+14]/[M+16] *m/z* 352.84 to *m/z* 391.21
	2.34E+07	3.60E+07	1.55E+06	1.64E+06	0.65	0.04	0.05
KVPRNQDWL	2.58E+07	3.66E+07	1.58E+06	1.69E+06	0.71	0.04	0.05
	2.81E+07	3.76E+07	2.13E+06	2.15E+06	0.75	0.06	0.06

3.3.3 Absolute quantitation of cytochrome c by coulometric mass spectrometry

With the success in quantifying a series of Trp-containing peptides, we took a step further to use our CMS method for the absolute quantitation of proteins. Cytochrome c from equine heart (104 amino acids, sequence shown in Figure 3.9a) was chosen as a test sample. A surrogate peptide GITWK digested from cytochrome c was identified and quantified using CMS. Blank solvent was first injected and no current peak was observed when +1.00 V was applied (Figure 3.9f). In contrast, an electric current peak from oxidation of GITWK was observed under the same potential (Figure 3.9g). Before oxidation, the +2 ion of GITWK was observed at *m/z* 302.68. As shown in Figure 3.9b, after the cell was turned on, ions of the M + 14, M + 16, and M + 32 products as well as small amount of cleavage product GITW + 14 were observed at m/z 309.67, 310.67, 318.67, and 490.23, respectively (Figure 3.9c). The oxidation yield for GITWK was measured to be 9.8% (Table 3.8) by comparing the peak area of *m/z* 302.68 before and after oxidation. On the basis of Equation 5 using the integration of electric current peak area from peptide oxidation and product ion intensity ratios, the oxidized amount of GITWK was calculated as 5.3 pmol. Further, according to the oxidation yield, the total amount of GITWK was measured to be 53.4 pmol from a triplicate experiment (Table 3.8). On the basis of the assumption that stoichiometrically one protein molecule produces one peptide molecule in theory, the measured protein amount is therefore 53.4 pmol, which is also close to the amount of

protein of 60 pmol (−11.0% error, Table 3.8) for generating the 6 μL of the protein digest that was injected. The −11.0% measurement error might be from the sample loss caused by the tryptic digestion of proteins to peptides.20 To further check our measurement accuracy, the same diluted cytochrome c digest sample was also measured using traditional isotope dilution method with an isotope labeled peptide GITWK^ (labeled at lysine, $^{13}C6$, $^{15}N2$). The concentration of the diluted digest sample was quantified to be 8.6 μM (injection volume 6 μL, total amount of 51.6 pmol) based on the known amount of the isotope labeled peptide GITWK^ added and the intensity ratio of both peptides (the calibration curve obtained was shown in Figure 3.10). The difference of the measured amount of surrogate peptide GITWK from cytochrome c digest between CMS (53.4 pmol) and isotope dilution method (51.6 pmol) was only 3.5%, validating the feasibility of using CMS for protein absolute quantitation based on the oxidation of tryptophan residue.

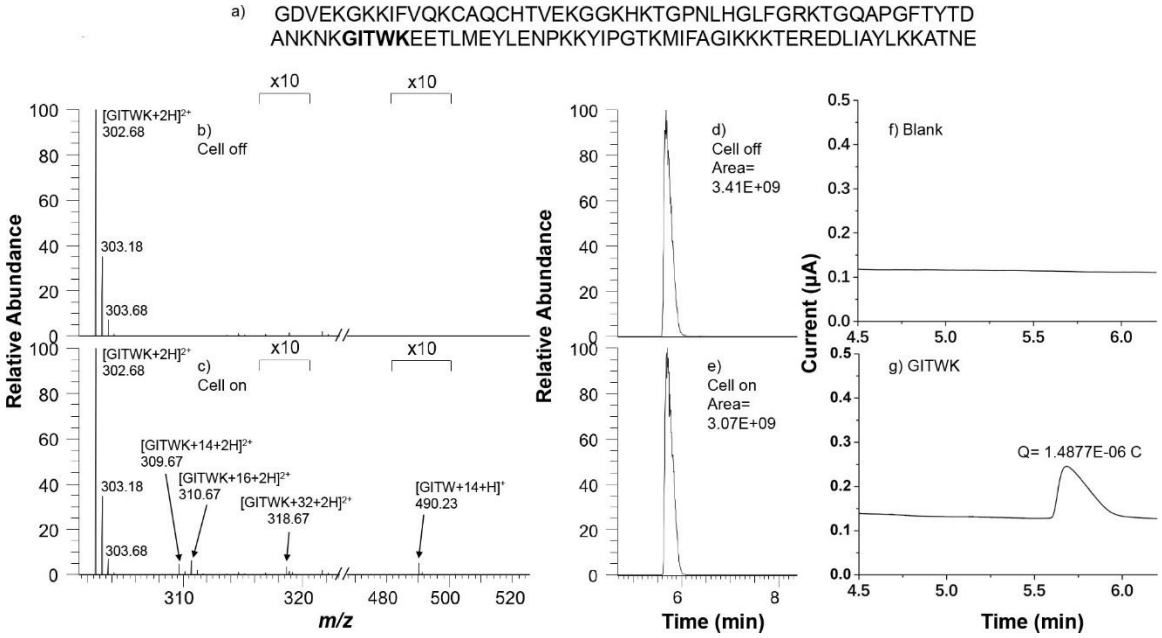

Figure 3.9 (a) Sequence of cytochrome c (the chosen surrogate peptide GITWK for CMS is highlighted in bold). MS spectra of GITWK from cytochrome c (b) when the cell was off and (c) when the cell was turned on (applied potential: +1.00 V). The oxidation product of GITWK was detected at *m/z* 309.67, m/z 310.67, *m/z* 318.67 and *m/z* 490.23. EICs of GITWK were acquired (d) when the cell was off and (e) when the cell was turned on (applied potential: + 1.00 V). Electric current diagrams were collected from (f) blank solvent and (g) the oxidation of GITWK.

Table 3.8 Electric Current and MS Data for Digested Cytochrome c (the Selected Surrogate Peptide: GITWK)

	Q (A*s)	Amount of the oxidized analyte (mol)	Oxidation yield	Measured amount (mol)	Averaged amount (pmol)	Theoretical amount (pmol)	Measurement error
	1.4787E-06	5.2261E-12	0.10205248	5.1210E-11			
GITWK	1.3725E-06	4.8861E-12	0.08889544	5.4965E-11	53.4	60	-11.0%
	1.4877E-06	5.3054E-12	0.09832663	5.3957E-11			

	EIC peak area of *m/z* 302.68 before electrolysis	EIC peak area of *m/z* 302.68 after electrolysis	Oxidation yield
	3391451913	3045345821	0.10205248
GITWK	3393338205	3091685904	0.08889544
	3406675603	3071708659	0.09832663

	Intensity for oxidized peptide ions				Intensity ratio		
	[M+14] *m/z* 309.67	[M+16] *m/z* 310.67	[M+32] *m/z* 318.67	[R_1W+14] *m/z* 490.23	[M+14]/[M+16] *m/z* 309.67 to *m/z* 310.67	[M+32]/[M+16] *m/z* 318.67 to *m/z* 310.67	[R_1W+14]/[M+16] *m/z* 490.23 to *m/z* 310.67
	5.76E+06	7.63E+06	4.06E+05	6.25E+05	0.76	0.05	0.06
GITWK	5.62E+06	7.80E+06	4.21E+05	6.07E+05	0.72	0.05	0.06
	5.47E+06	7.72E+06	4.47E+05	6.13E+05	0.71	0.06	0.06

*Note that GITWK+16 with +1 (at *m/z* 310.67) and +2 (at *m/z* 620.34) charge states were observed, while for the cleavage peptide fragment GITW+14, only single charge ion at *m/z* 490.23 was observed. The mole ratio of n4/n1 was calculated by using ratio of *m/z* 490.23 intensity to the sum of intensities of *m/z* 310.67 and *m/z* 620.34.

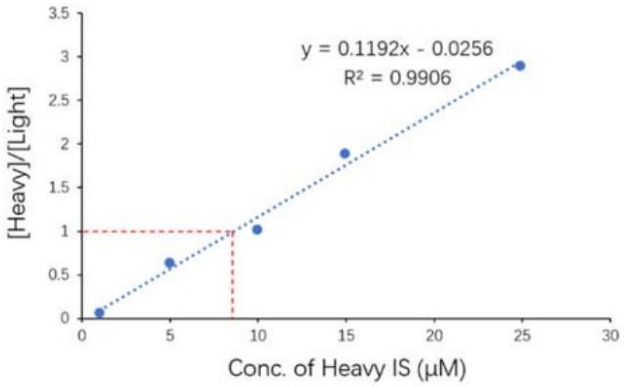

Figure 3.10 Calibration curve using isotope-labelled peptide GITWK^ as an internal standard for quantitation. (From the plot above, one can see that: when y=1, x=8.6 μM ($c_{[light]} = c_{[heavy]}$)).

In addition, in such an experiment of CMS quantitation of proteins, more than one surrogate peptide in protein digest could be quantified to obtain quantitation redundancy.20 For instance, in a separate trial, both GITWK and another tyrosinecontaining surrogate peptide TGQAPGFTYTDANK from the same cytochrome c digest were quantified together by CMS. Those two peptides were separated and quantified in the same LC/EC/MS run. The results showed that the GITWK and TGQAPGFTYTDANK were quantified to be 53.5 and 52.7 pmol by CMS (theoretical amount was 60.5 pmol based on the initial amount of cytochrome c used for digestion; data shown in Figure 3.11 and Table 3.9). The CMS quantitation results for two peptides agreed with each other well, with only 1.5% difference. This result demonstrates the feasibility of quantifying multipeptides in a single run and the reliability of CMS quantitation for a target protein based on different surrogate peptides.

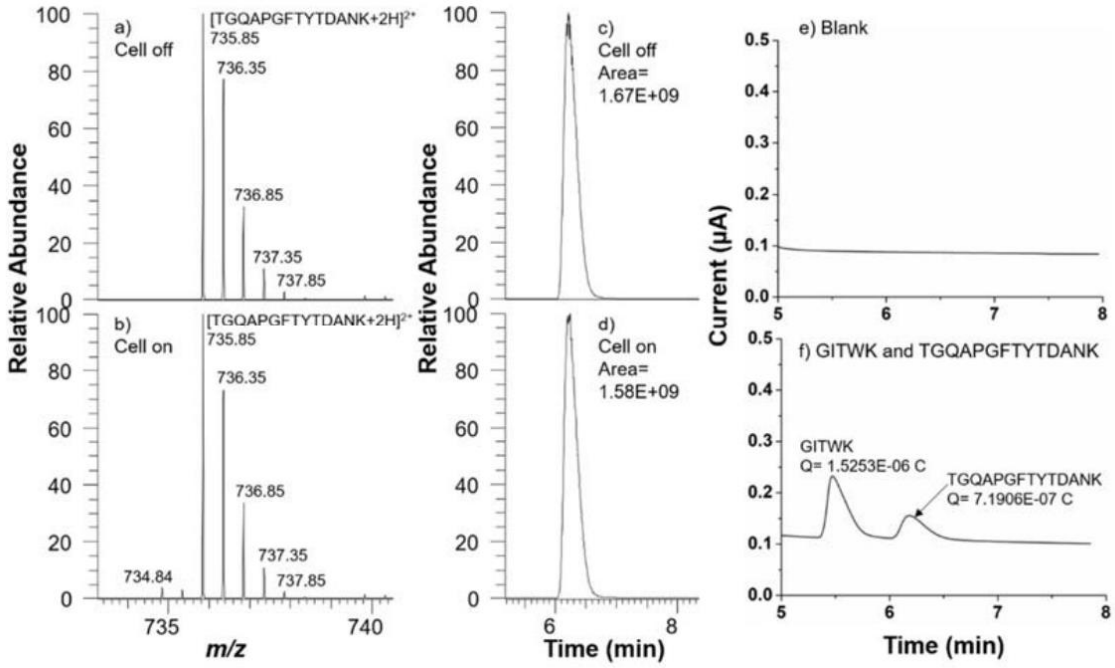

Figure 3.11 MS spectra of TGQAPGFTYTDANK (a) when the cell was off and (b) when the cell was turned on (applied potential: + 1.00 V). The oxidation product of TGQAPGFTYTDANK was detected at *m/z* 734.84. EICs of TGQAPGFTYTDANK were acquired (c) when the cell was off and (d) when the cell was turned on (applied potential: + 1.00 V). Electric current diagrams were collected from (e) blank solvent and (f) the oxidation of GITWK and TGQAPGFTYTDANK. MS spectra and EIC peaks of GITWK are not shown, as they are similar to what are seen in Figure 5. Note that in f, GITWK is shown to have a larger oxidation current than TGQAPGFTYTDANK.

Table 3.9 Electric Current and MS Data for Digested Cytochrome c (the Selected Surrogate Peptides are GITWK and TGQAPGFTYTDANK)

	Q (A*s)	Amount of the oxidized analyte (mol)	Oxidation yield	Measured amount (mol)	Averaged amount (pmol)	Theoretical amount (pmol)	Measurement error
	1.4764E-06	5.1702E-12	0.097637637	5.2953E-11			
GITWK	1.4668E-06	5.1473E-12	0.099652899	5.1652E-11	53.5	60.5	-11.6%
	1.5253E-06	5.3731E-12	0.096064883	5.5932E-11			

	EIC peak area of *m/z* 302.68 before electrolysis	EIC peak area of *m/z* 302.68 after electrolysis	Oxidation yield
	1153220362	1040622651	0.097637637
GITWK	1215324638	1094214014	0.099652899
	1268453129	1146599327	0.096064883

Table 3.9 Electric Current and MS Data for Digested Cytochrome c (the Selected Surrogate Peptides are GITWK and TGQAPGFTYTDANK) (Continued)

	Intensity for oxidized peptide ions				Intensity ratio		
	[M+14] *m/z* 309.67	[M+16] *m/z* 310.67	[M+32] *m/z* 318.67	[R_1W+14] *m/z* 490.23	[M+14]/[M+16] *m/z* 309.67 to *m/z* 310.67	[M+32]/[M+16] *m/z* 318.67 to *m/z* 310.67	[R_1W+14]/[M+16] *m/z* 490.23 to *m/z* 310.67
	2.29E+06	2.87E+06	1.67E+05	3.67E+05	0.80	0.06	0.07
GITWK	2.35E+06	2.99E+06	1.83E+05	3.52E+05	0.79	0.06	0.06
	2.33E+06	3.03E+06	1.79E+05	3.40E+05	0.77	0.06	0.06

	Q (A*s)	Amount of the oxidized analyte (mol)	Oxidation yield	Measured amount (mol)	Averaged amount (pmol)	Theoretical amount (pmol)	Measurement error
	7.4682E-07	3.8695E-12	0.078279445	4.9432E-11			
TGQAPGFTYTDANK	7.2707E-07	3.7672E-12	0.068433341	5.5049E-11	52.7	60.5	-12.9%
	7.1906E-07	3.7257E-12	0.069321312	5.3745E-11			

	EIC peak area of *m/z* 735.85 before electrolysis	EIC peak area of *m/z* 735.85 after electrolysis	Corrected EIC peak area* of *m/z* 735.85	Oxidation yield
	1588782909	1486018480	1464413865	0.078279445
TGQAPGFTYTDANK	1636891250	1546511840	1524873314	0.068433341
	1670190590	1575197527	1554410787	0.069321312

*Note that, after oxidation, the third isotopic peak of the oxidized peptide ion at *m/z* 734.84 overlaps with the peak of the remaining intact peptide ion at *m/z* 735.85 (Figure 3.11). The contribution to the EIC peak area of *m/z* 735.85 after oxidation from the third isotopic peak of *m/z* 734.84 was calculated, based on the EIC peak area of *m/z* 734.84 and α that is the theoretical ratio of the third isotopic peak and the first isotopic peak of *m/z* 735.85. Approximately, α equals to the ratio of the third isotopic peak and the first isotopic peak of *m/z* 735.85 before oxidation (that is 0.33). Thus, the corrected EIC peak area of *m/z* 735.85 after oxidation = EIC peak area of *m/z* 735.85 after oxidation- α × EIC peak area of *m/z* 734.84 after oxidation.

From the results shown above, one can see that the quantitation error between our measured and theoretical values is only −4.5% to +4.3% (Table 3.10). It clearly shows that CMS can be applicable for quantifying Trp-containing peptides and our assumption used for the calculation (Equations 1−3) is valid, although the oxidation undergoes multiple

pathways (Scheme 3.2). Indeed, M + 14 and M + 32 are structurally similar to M + 16, and the only differences among these products are from the substituents in the tryptophan side chains. The cleavage product is shorter than the product M + 16, and their ionization efficiency could have some differences so that the calculation of n4 used intensity ratios could have some errors. However, the detectable cleavage product was only observed in the oxidation of two peptides in our experiments and the cleavage product ion intensity were quite small in comparison to the sum of all other products (the ratio of the former to the latter is less than 3.4%). Thus, the measurement error of the oxidized peptide amount n from the estimated calculation of n4 should be very small. This explains why all the Trp-containing peptides were measured by CMS with good accuracy.

Table 3.10 Tist of Tryptophan-Containing Peptides Quantified by CMS in this Work

#	Name	Peptide sequence	Molecular weight (Da)	Measured amount (pmol)	Theoretical amount (pmol)	Quantitation measurement error
1	L-Tryptophylglycylglycine	WGG	318.3	87.1	89.0	-2.1%
2	Fibronectin adhesion-promoting peptide	WQPPRARI	1023.2	62.8	60.2	4.3%
3	gp 100 (25-33) human	KVPRNQDWL	1155.3	61.0	60.1	1.5%
4	BDC2.5 Mimotope	RTRPLWVRME	1343.6	58.7	60.1	-2.3%
5	Delta sleep inducing peptide	WAGGDASGE	848.8	57.7	60.4	-4.5%

The sensitivity of CMS based on the tryptophan oxidation was also evaluated by testing a series of low concentrations of peptide WGG ranging from 0.025 to 0.05 to 0.1 μM (3 μL injection volume). The quantitation results are shown in Table S10.A3 μL sample of 0.025 μM WGG (injection amount 75 fmol) was injected into LC/EC/MS for quantitation, and the measured peptide quantity was 74.1 fmol on average (−1.2% quantitation error, see detailed results in Table 3.11), suggesting a high quantitation sensitivity and accuracy. Indeed, in comparison to the CMS quantitation of Y-containing

peptides where 300 fmol of DRVY was successfully quantified,[115] the quantitation sensitivity of using W-containing peptide is improved, under a similar experimental condition. This is in line with our expectation mentioned before, based on our observation that W-containing peptide often provides a relatively high oxidation current upon oxidation. Besides, the peak width at half height of EIC peaks and their corresponding EC peaks for peptides studied are compared (Table 3.12). A slight peak broadening was observed EIC peaks, which might be caused by the extra dead volumes of the electrochemical flow cell and the connection tubing between EC and MS.

Table 3.11 Electric Current and MS Data for Sensitivity Evaluation of CMS Using WGG

	Q (A*s)	Amount of the oxidized analyte (mol)	Oxidation yield	Measured amount (mol)	Averaged amount (pmol)	Theoretical amount (pmol)	Measurement error
WGG 0.1 μM,3 μL	4.3892E-08	1.43057E-13	0.485322819	2.9477E-13	295.7	300	-1.4%
	4.5478E-08	1.48515E-13	0.487016882	3.0495E-13			
	3.9083E-08	1.2788E-13	0.44485814	2.8746E-13			
WGG 0.05 μM, 3 μL	2.2456E-08	7.3462E-14	0.470054906	1.5628E-13	156.7	150	4.5%
	2.3326E-08	7.6805E-14	0.490119304	1.5671E-13			
	2.2501E-08	7.4833E-14	0.476551469	1.5703E-13			
WGG 0.025 μM, 3 μL	1.1137E-08	3.6644E-14	0.50396206	7.2711E-14	74.1	75	-1.2%
	1.1592E-08	3.8232E-14	0.493502788	7.7470E-14			
	1.0557E-08	3.4705E-14	0.480551755	7.2220E-14			

Table 3.11 Electric Current and MS Data for Sensitivity Evaluation of CMS Using WGG (Continued).

	EIC peak area of *m/z* 319.14 before electrolysis	EIC peak area of *m/z* 319.14 after electrolysis	Oxidation yield
WGG 0.1μM, 3 μL	6547238	3369714	0.485322819
	6584127	3377546	0.487016882
	6173350	3427085	0.44485814
WGG 0.05 μM, 3 μL	3699070	1960304	0.470054906
	3837837	1956839	0.490119304
	3701959	1937785	0.476551469
WGG 0.025 μM, 3 μL	1969430	976912	0.50396206
	1955762	990588	0.493502788
	1926652	1000796	0.480551755

	Intensity for oxidized peptide ions			Intensity ratio	
	[M+14] *m/z* 333.12	[M+16] *m/z* 335.13	[M+32] *m/z* 351.13	[M+14]/[M+16] *m/z* 333.12 to *m/z* 335.13	[M+32]/[M+16] *m/z* 351.13 to *m/z* 335.13
WGG 0.1μM, 3 μL	6.10E+04	4.90E+04	9.43E+03	1.24	0.19
	7.34E+04	5.99E+04	1.16E+04	1.23	0.19
	5.86E+04	4.89E+04	9.92E+03	1.20	0.20
WGG 0.05 μM, 3 μL	4.08E+04	3.48E+04	8.02E+03	1.17	0.23
	4.15E+04	3.75E+04	9.02E+03	1.10	0.24
	3.95E+04	3.82E+04	8.66E+03	1.04	0.23
WGG 0.025 μM, 3 μL	1.51E+04	1.32E+04	2.74E+03	1.14	0.21
	1.49E+04	1.34E+04	2.95E+03	1.11	0.22
	1.56E+04	1.38E+04	3.16E+03	1.13	0.23

Table 3.12 Peak Width at Half Height of EIC and EC Peaks of Peptides Studied

#	Peptide sequence	Peak width at half height (EIC peak) min	Peak width at half height (EC peak) min
1	Aβ1-16	0.074	0.070
2	Aβ1-18	0.079	0.050
3	WGG	0.063	0.060
4	WQPPRARI	0.073	0.063
5	WAGGDASGE	0.056	0.053
6	KVPRNQDWL	0.095	0.078
7	RTRPLWVRME	0.072	0.06
8	GITWK	0.203	0.185

3.4. Conclusions

In this study, we demonstrated the viability of using CMS for the absolute quantitation of very long peptides such as Aβ peptide fragments (Aβ1−16 and Aβ1−28) based on the tyrosine oxidation. Moreover, to further extend the application of our method in peptides and protein quantitation, we also extended the CMS absolute quantitation to tryptophan-containing peptides. Good quantitation accuracy and sensitivity were achieved. Furthermore, absolute quantitation of protein (using cytochrome c as an example) was also demonstrated and confirmed with traditional isotope dilution method. One striking strength of our method is that there is no need for isotope-labeled internal standard and calibration curve which is routinely used in MS-based absolute quantitation, showing the advantage of cost and time efficiency for CMS. Since CMS has been shown to be capable of quantifying either peptides or proteins containing either tryptophan, tyrosine, or cysteine residues, it would have a good application potential in quantitative proteomics. To realize the application of CMS in the real proteomics world, reducing the current setup from micro scale to nanoscale (i.e., nanoLC and nanoESI) would be necessary. Such an experiment is underway.

CHAPTER 4

ABSOLUTE QUANTITATION OF DEAMIDATED PEPTIDES AND HOST CELL PROTEINS BY COULOMETRIC MASS SPECTROMETRY WITHOUT USING STANDARDS

A version of this work has been published in the *Analytical Chemistry* as the article: Ai, Y.; Gunawardena, H. P.; Li, X.; Kim, Y.-I.; Dewald, H. D.; Chen, H., Standard-Free Absolute Quantitation of Antibody Deamidation Degradation and Host Cell Proteins by Coulometric Mass Spectrometry. *Analytical Chemistry* **2022,** *94* (36), 12490-12499.

4.1 Introduction

Mass spectrometry (MS)-based quantitative measurement of protein abundance plays a significant role in both biomedical and clinical fields.[202-204] Elegant MS quantitation strategies such as stable isotope labeling with Stable isotope labeling using amino acids in cell culture (SILAC), Isotope Coded Affinity Tags (ICAT), Isobaric tags for relative and absolute quantitation (iTRAQ), Tandem mass tags (TMT), and label-free approaches provide information on relative alteration of protein abundance in a proteome-wide scale.[55, 68, 205-207] However, absolute quantitation of protein concentration in biological samples is crucial for clinical and pharmaceutical applications.[76, 208] In this regard, isotope dilution mass spectrometry (IDMS) is the most widely used approach with high accuracy to determine the absolute quantity of a protein in a complex mixture.[79] However, it is only applicable to quantify a limited number of proteins at a time due to the high cost and complexity of sample preparation. Label-free absolute quantitation methods[209, 210] allow a large number of proteins to be quantified at the proteome scale, but the accuracy compromises significantly due to the varied ionization efficiencies among peptides.[210] Thus, the development of methods for accurate peptide and protein quantitation without the use of isotope labeled standards is largely in need.

In recent years, protein-based pharmaceuticals (or biopharmaceuticals) such as therapeutic monoclonal antibodies (mAbs) have become increasingly important for disease

treatment. Therefore, to ensure patient safety, it is crucial to conduct impurity analysis and structural characterization of biopharmaceuticals for product reliability and consistency across the entire product life cycle. Host cell proteins (HCPs) are a major class of impurities derived from biotherapeutics production processes. HCPs that remain in the final drug product, especially for those degrading or immunogenic proteins, such as cathepsin D15 or phospholipase B like 2 (PLBL2),[211] have been shown to affect product quality and patient safety due to the immune response. The current standard approach to quantify HCPs is based on enzyme linked immunosorbent assay,[212, 213] which has a drawback in its detection selectivity. One recent example is the delayed Sanofi recombinant protein vaccine (prefusion S protein and preS dTM) against SARS-CoV-2.[214] A key polyclonal antibody reagent used to detect the SARS-CoV-2 preS protein was found to also recognize glycosylated HCPs, resulting in the significantly overestimated concentration (approximately four to six times) of preS protein in the formulated vaccine product. MS is emerging as an alternative way to characterize HCP contents,[215-217] but the existing MS methods might be hard to implement since either peptide or protein internal standards are needed for HCP quantitation, which takes time to synthesize. To satisfy the desire of tracking HCPs and their clearance within days of discovery, especially in a pandemic situation like COVID-19, it is urgent to offer a rapid quantitation method for high-risk HCPs, without the need of using standards, for timely process optimization and risk assessment.

In terms of characterization of biopharmaceuticals, another challenge is quantitative analysis of various (bio)chemical modifications of mAbs such as glycosylation, deamidation, and oxidation[154] since these modifications could change the therapeutics bioactivity and potentially cause immunogenicity.[148] Asparagine (Asn) deamidation is one of the main chemical modifications of interest for mAbs and is formed

via a succinimide (Asu) intermediate that can be subsequently hydrolyzed to aspartic acid (Asp) or iso-aspartic acid (isoAsp, Scheme 4.1), which is sensitive to environmental changes (e.g., temperature and pH) during the manufacturing process or long-term storage.[218, 219] In addition, deamidation of proteins such as many long-lived and disease-related proteins (e.g., β-amyloid protein and crystalline) as a spontaneous non-enzymatic process in vivo has been widely studied in human degenerative diseases and natural aging.[220, 221] LC/MS is commonly used for the relative quantitation of deamidation level based on the peak intensity or area ratio of the native and deamidated peptides. Absolute quantitation of deamidation is rare and only one study[222] used isotope-labeled synthetic peptide standards for quantifying native and deamidated peptides. However, absolute quantitation of the succinimide intermediate has never been done before due to lack of standards.

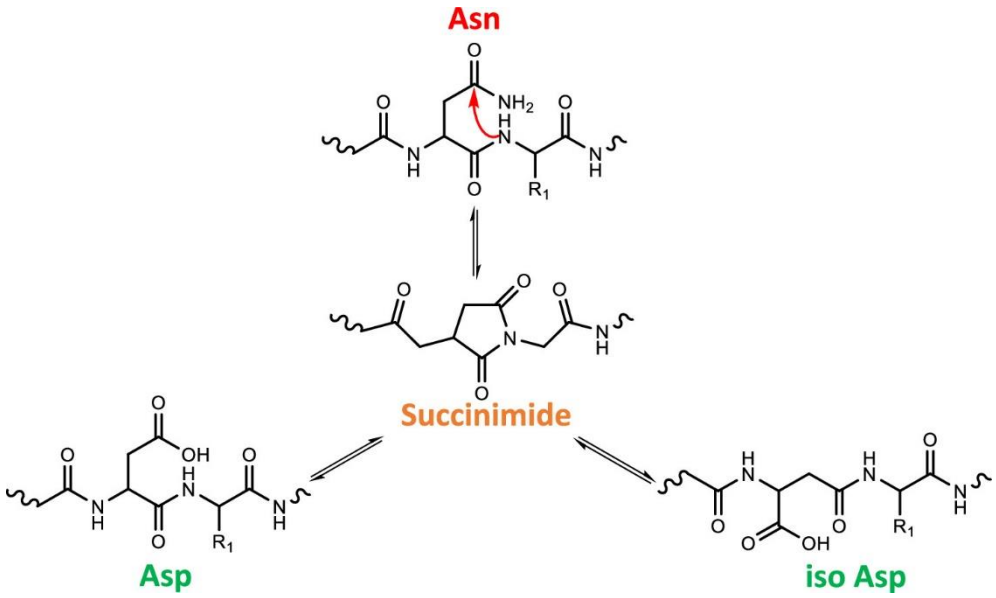

Scheme 4.1 Mechanism of asparagine deamidation to aspartic acids via a succinimide intermediate.

Recently, our laboratory developed coulometric mass spectrometry (CMS) for absolute quantitation of small organic molecules, peptides, and large protein molecules without the need of using standards or calibration curves.[109, 114, 115, 189, 223, 224] As illustrated

in Scheme 4.2, an electrochemically active peptide (e.g., those containing either tyrosine or tryptophan residue) is subjected to LC separation, electrochemical oxidation, and MS detection. Upon electrochemical oxidation, electron transfer occurs, resulting in an electrical current peak that can be integrated over time to obtain the total charge Q. According to Faraday's law, Q is proportional to the quantity of the oxidized peptide: $Q = nzF$, where n denotes the moles of the oxidized peptide, z is the number of electrons transferred per peptide, and F is the Faraday constant of 96,500 C/mol. Furthermore, the peptide oxidation yield Δi can be determined by measuring the relative change of the peptide extracted ion chromatogram (EIC) peak area upon electrolysis. Thus, the total amount of the peptide can be calculated as $n/(\Delta i) = Q/(zF\Delta i)$. As the protein can be enzymatically digested into peptides and the amount of peptide can reflect the quantity of its precursor protein, our CMS can also be used for absolute quantitation of proteins. However, previously, CMS was only used for the quantitation of single protein including mAb.[122, 223] This study explored CMS for multi-protein quantitation in one mixture sample in the same run and demonstrated the potential of CMS for absolute quantitation of low-abundant HCP in the presence of high-abundant NIST mAb 8671, without using standards. In addition, by using CMS, this study presents simultaneous quantitation of native and deamidated peptides as well as the succinimide intermediate from deamidation of Asn 318 residue of NIST 8671 mAb, for the first time.

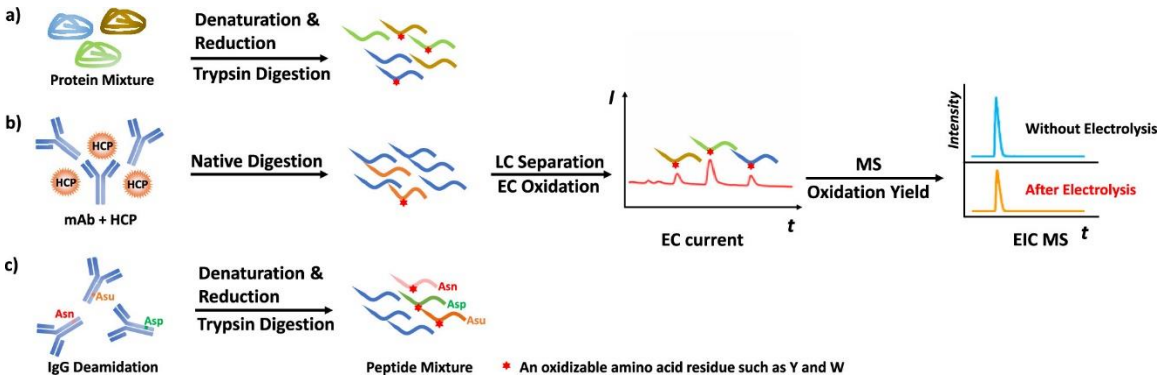

Scheme 4.2 Workflows showing absolute quantitation for (a) multiple proteins in a protein mixture, (b) HCPs in mab, and (c) mAb deamidation by CMS.

4.2 Experimental

4.2.1 Reagents and materials

β-Lactoglobulin B from bovine milk, α-lactalbumin from bovine milk and carbonic anhydrase from bovine erythrocytes were bought from Sigma-Aldrich (St. Louis, MO). Phospholipase B-like 2 protein (PLBL2, CHO-S–Purified) was purchased from Immunology Consultants Laboratory (Portland, OR). NIST monoclonal antibody reference material 8671 (NIST mAb, humanized IgG1k monoclonal antibody) was obtained from the National Institute of Standards and Technology (NIST, Gaithersburg, MD). Stable isotope-labeled peptide standards, VLVLDTDYK^ (labeled at lysine, ^{13}C6, ^{15}N2), DGPLTGTYR^ (labeled at arginine, ^{13}C6, ^{15}N4), LDQWLCEK^ (labeled at lysine, ^{13}C6, ^{15}N2), SFGWDLAK^ (labeled at lysine, ^{13}C6, ^{15}N2), and NPALWK^ (labeled at lysine, ^{13}C6, ^{15}N2) were purchased from Vivitide (Gardner, MA). Trypsin (sequencing grade), urea (electrophoresis grade), difluoroacetic acid (LC-MS grade), ammonium bicarbonate (bioultra grade), dithiothreitol (DTT, bioultra grade), and iodoacetamide (IAM, bioultra grade) were all bought from Sigma-Aldrich (St. Louis, MO). Acetonitrile (ACN, HPLC grade) and formic acid (HPLC grade) were bought from Fisher Scientific (Fair

Lawn, NJ). A Millipore Direct-Q5 purification system (Burlington, MA) was used to obtain purified water for sample preparation.

4.2.2 Apparatus

Our CMS experimental setup (Scheme 4.3) consisted of an ultra-performance liquid chromatography (UPLC, Waters, Milford, MA) coupled with an electrochemical thin-layer flow cell (BASi, West Lafayette, IN; cell dead volume: ca. 1 μL) and a highresolution Orbitrap Q Exactive mass spectrometer (Thermo Scientific, San Jose, CA). The electrochemical cell was equipped with either a glassy carbon disc (i.d. 3 mm) or a homemade boron-doped diamond (BDD) electrode (i.d. 8 mm) as the working electrode (WE). A Ag/AgCl (3 M NaCl) electrode was used as the reference electrode, and the cell stainless steel body served as the counter electrode. The glassy carbon WE was polished with alumina slurry, followed by rinsing with water before and after use. Pulse mode cleaning was applied for re-activation of BDD electrode between runs.

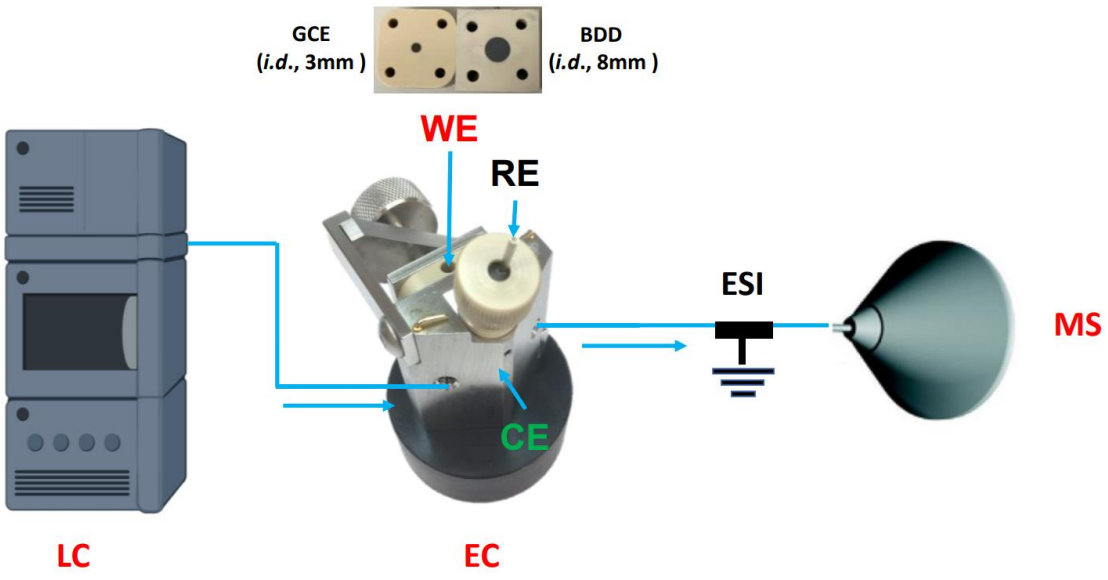

Scheme 4.3 Schematic drawing of the LC/EC/MS setup for CMS absolute quantitation of proteins.

A Waters reversed-phase column (BEH C18, 2.1 mm × 50 mm, 1.7 μm, Waters, Milford, MA) or an Agilent poroshell reversed-phase column (HPH−C18, 2.1 mm × 100 mm, 1.9 μm, Agilent, Santa Clara, CA) was used for peptide separation. A potential of +1.05 V (vs Ag/AgCl) was applied to the WE to trigger peptide oxidation. An Epsilon Eclipse potentiostat (BASi, West Lafayette, IN) was used to monitor and record the oxidation current. OriginPro 2018b was used to import and integrate the electric current peak to calculate the total electric charge of Q. Peptides flowing out of an electrochemical flow cell were online ionized by a heated electrospray ionization source with the following parameters: sheath gas flow rate, 35; auxiliary gas flow rate, 10; spray voltage, 4.0 kV; sweep gas flow rate, 0; capillary temperature, 300 °C; auxiliary gas heater temperature, 100 °C; and S-lens RF level, 50. Mass spectra were acquired by a Thermo Xcalibur (3.0.63).

4.2.3 Digestion of protein mixture

For CMS analysis of a protein mixture sample, 400 μL of a protein mixture containing *β*-lactoglobulin B (16.1 μM), α-lactalbumin (16.2 μM), and carbonic anhydrase (16.3 μM) in 50 mM ammonium bicarbonate (NH_4HCO_3, pH 8.0) were first denatured with 8 M urea, followed by dithiothreitol (DTT, 5 mM) reduction at 37 °C for 1 h and alkylation by iodoacetamide (IAM, 10 mM) at room temperature in the dark for 30 min. Then, DTT was added again to quench extra amount of IAM. The sample was subsequently desalted with Amicon Ultra-0.5, 3 kDa filters (Millipore Sigma). The desalted protein mixture was further diluted with 50 mM ammonium bicarbonate to 200 μL. Trypsin (20 μL, 0.5 μg/ μL) was added into 100 μL of desalted protein mixture sample (protein: enzyme = 20:1, w/w), incubated at 37 °C overnight, and quenched by formic acid. The digested protein mixture

sample was diluted with 0.1% formic acid to the final concentration of β-lactoglobulin B (3.49 μM), α-lactalbumin (3.51 μM), and carbonic anhydrase (3.52 μM) for CMS analysis.

4.2.4 LC elution gradient for the protein mixture sample

For LC/EC/MS analysis of the digested protein mixture sample containing β-lactoglobulin B (3.49 μM), α-lactalbumin (3.51 μM) and carbonic anhydrase (3.52 μM), the mobile phase flow rate was 200 μL/min. The mobile phase consisted of 0.1% formic acid in water (A) and 0.1% formic acid in ACN (B). The gradient used with (BEH C18, 2.1 mm × 50 mm, 1.7 μm) column was as follows: 0-2 min, increased from 5% to 8% B; 2-14 min, linear ramp from 8% to 11% B; 14-15 min, fast ramp from 11% to 12% B; 15-29 min, reached to 15% B; 29-10 min, climbed to 80% B and remained at 80% for 3 min before returned to 5% B. The injection volume was 3 μL per analysis. The BASi electrochemical cell was equipped with a 3 mm ID glassy carbon WE for peptide electrochemical oxidation.

4.2.5 Native digestion of spiked PLBL2

For CMS analysis of PLBL2 in mAb, 1 mg of NIST mAb (reference material 8671) in 200 μL of 100 mM ammonium bicarbonate was spiked with 5 μL of 0.1 or 1 μg/μL PLBL2 (mAb/PLBL2 = 2000:1 or 200:1 by weight). The sample was treated with 20 μL of 0.5 μg/μL trypsin at 37 °C overnight for native digestion.37 The digest was heated at 90 °C for 10 min and then centrifuged at 20000 g for 10 min to remove undigested mAb. The supernatant was vacuum-dried and reconstituted in 30 μL of H_2O/ACN:FA (95:5:0.1, v/v) for mAb/PLBL2 = 2000:1 sample or in 60 μL of H_2O/ACN:FA (95:5:0.1, v/v) for mAb/PLBL2 = 200:1 sample, prior to CMS analysis.

4.2.6 LC gradient for digested mAb spiked with PLBL2

For LC/EC/MS analysis of the native digest of mAb spiked with PLBL2, the reconstituted tryptic peptides were directly injected onto the Poroshell HPH-C18 column (2.1 mm × 100

mm, 1.9 μm) at a volume of 5 μL. Separation was performed using mobile phase A consisting of 0.1% formic acid in water and mobile phase B consisting of 0.1% formic acid in acetonitrile with a flow rate at 200 μL/min. The gradient condition was as follows: 0-15 min, increased from 5% to 13% B; 15-17 min, linear ramp from 13% to 15% B; 19-20 min, fast ramp from 15% to 85% B and remained at 85% for 5 min before returned to 5% B. The theoretical injection concentration of the spiked PLBL2 was 1.26 μM and 0.25 μM for 200:1 and 2000:1 (mAb:PLBL2) native digests, respectively. The BASi electrochemical cell was equipped with a homemade BDD electrode (i.d. 8 mm) for peptide electrochemical oxidation.

4.2.7 Digestion of NIST mAb

For deamidation quantitation, 20 μL of NIST mAb (10 mg/ mL) was added to 180 μL of 50 mM ammonium bicarbonate pH 8.1) containing 9 M urea. The denatured mAb was reduced by DTT (20 mM) at 37 °C for 1 h and alkylated by IAM (40 mM) at room temperature in the dark for 30 min. DTT was added again to quench extra amount of IAM. The sample was desalted and buffer-exchanged by Amicon Ultra 0.5, 10 kDa filters (Millipore Sigma) with 50 mM ammonium bicarbonate buffer. Then, 5 μL of trypsin (0.5 μg/μL) was added to 150 μL of the antibody sample solution for digestion at 37 °C for 4 h. After that, 20 μL of trypsin (0.5 μg/μL) was added again to the sample solution and incubated at 37 °C overnight. The digestion was quenched by adding formic acid to 1% (v/v) (mAb concentration 1.13 μg/μL). The digested mAb was further diluted with 0.1% formic acid to 0.38 μg/μL before CMS analysis. Detailed LC separation conditions for the samples mentioned above can be found in the Supporting Information.

4.2.8 LC gradient for NIST mAb N318 deamidation products

For LC/EC/MS analysis of NIST mAb N318 deamidation products, the mobile phase flow rate was kept at 200 μL/min. Mobile phase A was 0.1% DFA in water and mobile phase B was 0.1% DFA in acetonitrile. The gradient used with the Poroshell HPH-C18 column (2.1 mm × 100 mm, 1.9 μm) was 0−1 min, 5−10% solvent B; 1-2min, 10-25% solvent B; 2-18 min, 25-27% solvent B; 18−21 min, 27−33% solvent B; 21−22 min, 33−85% solvent B; 22−26 min, 85% solvent B; 27−30 min, 5% solvent B. The injection concentration of NIST mAb was 0.38 μg/μL. The injection volume was 5 μL per analysis. The BASi electrochemical cell was equipped with a homemade BDD electrode (i.d. 8 mm) for peptide electrochemical oxidation.

4.2.9 Protein expression and purification of Kai C

For KaiC expression and purification, the protein was purified by following the previously published protocol with minor modifications.[225, 226] Basically, the open reading frame of KaiC from *Synechococcus elongatus* was inserted into the protein expression vector pET-41a using NcoI and HindIII cloning sites. *Escherichia coli* BL21(DE3) was used for the overexpression of KaiC. *E. coli* culture containing the plasmid was grown in 1L LB at 37°C until A_{600} reached 0.6. The culture was cooled down to room temperature. When A_{600} reached 0.7, 100 μM isopropyl β-D-thiogalactopyranoside (IPTG) was added to overexpress the recombinant KaiC. After 16 hours of incubation at room temperature, the cells were harvested using a centrifuge. Then, the cell pellets were resuspended in the buffer (150 mM NaCl, 50 mM Tris·HCl, 5 mM $MgCl_2$, 1 mM EDTA, 1 mM DTT, 5 mM ATP, and pH = 7.2). The cells were lysated by using a chilled French press, followed by centrifugation at 20,000 × g for 60 min at 4 °C. The supernatant was filtered with a 0.45 μm vacuum filter to remove small particles. The GST-tagged KaiC was purified with a

GST column. Human rhinovirus 3C protease was added to cut the tag off. To separate KaiC from the GST-tag, the GST column was used again. After the purity was checked by SDS-PAGE, the sample was dialyzed with the reaction buffer (150 mM NaCl, 20 mM Tris·HCl, 1 mM ATP, and pH 8.0). The final protein concentration was determined as 9.6 μM by the Bradford protein assay. The protein stock was stored at −80 °C, prior to CMS quantitation.

4.2.10 Pellet digestion of Kai C

For protein digestion, 140 μL Kai C protein (9.6 μM as determined by Bradford protein assay) was precipitated from the expressed protein sample solution using cold acetone at −20°C overnight to remove salts and buffers. The protein pellet was obtained by centrifugation at 13 000g for 10 min. Then protein pellet was washed by cold acetone once and air-dried at room temperature. After that, a 100 μL of 0.05 μg/μL trypsin (in 50 mM NH_4HCO_3, pH 8.0) was added to dissolve the pellet. After brief vortexing, the sample solution was incubated in a water bath at 37 °C for 4 h. After that a second aliquot of trypsin (0.1 μg/μL, 50 μL) was added to the sample solution. The sample was incubated at 37°C overnight to achieve complete digestion. The digest sample was diluted to the final concentration of 2.5 μM by adding mobile phase A (water with 0.1% formic acid) before LC/EC/MS analysis.

4.2.11 LC elution gradient for Kai C

For LC/EC/MS analysis of digested Kai C, the system was operated at a flow rate of 200 μL/min. The gradient used with (BEH C18, 2.1 mm × 50 mm, 1.7 μm) column was as follows: the mobile phase B (acetonitrile with 0.1% formic acid) increased from 5% to 18% in 2 min, and reached 23% from 2 to 12 min. Then, the mobile phase B climbed to 80% in 1 min and remained at 80% for 4 min. After that the mobile phase B returned to 5% in 1 min and finally isocratic at 5% for 4 min. The concentration of digested Kai C was 2.5 μM

(from the Bradford protein assay measurement). The injection volume was 6 μL per analysis.

4.2.12 Isotope dilution MS measurement of protein mixture sample

The isotope-labelled peptide VLVLDTDYK^ (labeled at lysine, 13C6, 15N2), DGPLTGTYR^ (labeled at lysine, 13C6, 15N4) and LDQWLCEK^ (labeled at lysine, 13C6, 15N2) were spiked at different concentrations into 50 μL of digested protein mixture sample containing β-lactoglobulin B (6.98 μM), α-lactalbumin (7.02 μM)) and carbonic anhydrase (7.04 μM) respectively. Final volume was adjusted to 100 μL for all the spiked samples. The final solutions contained VLVLDTDYK^, DGPLTGTYR^ and LDQWLCEK at different concentrations (0.5, 1.0, 2.0, and 5.0 μM). The LC/MS was set at the mobile phase flow rate of 200 μL/min. The gradient condition was as follows: 0-2 min, increased from 5% to 8% B; 2-14 min, linear ramp from 8% to 11% B; 14- 15 min, fast ramp from 11% to 12% B; 15-29 min, reached to 15% B; 29-10 min, climbed to 80% B and remained at 80% for 3 min before returned to 5% B. The injection concentrations of β-lactoglobulin B, α-lactalbumin and carbonic anhydrase, 3.49 μM, 3.51 μM and 3.52 μM, respectively. The injection volume was 3 μL per analysis.

4.2.13 Isotope dilution MS measurement of NPALWK from PLBL2 (mAb :PLBL2= 200:1)

The isotope-labelled peptide NPALWK^ (labeled at lysine, 13C6, 15N4) was first diluted to 0.34 μM. Then 10 μL of 0.34 μM NPALWK^ was spiked into 10 μL of 4-fold diluted digest sample for analysis. The final concentration of spiked NPALWK^ was 0.17 μM and the final dilution factor for the protein digest was 8. The LC/MS was set at the mobile phase flow rate of 200 μL/min. The gradient condition was as follows: 0-15 min, increased from 5% to 13% B; 15-17 min, linear ramp from 13% to 15% B; 19-20 min, fast ramp from

15% to 85% B and remained at 85% for 5 min before returned to 5% B. The injection volume was 5 μL per analysis.

4.2.14 Isotope dilution MS measurement of NPALWK from PLBL2 (mAb :PLBL2= 2000:1)

The isotope-labelled peptide NPALWK^ (labeled at lysine, 13C6, 15N4) was first diluted to 0.05 μM. Then 10 μL of NPALWK^ was spiked into 10 μL of 2-fold dilution of digest sample for injection. The final concentration of NPALWK^ was 0.025 μM and the final dilution factor for the protein digest was 4. The LC/MS was set at the mobile phase flow rate of 200 μL/min. The gradient condition was as follows: 0-15 min, increased from 5% to 13% B; 15-17 min, linear ramp from 13% to 15% B; 19-20 min, fast ramp from 15% to 85% B and remained at 85% for 5 min before returned to 5% B. The injection volume was 5 μL per analysis.

4.2.15 Isotope dilution MS measurement of SFGWDLAK from Kai C

The isotope-labelled peptide SFGWDLAK^ (labeled at lysine, 13C6, 15N2) was spiked into the digested Kai C sample at the final concentrations of 0.49, 2.46, 4.92, and 9.84 μM, respectively. The LC/MS was set at the mobile phase flow rate of 200 μL/min. The mobile phase B (acetonitrile with 0.1% formic acid) increased from 5% to 18% in 2 min, and reached 23% from 2 to 12 min. Then, the mobile phase B climbed to 80% in 1 min and remained at 80% for 4 min. After that the mobile phase B returned to 5% in 1 min and finally isocratic at 5% for 4 min. The concentration of digested Kai C was 2.5 μM (from the Bradford protein assay measurement). The injection volume was 6 μL per analysis.

4.3 Results and Discussion

4.3.1 Absolute quantitation of protein mixture by coulometric mass spectrometry

Previously, we demonstrated that CMS can be used for absolute quantitation of a single protein based on quantitation of its surrogate peptides.30,34 In this study, we explored the possibility for using CMS for quantitation of multiple proteins in a mixture in one run. We reason that this would be straightforward as long as multiple surrogate peptides representing different proteins could be LC-separated. In this experiment, three proteins (sequences shown in Figures 4.1a and 4.2a), *β*-lactoglobulin B (178 amino acids, MW 18,276 Da), α-lactalbumin (142 amino acids, MW 14,175 Da), and carbonic anhydrase (260 amino acids, MW 29,100 Da), in a mixture sample were first digested, and three resulting oxidizable surrogate peptides containing either tyrosine or tryptophan, VLVLDTDYK, LDQWLCEK, and DGPLTGTYR, were selected for CMS analysis. Note that, besides the need of an oxidizable residue such as Y or W, the selection of peptides for CMS absolute quantitation is similar to the peptide selection for target proteomics quantitation (using SRM/PRM), including avoiding peptides prone to a chemical/post-translational modification such as deamidation or those bearing missed cleavages.38 As shown in Figure 4.1b, after the cell was turned on, the oxidation current peaks corresponding to LDQWLCEK and VLVLDTDYK were detected, which matched with the retention times of LDQWLCEK (20.4 min) and VLVLDTDYK (24.1 min) in their EICs (Figure 4.1h,j), whereas there was no current peak observed from blank sample control (Figure 4.1b inset). On the other hand, the +2 ion of LDQWLCEK was observed at m/z 546.26 when the cell was off (Figure 4.1c), while ions of the peptide oxidation products M + 14, M + 16, and M + 32 derived from tryptophan residue oxidation43 were observed at *m/z* 553.25, *m/z* 554.26, and *m/z* 562.26, respectively, when the cell was turned on (Figure 4.1d). The integrated EIC peak area of *m/z* 546.26 after oxidation (Figure 4.1h)

was smaller by 11.3% compared to that before oxidation (Figure 4.1g), suggesting that the oxidation yield for LDQWLCEK was 11.3% (see detailed data in Table 4.1). According to the calculation equation reported previously30 for CMS quantitation of W-containing peptides based on Faraday's law using the integrated oxidation current (i.e., Q = 2.29 × 10−7 C as shown in Figure 4.1b) and product intensity ratios (see detailed calculations in Table 4.1), the amount of the oxidized LDQWLCEK was calculated as 0.86 pmol. In combination of the oxidation yield of 11.3%, the measured amount of LDQWLCEK was 7.6 pmol. The average amount of a triplicate measurement was 7.9 pmol (CV: 5.7%, Table 4.1). Similarly, as shown in Figure 4.1e, without oxidation, the +2 ion of VLVLDTDYK, a tyrosine containing peptide from β-lactoglobulin B, was observed at *m/z* 533.30. After electrolysis, the +2 ion of the oxidized VLVLDTDYK product was observed at *m/z* 532.29 (Figure 4.1f). The EICs of the +2 ion of VLVLDTDYK (*m/z* 533.30) without and with oxidation are shown in Figure 4.1i, j, respectively. By comparing the two EIC peak areas before and after oxidation, the oxidation yield for VLVLDTDYK was calculated to be 9.6% (Table 4.2). The amount of oxidized VLVLDTDYK was calculated to be 0.72 pmol based on Faraday's law (n = Q/(zF)) and a two-electron transfer process involved in the Y residue oxidation35 (z = 2, Q = 1.39 × 10^{-7} C, as shown in Figure 4.1b). Therefore, the measured amount of VLVLDTDYK was 7.5 pmol (Table 4.2). In a triplicate measurement, the averaged quantity of this peptide measured by CMS was 7.8 pmol (CV: 10.3%, Table 4.2). DGPLTGTYR, another tyrosine-containing peptide from carbonic anhydrase which eluted out at 9.5 min (earlier than LDQWLCEK and VLVLDTDYK, Figure 4.1) was also quantified to be 9.2 pmol by CMS (CV: 5.8%, Table 4.3).

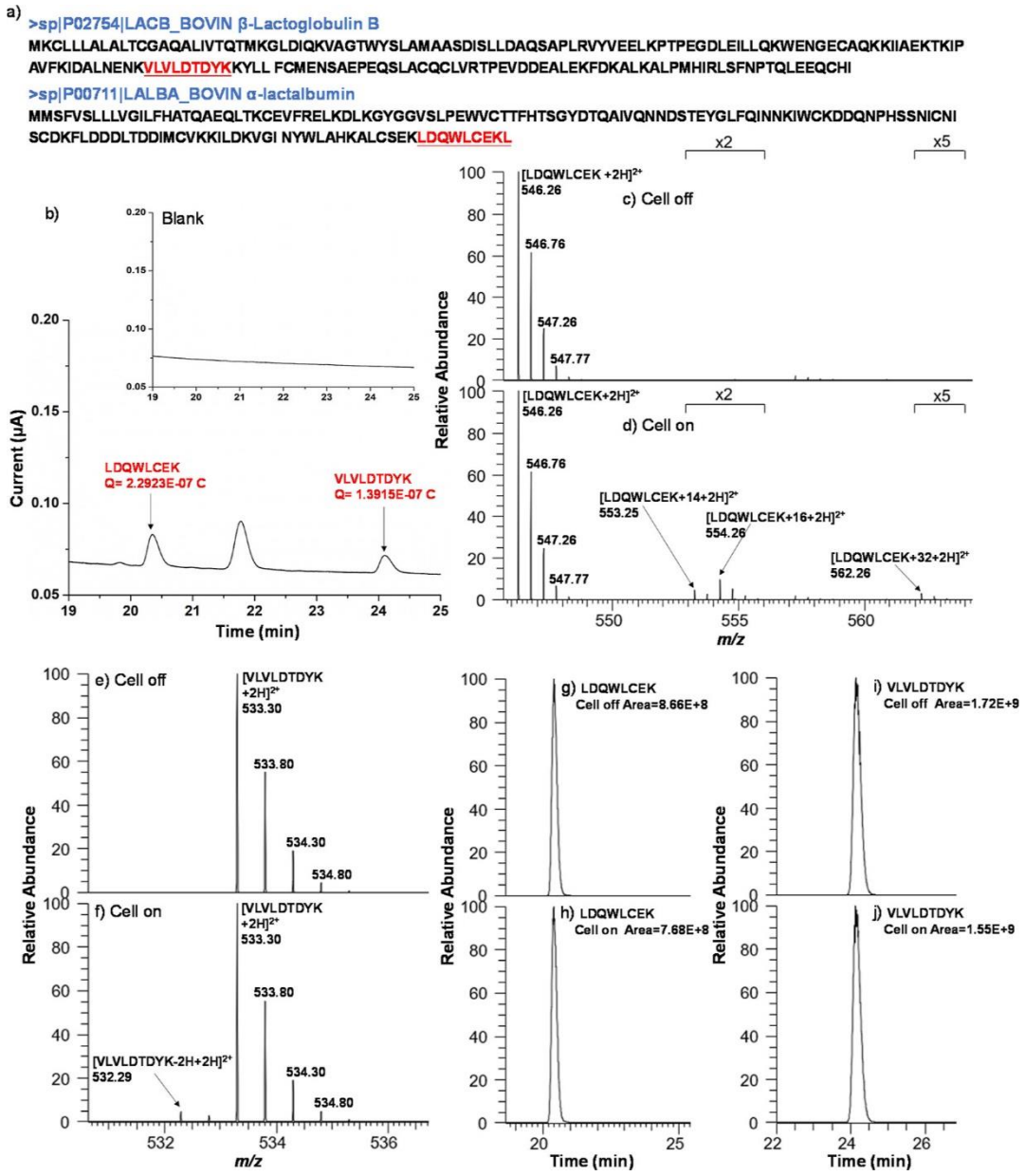

Figure 4.1 (a) Sequences of β-lactoglobulin B and α-lactalbumin (the chosen surrogate peptides VLVLDTDYK and LDQWLEK for CMS quantitation are highlighted in red); (b) electric current diagrams were collected from oxidation of blank solvent (inset) and the digested protein sample after LC separation; MS spectra of LDQWLEK (c) without oxidation and (d) with oxidation (applied potential: +1.05 V). MS spectra of VLVLDTDYK (e) without oxidation and (f) with oxidation (applied potential: + 1.05 V). EICs of LDQWLEK are shown in (g) without oxidation and (h) with oxidation (applied potential: + 1.05 V); EICs of VLVLDTDYK were acquired (i) without oxidation and (j) with oxidation (applied potential: + 1.05 V).

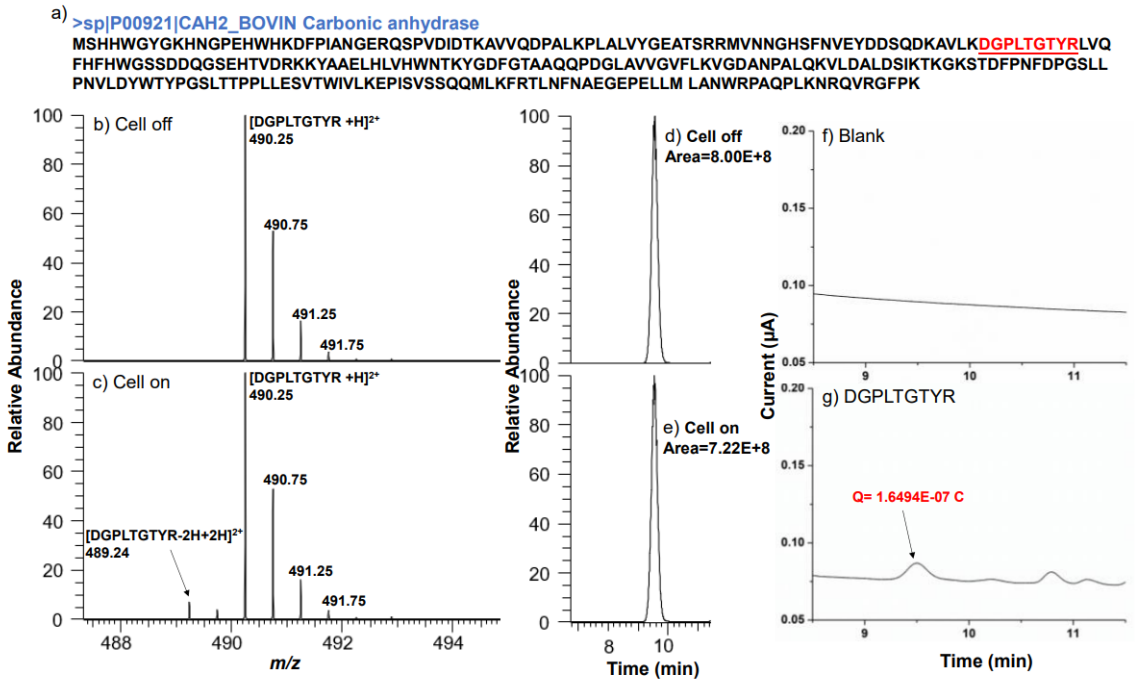

Figure 4.2 (a) Sequence of carbonic anhydrase (the chosen surrogate peptide DGPLTGTYR for CMS is highlighted in red); ESI-MS spectra of DGPLTGTYR when the applied potential was b) 0 V and c) +1.05 V. The peak of the oxidation product was seen at *m/z* 489.24 in c). EICs of DGPLTGTYR were recorded when the cell was off d) and e) when the cell was turned on (applied potential: +1.05 V). Electric current responses were due to the oxidation of f) the blank solvent and g) DGPLTGTYR.

Table 4.1 Electric Current and MS Data of the Selected Surrogate Peptide LDQWLCEK from α-lactalbumin

	Q (A*s)	Amount of the oxidized analyte (mol)	Oxidation yield	Measured amount (mol)	Averaged amount (pmol)	Theoretical amount (pmol)	Measurement error	CV (%)
	2.1480E-07	8.0972E-13	0.10432376	7.7616E-12				
LDQWLCEK	2.1549E-07	8.1123E-13	0.09621663	8.4313E-12	7.92	10.53	-24.8	5.7
	2.2923E-07	8.5822E-13	0.113297898	7.5749E-12				

Table 4.1 Electric Current and MS Data of the Selected Surrogate Peptide LDQWLCEK from α-lactalbumin (Continued)

	Averaged amount (pmol)	Measured amount (pmol) by IDMS	Discrepancy between CMS and IDMS
LDQWLCEK	7.92	8.07	-1.7%

	EIC peak area of *m/z* 546.26 before electrolysis	EIC peak area of *m/z* 546.26 after electrolysis	Oxidation yield
	876870084	785391700	0.10432376
LDQWLCEK	893835847	807833974	0.09621663
	866313390	768161904	0.113297898

	Intensity for oxidized peptide ions			Intensity ratio	
	[M+14] *m/z* 553.25	[M+16] *m/z* 554.26	[M+32] *m/z* 562.26	[M+14]/[M+16] *m/z* 553.25 to *m/z* 554.26	[M+32]/[M+16] *m/z* 562.26 to *m/z* 554.26
	7.29E+05	1.53E+06	1.86E+05	0.48	0.12
LDQWLCEK	6.02E+05	1.28E+06	1.71E+05	0.47	0.13
	6.52E+05	1.31E+06	1.65E+05	0.50	0.13

Table 4.2 Electric Current and MS Data of the Selected Surrogate Peptide VLVLDTDYK from β-lactoglobulin B

	Q (A*s)	Amount of the oxidized analyte (mol)	Oxidation yield	Measured amount (mol)	Averaged amount (pmol)	Theoretical amount (pmol)	Measurement error	CV (%)
	1.2559E-07	6.5070E-13	0.090405399	7.1976E-12				
VLVLDTDYK	1.2674E-07	6.5666E-13	0.075166422	8.7361E-12	7.82	10.47	-25.3	10.3
	1.3915E-07	7.2101E-13	0.095615037	7.5407E-12				

Table 4.2 Electric Current and MS Data of the Selected Surrogate Peptide VLVLDTDYK from β-lactoglobulin B (Continued)

	Averaged amount (pmol)	Measured amount (pmol) by IDMS	Discrepancy between CMS and IDMS
VLVLDTDYK	7.82	8.10	-3.5%

	EIC peak area of *m/z* 533.29 before electrolysis	EIC peak area of *m/z* 533.29 after electrolysis	Oxidation yield
	1700360389	1546638630	0.090405399
VLVLDTDYK	1744963819	1613801133	0.075166422
	1716369241	1552258532	0.095615037

Table 4.3 Electric Current and MS Data of the Selected Surrogate Peptide DGPLTGTYR from Carbonic Anhydrase

	Q (A*s)	Amount of the oxidized analyte (mol)	Oxidation yield	Measured amount (mol)	Averaged amount (pmol)	Theoretical amount (pmol)	Measurement error	CV (%)
	1.4362E-07	7.4412E-13	0.07611963	9.7757E-12				
DGPLTGTYR	1.3714E-07	7.1057E-13	0.079434365	8.9454E-12	9.17	10.56	-13.2	5.8
	1.6494E-07	8.5462E-13	0.097353398	8.7786E-12				

	Averaged amount (pmol)	Measured amount (pmol) by IDMS	Discrepancy between CMS and IDMS
DGPLTGTYR	9.17	8.76	-4.7%

Table 4.3 Electric Current and MS Data of the Selected Surrogate Peptide DGPLTGTYR from Carbonic Anhydrase (Continued)

	EIC peak area of *m/z* 490.25 before electrolysis	EIC peak area of *m/z* 490.25 after electrolysis	Oxidation yield
	804497429	743259382	0.07611963
DGPLTGTYR	829398748	763515985	0.079434365
	800128809	722233551	0.097353398

To confirm the CMS quantitation result, IDMS was used for comparison. Three isotopically labeled peptides, VLVLDTDYK̂ (labeled at lysine, ^{13}C6, and ^{15}N2), DGPLTGTYR̂ (labeled at arginine, ^{13}C6, and ^{15}N4), and LDQWLCEK̂ (labeled at lysine, ^{13}C6, and ^{15}N2), were spiked at various amounts into the same protein digest sample. The amounts of these surrogate peptides were determined by IDMS to be 8.1 pmol for LDQWLCEK, 8.1 pmol for VLVLDTDYK, and 8.8 pmol for DGPLTGTYR (Figure 4.3, Supporting Information), which are close to the corresponding CMS results of 7.9, 7.8, and 9.2 pmol, respectively. The difference between our CMS and isotope dilution method was less than 5% for these three surrogate peptides (Table 4.4), underscoring the accuracy of CMS method for peptide quantitation in a mixture. Furthermore, we compared the moles of surrogate peptides measured by CMS with the theoretical amounts of their precursor proteins (calculated by weight) and deviations being −24.8% (α-lactalbumin), −25.3% (*β*-lactoglobulin B), and −13.2% (carbonic anhydrase), as shown in Table 4.4. The quantitation errors of three proteins are most likely to result from the sample loss during the tryptic digestion and sample handling. Indeed, when we measured the amount of all peptides from the three protein mixture digest using the colorimetric peptide assay commercial kit (Thermo Scientific, San Jose, CA), the peptide recovery from the sample preparation including digestion was 86%, which is in line with the observed difference

between the surrogate peptide amounts measured by CMS with their precursor protein amounts as mentioned above. It has been reported that the trypsin digestion efficiency is protein dependent and related to different digestion conditions.39 Nevertheless, the CMS peptide quantitation results are close to their precursor protein quantities. Thus, this result demonstrates the capability of CMS in absolute quantitation of multiple proteins during one CMS experiment. To the best of our knowledge, this is the first time of demonstration for absolute quantitation of multiple proteins by MS without using standards.

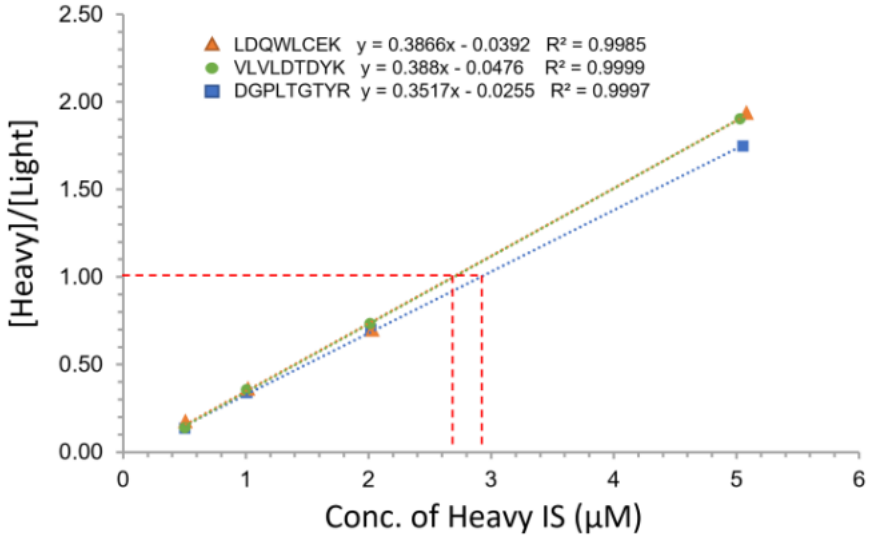

Figure 4.3 Calibration curves using isotope-labelled peptide LDQWLCEK^, VLVLDTDYK^ and DGPLTGTYR^ spiked at various amounts in the digested protein mixture sample as internal standards for quantitation (The dilution curves were established for each pair of endogenous/isotopically labeled peptides based on ion intensity ratio plotted against the concentrations of the spiked heavy peptides; From the plot above, one can see that: when y=1, $c_{[light]} = c_{[heavy]}$. So, the measured concentration of the light peptide LDQWLCEK from α-lactalbumin was 2.69 µM. The measured concentration of the light peptide VLVLDTDYK from β-Lactoglobulin B was 2.70 µM. The measured concentration of the light peptide DGPLTGTYR from carbonic anhydrase was 2.92 µM.)

Table 4.4 Comparison of Surrogate Peptides from Protein Samples Quantified by CMS and IDMS.

protein	Surrogate peptide	Measured amount (pmol) by CMS	Measured amount (pmol) by IDMS	Discrepancy between CMS and IDMS	Theoretical protein amount (pmol)	Measurement error (%)
β-Lactoglobulin B	VLVLDTDYK	7.82	8.10	-3.5%	10.47	-25.3
α-lactalbumin	LDQWLCEK	7.92	8.07	-1.7%	10.53	-24.8
Carbonic anhydrase	DGPLTGTYR	9.17	8.76	4.7%	10.56	-13.2
PLBL2 (mAb:PLBL2=200:1)	NPALWK	3.9	4.1	-4.9%	6.3	-38.2
PLBL2 (mAb:PLBL2=2000:1)	NPALWK	0.83	0.88	-5.7%	1.3	-36.2

4.3.2 Absolute quantitation of spiked PLBL2 in NIST mAb 8671 by coulometric mass spectrometry

PLBL2, a 66KDa HCP that frequently co-purifies with mAb preparations produced in Chinese hamster ovary (CHO) cells, is one lipase to potentially cause the enzymatic degradation of common formulation surfactants polysorbates 20 and 80[164] and would produce unwanted immunogenic effects in patients.[215] The existing MS-based quantitation methods need standards for quantitation of HCPs such as PLBL2, which are time-consuming to synthesize and to order and thus difficult to satisfy the desire of rapidly tracking HCPs, as mentioned before. We reason that CMS could be a choice of method for this task as it does not need standards. As a demonstration, we applied CMS for the absolute quantitation of PLBL2 spiked in NIST mAb 8671 at two spiking levels (i.e., mAb/PLBL2 = 200:1 and 2000:1).

As it is challenging to quantify a low-abundant protein in the presence of excess mAb, we adopted a native digestion approach originally developed by Huang et al.[173] In this approach, trypsin is directly added to the pH-adjusted mAb sample under native (non-denaturing) conditions. As native mAb is relatively resistant to the low concentration of trypsin digestion, after overnight digestion, an intact and minimally digested mAb was

denatured after heat treatment and then depleted from the digest solution via precipitation, while the supernatant contains enriched digested PLBL2.

NPALWK, a surrogate peptide identified from PLBL2 (sequence shown in Figure 4.4a), was separated and quantified with CMS. When the cell was off (Figure 4.4b), the +2 ion of NPALWK was observed at *m/z* 364.71. After electrolysis (Figure 2c), the oxidation product peaks corresponding to M + 14, M + 16, and M + 32 were observed at *m/z* 371.70, *m/z* 372.71, and *m/z* 380.70, respectively. The oxidation yield for NPALWK was measured to be 16.3% (Table 4.5) by comparing the EIC peak area of *m/z* 364.71 before (Figure 3.3d) and after oxidation (Figure 3.3e). Figure 3.3g shows the electric current peak from oxidation of NPALWK, from which the amount of oxidized NPALWK was calculated to be 0.64 pmol (the calculation was similar to that for LDQWLCEK shown in Table S1, Supporting Information). Therefore, the measured amount of NPALWK was 3.9 pmol (Table 4.5). For confirmation, an isotope-labeled peptide NPALWK̂(labeled at lysine, ^{13}C6, and ^{15}N4) was purchased and used as an internal standard to quantify NPALWK in the same digest sample. By this traditional isotope dilution method, NPALWK was measured to be 4.1 pmol (Table 4.5). Again, the discrepancy of the quantitation results between CMS and IDMS was small (−4.9%, Table 4.4).

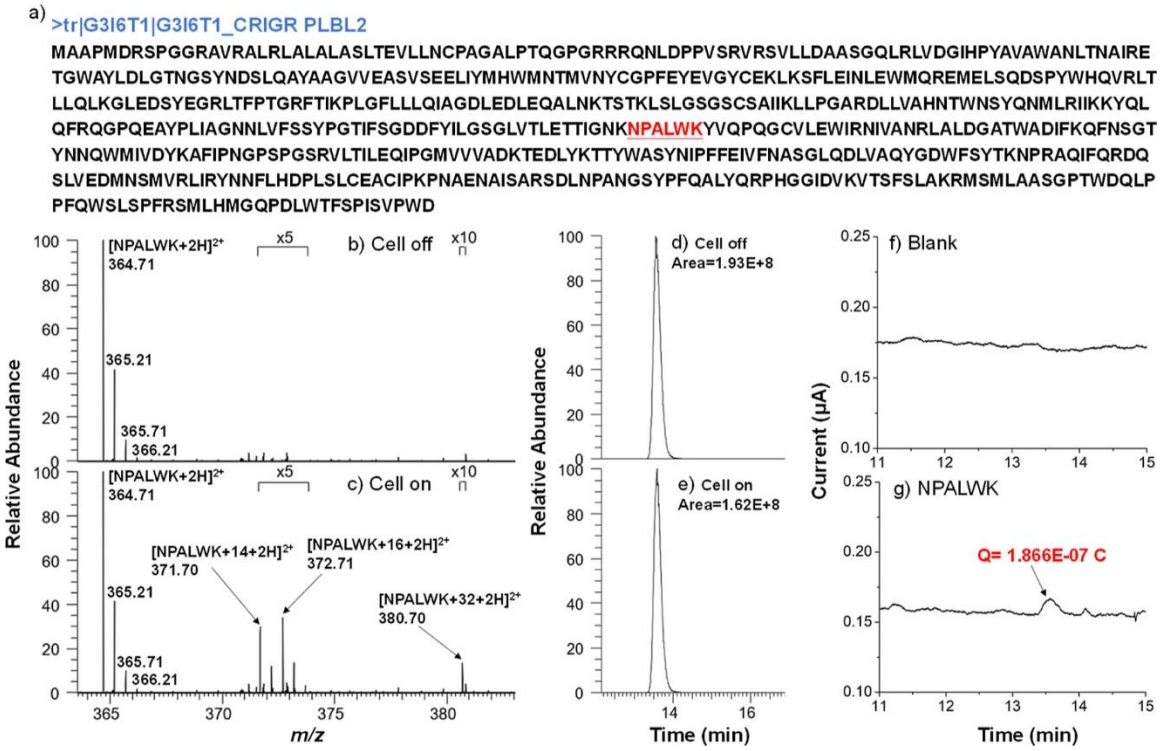

Figure 4.4 (a) Sequence of PLBL2 (the chosen surrogate peptide NPALWK is highlighted in red). MS spectra of NPALWK from the digested sample (mAb/PLBL2 = 200:1) (b) when the cell was off and (c) when the cell was turned on (applied potential: +1.05 V). The oxidation product of NPALWK was detected at *m/z* 371.70, *m/z* 372.71, and *m/z* 380.70. EICs of NPALWK were acquired (d) when the cell was off and (e) when the cell was turned on (applied potential: +1.05 V). Electric current diagrams were collected from oxidation of (f) blank solvent and (g) NPALWK.

Table 4.5 Electric Current and MS Data of the Selected Surrogate Peptide NPALWK from PLBL2 in the Sample of mAb:PLBL2=200:1

	Q (A*s)	Amount of the oxidized analyte (mol)	Oxidation yield	Measured amount (mol)	Theoretical amount (pmol)	Measurement error
NPALWK	1.8660E-07	6.3562E-13	0.163148	3.9	6.3	-38.2%

	Measured amount (pmol) by CMS	Measured amount (pmol) by IDMS	Discrepancy between CMS and IDMS
NPALWK	3.9	4.1	-4.9%

Table 4.5 Electric Current and MS Data of the Selected Surrogate Peptide NPALWK from PLBL2 in the Sample of mAb:PLBL2=200:1 (Continued)

	EIC peak area of *m/z* 364.71 before electrolysis	EIC peak area of *m/z* 364.71 after electrolysis	Oxidation yield
NPALWK	193400165	161847276	0.163148

	Intensity for oxidized peptide ions			Intensity ratio	
	[M+14] *m/z* 371.70	[M+16] *m/z* 372.71	[M+32] *m/z* 380.70	[M+14]/[M+16] *m/z* 371.70 to *m/z* 372.71	[M+32]/[M+16] *m/z* 380.70 to *m/z* 372.71
NPALWK	3.41E+05	3.84E+05	7.69E+04	0.89	0.20

Considering that the residual HCP present in the down-stream purification pool as well as in the final product is at very low level, we further reduced the spiked PLBL2 to 500 ppm (i.e., mAb/PLBL2 = 2000:1). As shown in Figure 4.5a and b, after oxidation, the oxidation product peaks of NPALWK were detected with a much smaller oxidation current peak observed in Figure 4.5f ($Q = 3.96 \times 10^{-8}$ C). Based on the oxidation yield from EIC peak area change (Figure 4.5c,d) and the Q value, the measured amount of NPALWK was calculated to be 0.83 pmol (Table 4.6). The originally spiked PLBL2 protein quantity in this mAb sample (mAb/PLBL2 = 2000:1) was 1.3 pmol. In comparison, the two mol values have a relatively large deviation (36.2%, Table 4.4), probably due to the native digestion protocol without denaturation and DTT reduction (for removal of excess amount of mAb), which might reduce the digestion efficiency of PLBL2. Nevertheless, again, this CMS peptide quantitation result was close to the quantity of 0.88 pmol determined by the isotope dilution method result (Table 4.6) with a small discrepancy at −5.7% (Table 4.4). These results indicate that CMS could be used for absolute quantitation of very low abundant proteins (i.e., PLBL2) in the presence of a highly abundant predominant protein (NIST mAb 8671). It indicates that CMS might be applicable to track the clearance of a specific

known HCP under various process conditions after shotgun proteomics identification. No need for standards would make this CMS strategy more suitable to meet the need of rapid quantitation of HCPs after their identification.

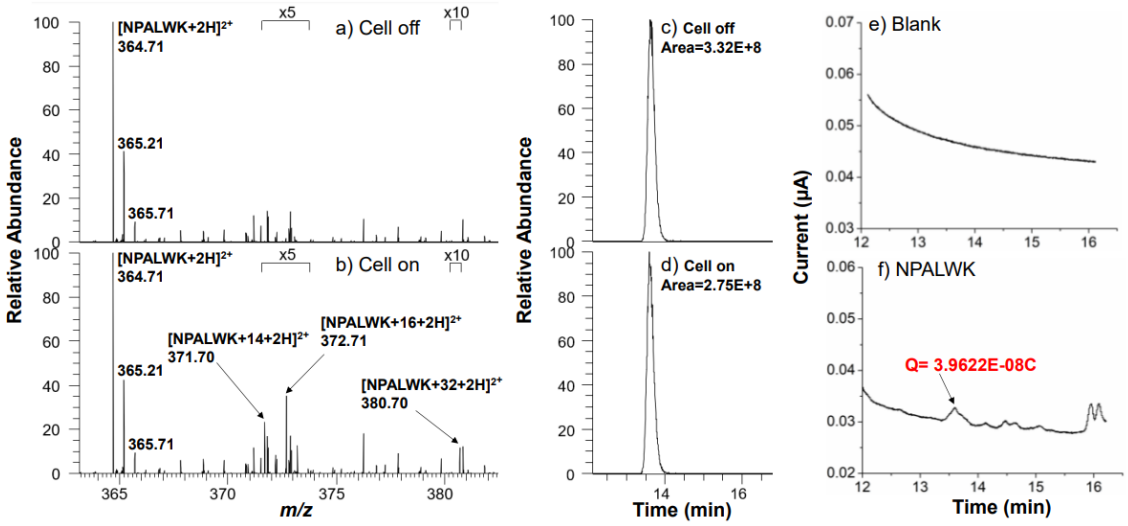

Figure 4.5 MS spectra of NPALWK from the digested sample (mAb:PLBL2=2000:1) (a) when the cell was off and (b) when the cell was turned on (applied potential: +1.05 V). The oxidation product of NPALWK was detected at *m/z* 371.70, *m/z* 372.71, and *m/z* 380.70. EICs of NPALWK were acquired (c) when the cell was off and (d) when the cell was turned on (applied potential: +1.05 V). Electric current diagrams were collected from oxidation of (e) a blank solvent and (f) NPALWK.

Table 4.6 Electric Current and MS Data of the Selected Surrogate Peptide NPALWK from PLBL2 in the Sample of mAb:PLBL2= 2000:1

	Q (A*s)	Amount of the oxidized analyte (mol)	Oxidation yield	Measured amount (mol)	Theoretical amount (pmol)	Measurement error
NPALWK	3.9622E-08	1.4181E-13	0.170597251	0.83	1.3	-36.2%

	Measured amount (pmol) by CMS	Measured amount (pmol) by IDMS	Discrepancy between CMS and IDMS
NPALWK	0.83	0.88	-5.7%

Table 4.6 Electric Current and MS Data of the Selected Surrogate Peptide NPALWK from PLBL2 in the Sample of mAb:PLBL2= 2000:1 (Continued)

	EIC peak area of *m/z* 364.71 before electrolysis	EIC peak area of *m/z* 364.71 after electrolysis	Oxidation yield
NPALWK	33161824	27504508	0.170597251

	Intensity for oxidized peptide ions			Intensity ratio	
	[M+14] *m/z* 371.70	[M+16] *m/z* 372.71	[M+32] *m/z* 380.70	[M+14]/[M+16] *m/z* 371.70 to *m/z* 372.71	[M+32]/[M+16] *m/z* 380.70 to *m/z* 372.71
NPALWK	4.66E+04	7.25E+04	1.22E+04	0.64	0.17

The sensitivity of HCP analysis by CMS is limited by the signal-to-noise ratio of electric current when the surrogate peptide concentration is low. To further improve the sensitivity of our CMS in HCP quantitation, our future study would focus on using microelectrodes for peptide oxidation to gain an enhanced signal-to-noise ratio in the electric current measurement.

4.3.3 Absolute quantitation of total and deamidated peptides from NIST mAb heavy chain

Deamidation of asparagine (Asn) residues to Asp or isoAsp is a common chemical modification and degradation pathway that occurs during the manufacturing and storage of monoclonal antibodies (mAbs). Previous studies have shown that the degradation products as well as the succinimide intermediate (Scheme 4.1) can cause serious quality and safety issues,[227, 228] such as aggregation, intermolecular crosslinking, activity loss, and immunogenicity. Therefore, mAb deamidation needs to be closely monitored. So far, absolute quantitation of deamidation is rare[222] and absolute quantitation of the succinimide intermediate has never been done before due to the lack of standards. In this study, we

demonstrated simultaneous identification and absolute quantification of mAb deamidation degradation by CMS, as illustrated in the workflow of Scheme 4.2c.

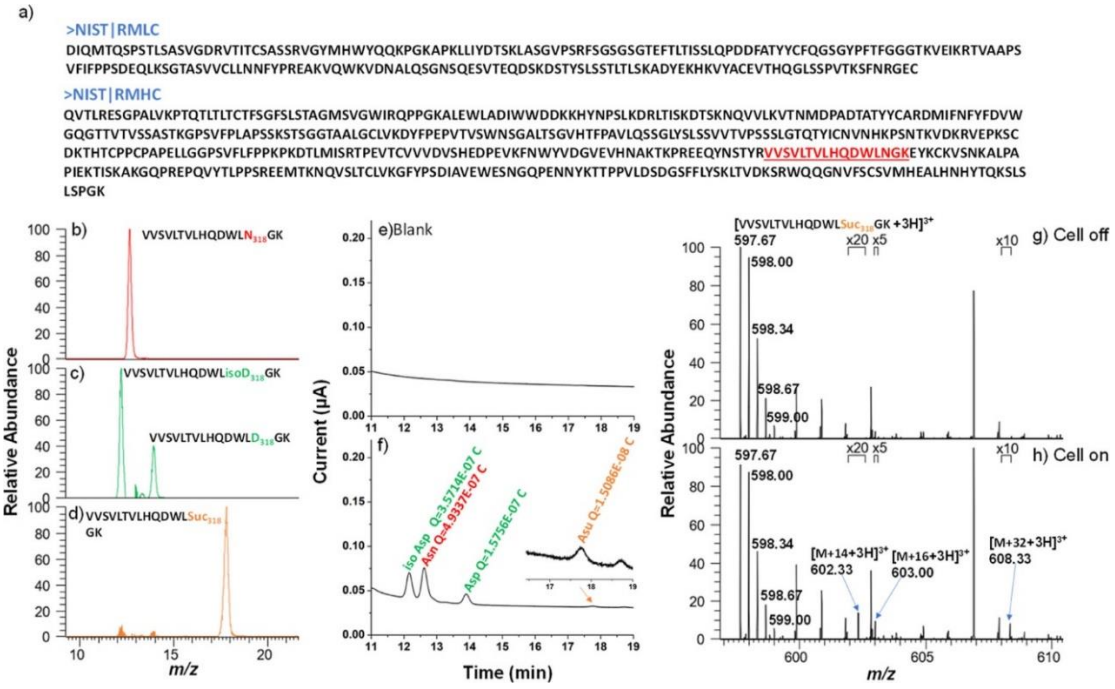

Figure 4.6 (a) Sequence of an NIST 8671 light chain and heavy chain (the chosen N318 surrogate peptide VVSVLTVLHQDWLN318GK from HC is highlighted in red). EICs of (b) unmodified peptide VVSVLTVLHQDWLN318GK and (c) deamidated peptides VVSVLTVLHQDWLisoD318GK and VVSVLTVLHQDWLD318GK and (d) succinimide intermediate VVSVLTVLHQDWLSuc318GK. Electric oxidation current diagrams are shown due to the oxidation of (e) solvent blank and (f) mAb digest. The MS spectra of the succinimide intermediate VVSVLTVLHQDWLSuc318GK was recorded (g) without oxidation and (h) with oxidation (applied potential: +1.05 V).

Briefly, the tryptic NIST mAb digest was subjected to LC separation using DFA as the acidic modifier. The residue N318 site from the heavy chain (HC, Figure 4.6a) was chosen for examination, and Figure 4.5b−d shows the EICs of four different peptide forms, including the unmodified peptide VVSVLTVLHQDWLN318GK, two deamidation peptides VVSVLTVLHQDWLisoD 318 G K and VVSVLTVLHQDWLD318GK, and the succinimide intermediate VVSVLTVLHQDWLSuc318GK from a 30-min LC gradient elution (note that VVSVLTVLHQDWLisoD318GK and VVSVLTVLHQDWLD318GK were assigned based on their elution order in reversed phase LC[229]).

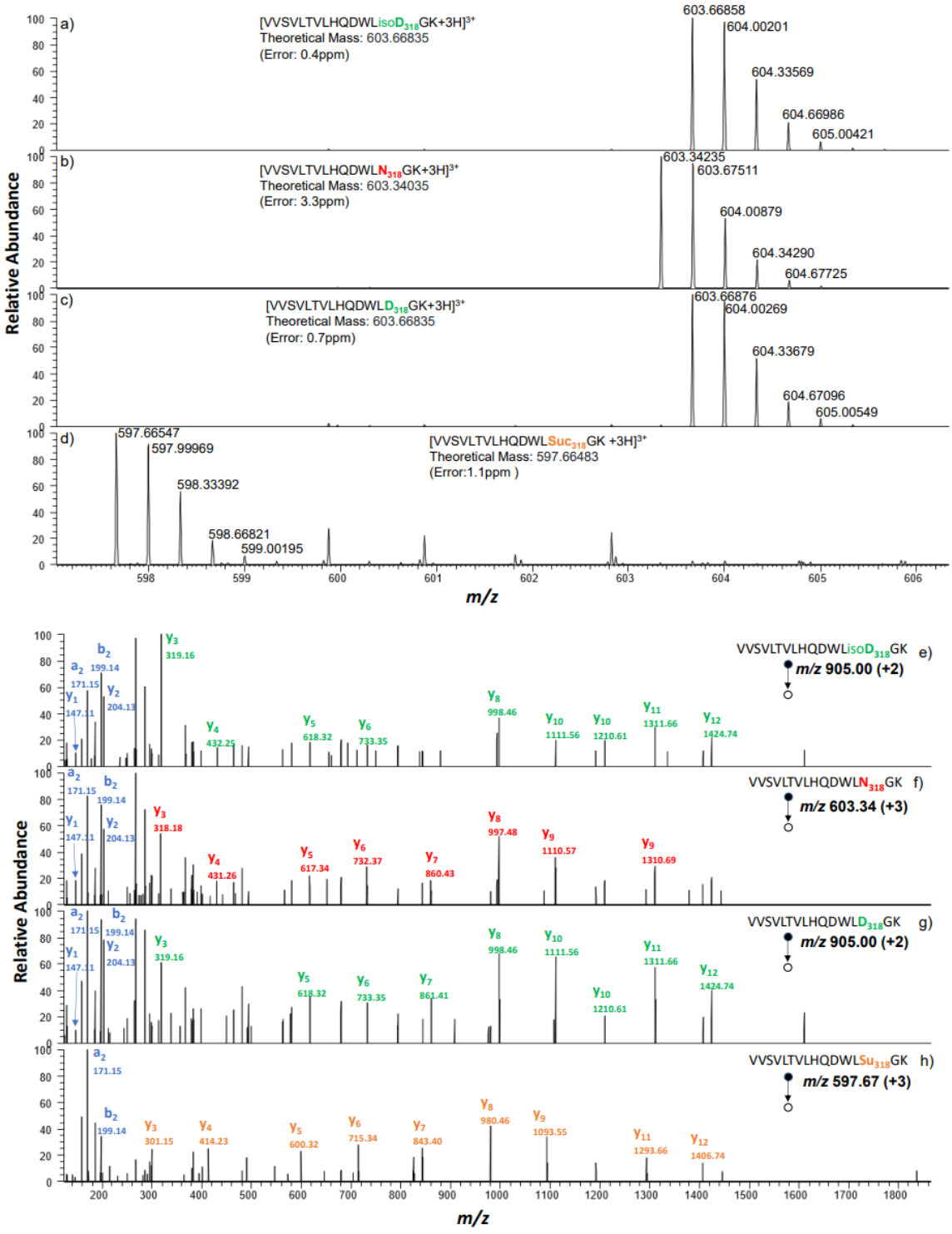

Figure 4.7 Accurate mass measurements of (a) VVSVLTVLHQDWLisoD318GK (b) VVSVLTVLHQDWLN318GK, (c) VVSVLTVLHQDWLD318GK, and (d) VVSVLT-VLHQDWLSuc318GK; MS/MS spectra of (e) VVSVLTVLHQDWLisoD318GK, (f) VVSVLTVLHQDWLN318GK, (g) VVSVLTVLHQDWLD318GK, and (h) VVSV-LTVLHQDWLSuc318GK.

The molecular mechanism of Asn deamidation has been well studied,[230] in which the side-chain carbonyl group of Asn is attacked by the NH group of the adjacent amide to generate a cyclic succinimide intermediate (Scheme 4.1). The succinimide intermediate can be further hydrolyzed into isoAsp or Asp. Mass measurements of unmodified peptide, deamidated products, and succinimide intermediate matched very well with their theoretical masses (<5 ppm mass error, Figures 4.7a-d). To further confirm these identifications and localize the modification sites, MS/MS spectra were acquired (Figures 4.7e-h). As shown in Figures 4.7e, f and g, y1 and y2 ions showed the same m/z for both unmodified and deamidated forms. Starting from y3 ion, y ions from deamidated peptides were 1 Da heavier than the corresponding y ions from the unmodified peptide, which matched with the fact that the deamidation site was the 3rd asparagine residue from the C-terminus. As shown in Figure 4.7h, y3 to y12 from the succinimide intermediate were 17 Da less than the corresponding y ions from the unmodified peptide (Figure 4.7f), which was also in line with occurrence of modification on the 3rd asparagine residue from C terminal.

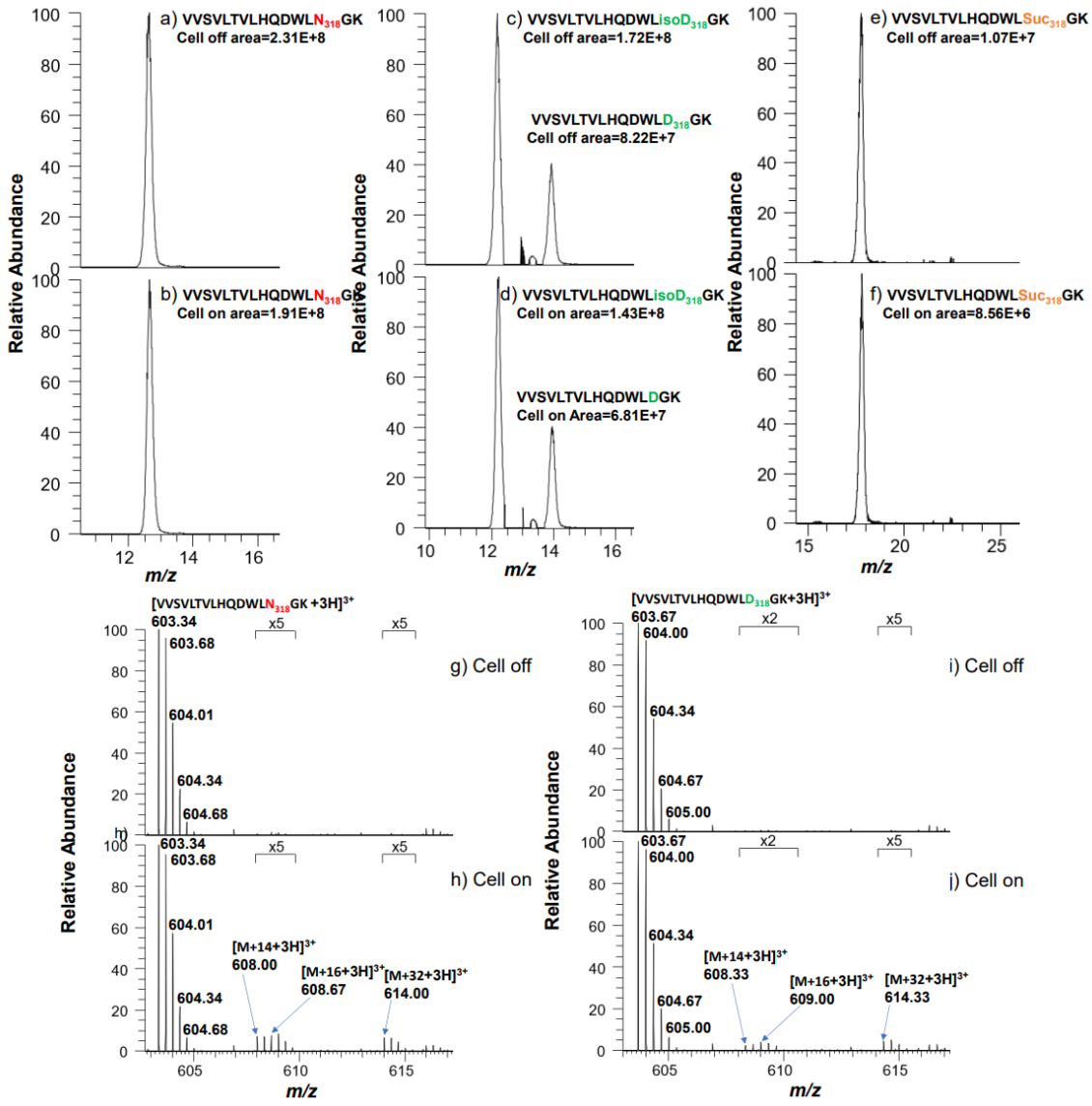

Figure 4.8 EICs of VVSVLTVLHQDWLN318GK were acquired (a) when the cell was off and (b) when the cell was turned on (applied potential: +1.05 V); EICs of VVSVLTVLHQDWLD318GK were acquired (c) when the cell was off and (d) when the cell was turned on (applied potential: +1.05 V); EICs of VVSVLTVLHQDWLSuc318GK were shown in (e) when the cell was off and (f) when the cell was turned on (applied potential: +1.05 V); MS spectra of VVSVLTVLHQDWLN318GK from the NIST mAb tryptic digest (g) when the cell was off and (h) when the cell was turned on (applied potential: +1.05 V). The oxidized product peak was detected at *m/z* 608.00, *m/z* 608.67 and *m/z* 614.00 in (h); MS spectra of VVSVLTVLHQDWLD318GK from NIST mAb tryptic digest (i) when the cell was off and (j) when the cell was turned on (applied potential: +1.05 V). The oxidation product of VVSVLTVLHQDWLSuc318GK was detected at *m/z* 608.33, *m/z* 609.00, and *m/z* 614.33.

After identification of four different forms of VVSVLTVLHQDWLN318GK, CMS was used for their absolute quantification. As shown in Figure 4.6e, no oxidation

current was observed for a blank solvent when the cell was turned on at +1.05 V. After injection of the NIST mAb digest sample, four oxidation current peaks corresponding to four peptides were recorded shown in Figure 4.6f. At the same time, the oxidation products were monitored with online MS detection, which further confirmed the occurrence of electrochemical oxidation of those tryptophan-containing peptides (Figure S5). For example, as shown in Figure 4.6g, before electrolysis, a +3 ion of VVSVLTVLHQDWLSuc318GK was observed at *m/z* 597.67; after electrolysis, the oxidation product ions at *m/z* 602.33 (M + 14 ion), *m/z* 603.00 (M + 16 ion), and m/z 608.33 (M + 32 ion) were observed in Figure 4.6h. The amount of oxidized VVSVLTVLHQDWLSuc318GK was calculated as 0.050 pmol based on the charge (Q = 1.51 × 10−8 C, Figure 4.6f) and the intensity ratios of the oxidation products observed (Table 4.7). Based on the EIC peak change for *m/z* 597.67 upon oxidation (Figure 4.6g,h), the oxidation yield for VVSVLTVLHQDWLSuc318GK was measured as 20.1% (Table S8). Therefore, the total amount of VVSVLTVLHQDWLSuc318GK was measured to be 0.25 pmol (Table 4.7). Simultaneously, the deamidated peptides as well as the unmodified peptide were also quantified by CMS. As shown in Figure 4.6f, after cell on, the current peaks corresponding to Asp and isoAsp together with Asn were recorded in the same LC run. For deamidated peptides, after oxidation, ions of the M + 14, M + 16, and M + 2 products were detected at *m/z* 608.33, *m/z* 609.00, and *m/z* 614.33, respectively (as exemplified by VVSVLTVLHQDWLD318GK shown in Figures S5i,j). The oxidation yields for VVSVLTVLHQDWLisoD 318 G K and VVSVLTVLHQDWLD318GK were measured by comparing the EIC peptide peak areas before and after oxidation (Figures 4.6c,d). Thus, VVSVLTVLHQDWLisoD318GK and VVSVLTVLHQDWLD318GK were determined to be 7.1 and 2.9 pmol, respectively (Table 4.7). The unmodified peptide VVSVLTVLHQDWLN318GK was quantified using CMS as well and the measured

amount was 9.0 pmol (Table 4.7). Therefore, the total amount of N318 tryptic peptides measured by CMS involving four different forms was 19.3 pmol. Considering that the NIST mAb (MW: ca. 150 kDa) contains two heavy chains, the measured mAb amount would be 9.66, which was close to the amount of mAb used for digestion (12.7 pmol). Therefore, the measurement error of protein quantity was −23.7% (Table 4.7), which is again probably due to the sample loss from the digestion step. Indeed, sample loss up to 32% during antibody digestion was reported before.45 Furthermore, the measured amount o f VVSVLTVLHQDWLSuc318GK (0.25 pmol) was much lower than the deamidation products (10.0 pmol in total), which is also in line with the fact that VVSVLTVLHQDWLSuc318GK is an intermediate and its conversion to deamidation products is fast.

Table 4.7 Electric Current and MS Data for N318 Deamidation Quantitation

	Q (A*s)	Amount of the oxidized analyte (mol)	Oxidation yield	Measured amount (mol)	Sum of measured peptide amount (pmol)	Sum of measured mAb amount (pmol)	Theoretical mAb amount (pmol)	Measurement error
Asn	4.9337E-07	1.5888E-12	0.175684586	9.04329E-12				
isoAsp	3.5714E-07	1.2044E-12	0.168892573	7.13117E-12	19.32	9.66	12.7	-23.7%
Asp	1.5756E-07	4.9462E-13	0.170834087	2.89532E-12				
Asu	1.5086E-08	5.0247E-14	0.200619034	2.50461E-13				

Table 4.7 Electric Current and MS Data for N318 Deamidation Quantitation (Continued)

	EIC peak area (before electrolysis)	EIC peak area (after electrolysis)	Oxidation yield
	m/z 603.34	*m/z* 603.34	
Asn	231492648	190822958	0.175684586
	m/z 603.67	*m/z* 603.67	
isoAsp	172141655	143068208	0.168892573
Asp	82154266	68119517	0.170834087
	m/z 597.67	*m/z* 597.67	
Asu	10714108	8564654	0.200619034

	Intensity for oxidized peptide ions			Intensity ratio	
	[M+14] *m/z* 608.00	[M+16] *m/z* 608.67	[M+32] *m/z* 614.00	[M+14]/[M+16] *m/z* 608.00 to *m/z* 608.67	[M+32]/[M+16] *m/z* 614.00 to *m/z* 608.67
Asn	1.62E+05	2.15E+05	1.73E+05	0.75	0.80
	[M+14] *m/z* 608.33	[M+16] *m/z* 609.00	[M+32] *m/z* 614.33	[M+14]/[M+16] *m/z* 608.33 to *m/z* 609.00	[M+32]/[M+16] *m/z* 614.33 to *m/z* 609.00
isoAsp	1.31E+05	1.93E+05	9.26E+04	0.68	0.48
Asp	5.41E+04	6.60E+04	6.87E+04	0.82	1.04
	[M+14] *m/z* 602.33	[M+16] *m/z* 603.00	[M+32] *m/z* 608.33	[M+14]/[M+16] *m/z* 602.33 to *m/z* 603.00	[M+32]/[M+16] *m/z* 608.33 to *m/z* 603.00
Asu	5.47E+03	8.60E+03	5.28E+03	0.64	0.61

In the past, most of the quantitation of deamidation products was based on relative quantitation due to the difficulty in obtaining standards. The relative quantitation was made by comparing the peak intensity or ion counts, which could lead to errors as different peptides could have different ionization efficiency. In comparison to an unmodified peptide containing N, the deamidation products contain the acidic residue D or iso D, which could have a reduced ionization efficiency in the positive ion mode. As previously reported,[231] amino acids with higher hydrophobicity would have higher ionization efficiency. For the

succinimide peptide intermediate, it lacks the polar amide side group and would be more hydrophobic than the unmodified peptide; therefore, the ionization efficiency of the succinimide peptide might increase compared with the unmodified peptide. Thus, quantitation using peak area or intensity would overestimate the succinimide peptide quantity. Indeed, while the EIC peak intensity ratio of the succinimide intermediate VVSVLTVLHQDWLSuc318GK to the unmodified peptide VVSVLTVLHQDWL-N318GK was 0.05, our CMS quantitation result showed the absolute quantity ratio of the two peptides was only 0.03 (Figure 4.6b). In addition, the abundance of the deamidated peptides was slightly underestimated based on the relative quantitation by EIC peak area (deamidation products/ unmodified peptide = 1.10) in comparison with the CMS absolute quantitation (deamidation products/unmodified peptide = 1.11, Figure 4.6a). These results indicate that CMS can be used for monitoring mAb deamidation degradation and also for quantitation of peptides with modifications where standards are hard to access. Furthermore, since deamidation is a nonenzymatic and spontaneous post-translational modification (PTM) which is also strongly associated with aging proteome instability and degenerative diseases,48 novel quantitation strategies such as CMS may facilitate the investigation of the disease mechanisms and monitoring aging process.

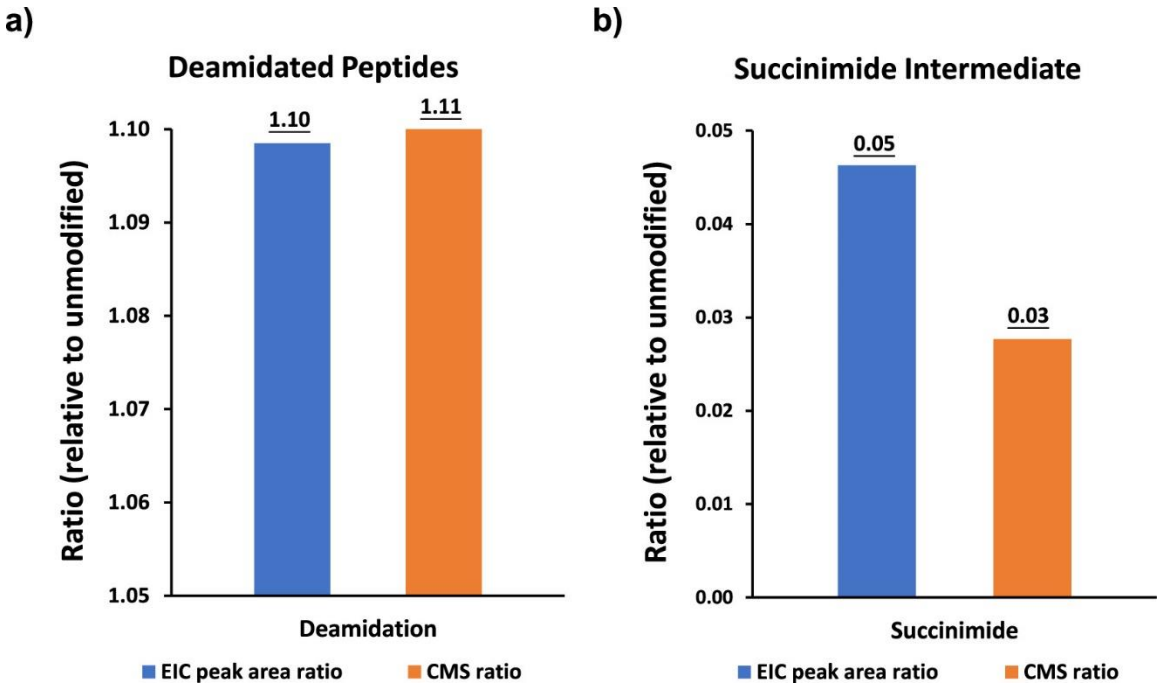

Figure 4.9 Comparison of quantitation results for the deamidated products (a) and succinimide intermediate (b) as measured based on the EIC peak areas and CMS absolute quantitation.

To fully explore the CMS application for real biological sample quantitation, KaiC (MW 58 kD), one of the essential circadian clock proteins isolated from Escherichia coli, 49 was also tested with CMS. Our results showed that the quantity of one surrogate peptide SFGWDLAK from KaiC measured by CMS and by the traditional isotope dilution method just differed by 1.3% (see details in Figures 4.10 and 4.11 and Table 4.8), suggesting the potential of CMS for real sample quantitation.

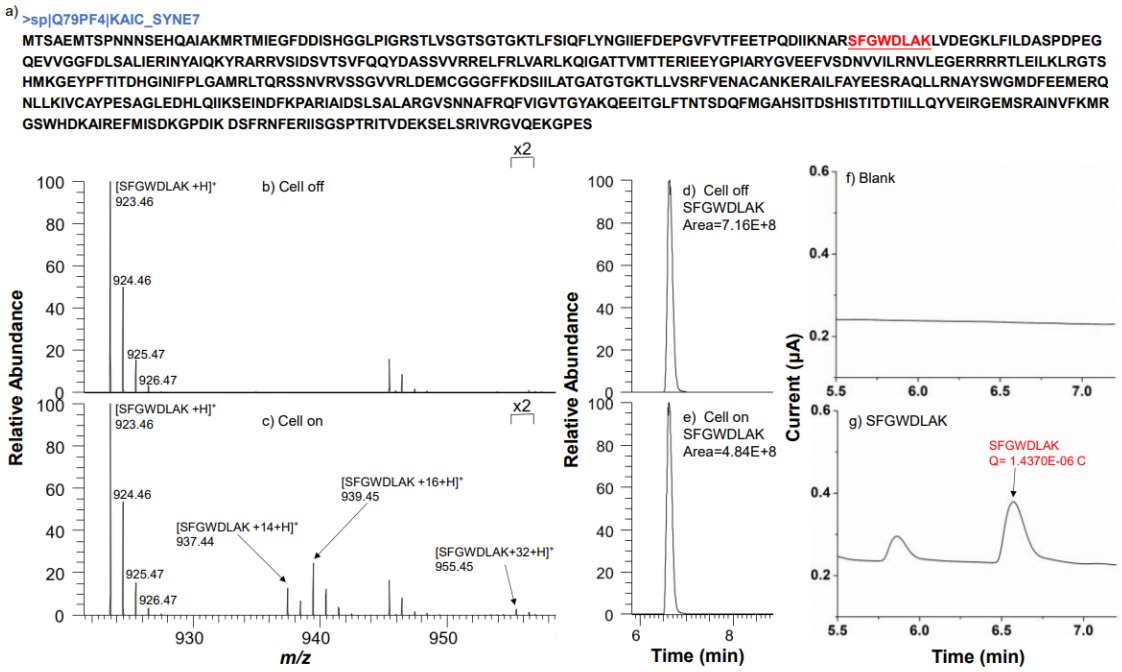

Figure 4.10 (a) Sequence of KaiC (the chosen surrogate peptide SFGWDLAK for CMS is highlighted in red); MS spectra of SFGWDLAK from the KaiC digest (b) when the cell was off and (c) when the cell was turned on (applied potential: +1.05 V). The oxidation products of SFGWDLAK were detected at *m/z* 937.44, *m/z* 939.45, and *m/z* 955.45; EICs of SFGWDLAK are shown in (d) when the cell was off and (e) when the cell was turned on (applied potential: +1.05 V); Electric current diagrams were collected from (f) blank solvent and (g) the oxidation of SFGWDLAK.

Table 4.8 Electric Current and MS Data for Digested KaiC from E. coli (the Selected Surrogate Peptide: SFGWDLAK)

	Q (A*s)	Amount of the oxidized analyte (mol)	Oxidation yield	Measured amount (mol)	Averaged amount (pmol)	Measured amount (mol) by Bradford	Measurement error	CV (%)
	1.3832E-06	5.2088E-12	0.354520725	1.4693E-11				
SFGWDLAK	1.3570E-06	5.1549E-12	0.324155001	1.5903E-11	15.8	15.0	4.0%	6.8
	1.4370E-06	5.4369E-12	0.323190172	1.6823E-11				

Table 4.8 Electric Current and MS Data for Digested KaiC from E. coli (the Selected Surrogate Peptide: SFGWDLAK) (Continued)

	Averaged amount (pmol)	Measured amount (pmol) by IDMS	Discrepancy between CMS and IDMS
SFGWDLAK	15.8	15.6	1.3%

	EIC peak area of *m/z* 923.46 before electrolysis	EIC peak area of *m/z* 923.46 after electrolysis	Oxidation yield
	721552394	465747116	0.354520725
SFGWDLAK	696487474	470717576	0.324155001
	715784652	484450087	0.323190172

	Intensity for oxidized peptide ions			Intensity ratio	
	[M+14] *m/z* 937.44	[M+16] *m/z* 939.45	[M+32] *m/z* 955.45	[M+14]/[M+16] *m/z* 937.44 to *m/z* 939.45	[M+32]/[M+16] *m/z* 955.45 to *m/z* 939.45
	3.91E+06	7.16E+06	4.01E+05	0.55	0.06
SFGWDLAK	3.50E+06	6.85E+06	4.15E+05	0.51	0.06
	3.62E+06	6.93E+06	4.33E+05	0.52	0.06

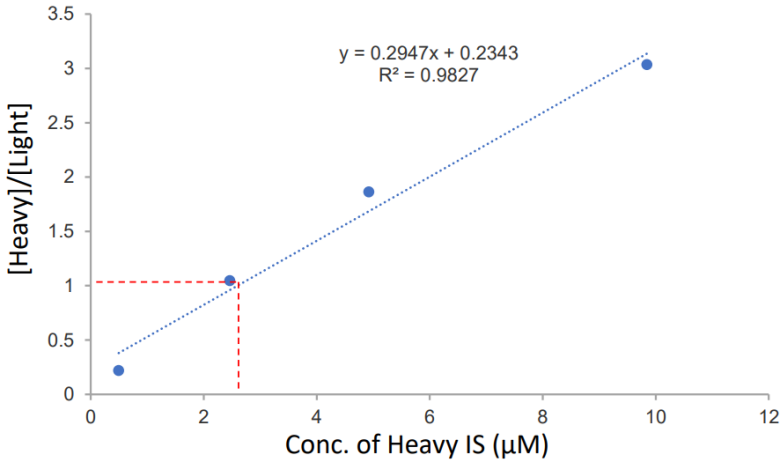

Figure 4.11 Calibration curve using isotope-labelled peptide SFGWDLAK^ as an internal standard for quantitation (From the plot above, one can see that: when y=1, x=2.6 µM ($c_{[light]} = c_{[heavy]}$). So, the measured concentration of the light peptide SFGWDLAK from KaiC digest was 2.6 µM).

4.4 Conclusions

In this study, we demonstrated the feasibility of using CMS for absolute quantitation of multiple proteins from a mixture sample in one run, for the first time. In addition, our work also demonstrated CMS as a novel absolute quantitation approach towards HCP quantitation by the evaluation of one HCP model consisting of one problematic HCP (PLBL2) with known ppm levels in a mAb drug substance material. The CMS quantitation results of both experiments were validated by the reference isotope dilution method with good accuracy. These results show the capability for CMS for multiplex protein quantitation and for measuring low-level proteins. Furthermore, CMS was demonstrated to enable simultaneously absolute quantitation of the unmodified, deamidated, and the succinimide intermediate peptides, in which the lack of internal standards is often an issue. Because of no need for internal standards, CMS can save time and cost for quantitative protein analysis and could support the rapid method development during biopharmaceutical drug discovery and manufacturing process.

CHAPTER 5

FUTURE WORK

We are planning to develop the large-scale CMS quantitation to enable the absolute quantitation of multiple proteins in the real biological sample such as the quantitation of high-risk HCPs during the different process stage as well as biomarker quantitation in human body fluids. Considering the complexity of the real sample, the pre-treatment steps prior to CMS including protein/peptide fractionation, or multidimensional online separation would be necessary. As no standards are required for CMS, it would be a powerful quantitation tool to significantly reduce the time and cost, especially for large-scale quantitation. On the other hand, to increase the throughput, we plan to create an automatic workflow for data analysis by integrated software solution which can perform the protein database search, surrogate peptide selection, electric current peak matching, as well as the peak deconvolution and integration.

Besides, we are also planning on the phosphotyrosine quantitation with CMS. Tyrosine phosphorylation is a dynamic reversible post-translational modification which is essential in mediating cellular communication and in the regulation of cell growth and oncogenic transformation. To understand the biological effects of tyrosine phosphorylation, it is necessary to not only identify the specific sites of phosphorylation, but also to quantify how phosphorylation levels on these sites may be altered under specific physiological conditions. Phosphopeptides are typically measured by normalizing the signal strength to examine quantitative changes at a site-specific level. Absolute quantitation involving isotope labeling and internal standards provides more robust, reliable, and precise quantitative results. However, syntheses of those standard compounds

can be highly costly and time-consuming. In addition, isotope labeled phosphopeptide standards are often unavailable. Therefore, we expect the standard-free CMS quantitation to address this issue.

REFERENCES

1. Bain, R. M.; Pulliam, C. J.; Cooks, R. G., Accelerated Hantzsch electrospray synthesis with temporal control of reaction intermediates. *Chemical Science* **2015,** *6* (1), 397-401.

2. Banerjee, S.; Zare, R. N., Syntheses of isoquinoline and substituted quinolines in charged microdroplets. *Angewandte Chemie* **2015,** *127* (49), 15008-15012.

3. Basuri, P.; Gonzalez, L. E.; Morato, N. M.; Pradeep, T.; Cooks, R. G., Accelerated microdroplet synthesis of benzimidazoles by nucleophilic addition to protonated carboxylic acids. *Chemical Science* **2020,** *11* (47), 12686-12694.

4. Cooks, R. G.; Yan, X., Mass spectrometry for synthesis and analysis. *Annual Review of Analytical Chemistry* **2018,** *11*, 1-28.

5. Wei, Z.; Li, Y.; Cooks, R. G.; Yan, X., Accelerated reaction kinetics in microdroplets: Overview and recent developments. *Annual Review of Physical Chemistry* **2020,** *71*, 31-51.

6. Yan, X.; Bain, R. M.; Cooks, R. G., Organic reactions in microdroplets: Reaction acceleration revealed by mass spectrometry. *Angewandte Chemie International Edition* **2016,** *55* (42), 12960-12972.

7. Girod, M.; Moyano, E.; Campbell, D. I.; Cooks, R. G., Accelerated bimolecular reactions in microdroplets studied by desorption electrospray ionization mass spectrometry. *Chemical Science* **2011,** *2* (3), 501-510.

8. Müller, T.; Badu‐Tawiah, A.; Cooks, R. G., Accelerated Carbon-Carbon Bond‐Forming Reactions in Preparative Electrospray. *Angewandte Chemie* **2012,** *124* (47), 12002-12005.

9. Badu-Tawiah, A. K.; Campbell, D. I.; Cooks, R. G., Accelerated C–N bond formation in dropcast thin films on ambient surfaces. *Journal of the American Society for Mass Spectrometry* **2012,** *23* (9), 1461-1468.

10. Yan, X.; Augusti, R.; Li, X.; Cooks, R. G., Chemical reactivity assessment using reactive paper spray ionization mass spectrometry: the Katritzky reaction. *ChemPlusChem* **2013,** *78* (9), 1142-1148.

11. Bain, R. M.; Pulliam, C. J.; Yan, X.; Moore, K. F.; Müller, T.; Cooks, R. G., Mass spectrometry in organic synthesis: Claisen–Schmidt Base-catalyzed condensation and Hammett correlation of substituent effects. *Journal of Chemical Education* **2014,** *91* (11), 1985-1989.

12. Lee, J. K.; Banerjee, S.; Nam, H. G.; Zare, R. N., Acceleration of reaction in charged microdroplets. *Quarterly Reviews of Biophysics* **2015,** *48* (4), 437-444.

13. Bain, R. M.; Pulliam, C. J.; Ayrton, S. T.; Bain, K.; Cooks, R. G., Accelerated hydrazone formation in charged microdroplets. *Rapid Communications in Mass Spectrometry* **2016,** *30* (16), 1875-1878.

14. Lee, J. K.; Kim, S.; Nam, H. G.; Zare, R. N., Microdroplet fusion mass spectrometry for fast reaction kinetics. *Proceedings of the National Academy of Sciences* **2015,** *112* (13), 3898-3903.

15. Lee, J. K.; Nam, H. G.; Zare, R. N., Microdroplet fusion mass spectrometry: Accelerated kinetics of acid-induced chlorophyll demetallation. *Quarterly Reviews of Biophysics* **2017,** *50*, e2.

16. Bain, R. M.; Pulliam, C. J.; Thery, F.; Cooks, R. G., Accelerated chemical reactions and organic synthesis in Leidenfrost droplets. *Angewandte Chemie International Edition* **2016,** *55* (35), 10478-10482.

17. Li, Y.; Liu, Y.; Gao, H.; Helmy, R.; Wuelfing, W. P.; Welch, C. J.; Cooks, R. G., Accelerated forced degradation of pharmaceuticals in levitated microdroplet reactors. *Chemistry–A European Journal* **2018,** *24* (29), 7349-7353.

18. Yan, X.; Cheng, H.; Zare, R. N., Two‐phase reactions in microdroplets without the use of phase‐transfer catalysts. *Angewandte Chemie* **2017,** *129* (13), 3616-3619.

19. Chabinyc, M. L.; Craig, S. L.; Regan, C. K.; Brauman, J. I., Gas-phase ionic reactions: dynamics and mechanism of nucleophilic displacements. *Science* **1998,** *279* (5358), 1882-1886.

20. Cheng, H.; Tang, S.; Yang, T.; Xu, S.; Yan, X., Accelerating electrochemical reactions in a voltage‐controlled interfacial microreactor. *Angewandte Chemie International Edition* **2020,** *59* (45), 19862-19867.

21. Tang, S.; Fan, L.; Cheng, H.; Yan, X., Incorporating electro-epoxidation into electrospray ionization mass spectrometry for simultaneous analysis of negatively and positively charged unsaturated glycerophospholipids. *Journal of the American Society for Mass Spectrometry* **2020,** *32* (9), 2288-2295.

22. Tang, S.; Cheng, H.; Yan, X., On‐demand electrochemical epoxidation in nano‐electrospray ionization mass spectrometry to locate carbon‐carbon double bonds. *Angewandte Chemie International Edition* **2020,** *59* (1), 209-214.

23. Wei, Z.; Zhang, X.; Wang, J.; Zhang, S.; Zhang, X.; Cooks, R. G., High yield accelerated reactions in nonvolatile microthin films: chemical derivatization for analysis of single-cell intracellular fluid. *Chemical Science* **2018,** *9* (40), 7779-7786.

24. Banerjee, S.; Sathyamoorthi, S.; Du Bois, J.; Zare, R. N., Mechanistic analysis of a copper-catalyzed C–H oxidative cyclization of carboxylic acids. *Chemical Science* **2017,** *8* (10), 7003-7008.

25. Chen, S.; Wan, Q.; Badu‐Tawiah, A. K., Picomole‐scale real‐time photoreaction screening: discovery of the visible‐light‐promoted dehydrogenation of tetrahydroquinolines under ambient conditions. *Angewandte Chemie* **2016,** *128* (32), 9491-9495.

26. Banerjee, S.; Basheer, C.; Zare, R. N., A study of heterogeneous catalysis by nanoparticle‐embedded paper‐spray ionization mass spectrometry. *Angewandte Chemie International Edition* **2016,** *55* (41), 12807-12811.

27. Yan, X.; Sokol, E.; Li, X.; Li, G.; Xu, S.; Cooks, R. G., On‐line reaction monitoring and mechanistic studies by mass spectrometry: Negishi cross‐coupling, hydrogenolysis, and reductive amination. *Angewandte Chemie International Edition* **2014,** *53* (23), 5931-5935.

28. Wleklinski, M.; Loren, B. P.; Ferreira, C. R.; Jaman, Z.; Avramova, L.; Sobreira, T. J.; Thompson, D. H.; Cooks, R. G., High throughput reaction screening using desorption electrospray ionization mass spectrometry. *Chemical Science* **2018,** *9* (6), 1647-1653.

29. Li, J.; Liu, C.; Chen, H.; Zare, R. N., Accelerated Oxidation of Organic Sulfides by Microdroplet Chemistry. *The Journal of Organic Chemistry* **2021,** *86* (7), 5011-5015.

30. Nie, H.; Wei, Z.; Qiu, L.; Chen, X.; Holden, D. T.; Cooks, R. G., High-yield gram-scale organic synthesis using accelerated microdroplet/thin film reactions with solvent recycling. *Chemical Science* **2020,** *11* (9), 2356-2361.

31. Liu, C.; Li, J.; Chen, H.; Zare, R. N., Scale-up of microdroplet reactions by heated ultrasonic nebulization. *Chemical Science* **2019,** *10* (40), 9367-9373.

32. Brownridge, P.; Beynon, R. J., The importance of the digest: proteolysis and absolute quantification in proteomics. *Methods* **2011,** *54* (4), 351-360.

33. He, Y.; Zhong, W.; Yeung, E. S., Multiplexed on-column protein digestion and capillary electrophoresis for high-throughput comprehensive peptide mapping. *Journal of Chromatography B* **2002,** *782* (1-2), 331-341.

34. Proc, J. L.; Kuzyk, M. A.; Hardie, D. B.; Yang, J.; Smith, D. S.; Jackson, A. M.; Parker, C. E.; Borchers, C. H., A quantitative study of the effects of chaotropic agents, surfactants, and solvents on the digestion efficiency of human plasma proteins by trypsin. *Journal of Proteome Research* **2010,** *9* (10), 5422-5437.

35. Switzar, L.; Giera, M.; Lingeman, H.; Irth, H.; Niessen, W. M., Protein digestion optimization for characterization of drug–protein adducts using response surface modeling. *Journal of Chromatography A* **2011,** *1218* (13), 1715-1723.

36. Norrgran, J.; Williams, T. L.; Woolfitt, A. R.; Solano, M. I.; Pirkle, J. L.; Barr, J. R., Optimization of digestion parameters for protein quantification. *Analytical Biochemistry* **2009,** *393* (1), 48-55.

37. Park, Z.-Y.; Russell, D. H., Thermal denaturation: a useful technique in peptide mass mapping. *Analytical Chemistry* **2000,** *72* (11), 2667-2670.

38. Bark, S. J.; Muster, N.; Yates, J. R.; Siuzdak, G., High-temperature protein mass mapping using a thermophilic protease. *Journal of the American Chemical Society* **2001,** *123* (8), 1774-1775.

39. Gao, M.; Deng, C.; Zhang, X., Magnetic nanoparticles-based digestion and enrichment methods in proteomics analysis. *Expert Review of Proteomics* **2011,** *8* (3), 379-390.

40. Ji, J.; Zhang, Y.; Zhou, X.; Kong, J.; Tang, Y.; Liu, B., Enhanced protein digestion through the confinement of nanozeolite-assembled microchip reactors. *Analytical Chemistry* **2008,** *80* (7), 2457-2463.

41. Dulay, M. T.; Eberlin, L. S.; Zare, R. N., Protein analysis by ambient ionization mass spectrometry using trypsin-immobilized organosiloxane polymer surfaces. *Analytical Chemistry* **2015,** *87* (24), 12324-12330.

42. Zheng, Q.; Zhang, H.; Chen, H., Integration of online digestion and electrolytic reduction with mass spectrometry for rapid disulfide-containing protein structural analysis. *International Journal of Mass Spectrometry* **2013,** *353*, 84-92.

43. Russell, W. K.; Park, Z.-Y.; Russell, D. H., Proteolysis in mixed organic− aqueous solvent systems: applications for peptide mass mapping using mass spectrometry. *Analytical Chemistry* **2001,** *73* (11), 2682-2685.

44. Wall, M. J.; Crowell, A. M.; Simms, G. A.; Liu, F.; Doucette, A. A., Implications of partial tryptic digestion in organic–aqueous solvent systems for bottom-up proteome analysis. *Analytica Chimica Acta* **2011,** *703* (2), 194-203.

45. Kang, J.; Hick, L. A.; Price, W. E., Using calibration approaches to compensate for remaining matrix effects in quantitative liquid chromatography/electrospray ionization multistage mass spectrometric analysis of phytoestrogens in aqueous environmental samples. *Rapid Communications in Mass Spectrometry: An International Journal Devoted to the Rapid Dissemination of Up‐to‐the‐Minute Research in Mass Spectrometry* **2007,** *21* (24), 4065-4072.

46. Lopez-Ferrer, D.; Capelo, J.; Vazquez, J., Ultra fast trypsin digestion of proteins by high intensity focused ultrasound. *Journal of Proteome Research* **2005,** *4* (5), 1569-1574.

47. Basile, F.; Hauser, N., Rapid online nonenzymatic protein digestion combining microwave heating acid hydrolysis and electrochemical oxidation. *Analytical Chemistry* **2011,** *83* (1), 359-367.

48. Zhong, X.; Chen, H.; Zare, R. N., Ultrafast enzymatic digestion of proteins by microdroplet mass spectrometry. *Nature Communications* **2020,** *11* (1), 1049.

49. Rainer, T.; Eidelpes, R.; Tollinger, M.; Müller, T., Microdroplet Mass Spectrometry Enables Extremely Accelerated Pepsin Digestion of Proteins. *Journal of the American Society for Mass Spectrometry* **2021,** *32* (7), 1841-1845.

50. Ma, C.-H.; Chen, C.-L.; Hsu, C.-C., Real-time bottom-up characterization of protein mixtures enabled by online microdroplet-assisted enzymatic digestion (MAED). *Chemical Communications* **2023,** *59* (84), 12585-12588.

51. Aebersold, R.; Burlingame, A. L.; Bradshaw, R. A., Western blots versus selected reaction monitoring assays: time to turn the tables? *Molecular & Cellular Proteomics* **2013,** *12* (9), 2381-2382.

52. Hoofnagle, A. N.; Wener, M. H., The fundamental flaws of immunoassays and potential solutions using tandem mass spectrometry. *Journal of Immunological Methods* **2009,** *347* (1-2), 3-11.

53. Pan, S.; Aebersold, R.; Chen, R.; Rush, J.; Goodlett, D. R.; McIntosh, M. W.; Zhang, J.; Brentnall, T. A., Mass spectrometry based targeted protein quantification: methods and applications. *Journal of Proteome Research* **2009,** *8* (2), 787-797.

54. Hawkridge, A. M., Practical considerations and current limitations in quantitative mass spectrometry-based proteomics. In *Quantitative Proteomics*, Eyers, C. E.; Gaskell, S., Eds. The Royal Society of Chemistry: 2014.

55. Gygi, S. P.; Rist, B.; Gerber, S. A.; Turecek, F.; Gelb, M. H.; Aebersold, R., Quantitative analysis of complex protein mixtures using isotope-coded affinity tags. *Nature Biotechnology* **1999,** *17* (10), 994-999.

56. Han, D. K.; Eng, J.; Zhou, H.; Aebersold, R., Quantitative profiling of differentiation-induced microsomal proteins using isotope-coded affinity tags and mass spectrometry. *Nature Biotechnology* **2001,** *19* (10), 946-951.

57. Ong, S.-E.; Foster, L. J.; Mann, M., Mass spectrometric-based approaches in quantitative proteomics. *Methods* **2003,** *29* (2), 124-130.

58. Sechi, S.; Oda, Y., Quantitative proteomics using mass spectrometry. *Current Opinion in Chemical Biology* **2003,** *7* (1), 70-77.

59. Goshe, M. B.; Smith, R. D., Stable isotope-coded proteomic mass spectrometry. *Current Opinion in Biotechnology* **2003,** *14* (1), 101-109.

60. Tao, W. A.; Aebersold, R., Advances in quantitative proteomics via stable isotope tagging and mass spectrometry. *Current Opinion in Biotechnology* **2003,** *14* (1), 110-118.

61. Ong, S.-E.; Mann, M., Mass spectrometry–based proteomics turns quantitative. *Nature Chemical Biology* **2005,** *1* (5), 252-262.

62. Regnier, F. E.; Julka, S., Primary amine coding as a path to comparative proteomics. *Proteomics* **2006,** *6* (14), 3968-3979.

63. Yao, X.; Freas, A.; Ramirez, J.; Demirev, P. A.; Fenselau, C., Proteolytic 18O labeling for comparative proteomics: model studies with two serotypes of adenovirus. *Analytical Chemistry* **2001,** *73* (13), 2836-2842.

64. Stewart, I. I.; Thomson, T.; Figeys, D., 18O labeling: a tool for proteomics. *Rapid Communications in Mass Spectrometry* **2001,** *15* (24), 2456-2465.

65. Thompson, A.; Schäfer, J.; Kuhn, K.; Kienle, S.; Schwarz, J.; Schmidt, G.; Neumann, T.; Hamon, C., Tandem mass tags: a novel quantification strategy for comparative analysis of complex protein mixtures by MS/MS. *Analytical Chemistry* **2003,** *75* (8), 1895-1904.

66. Ross, P. L.; Huang, Y. N.; Marchese, J. N.; Williamson, B.; Parker, K.; Hattan, S.; Khainovski, N.; Pillai, S.; Dey, S.; Daniels, S., Multiplexed protein quantitation in Saccharomyces cerevisiae using amine-reactive isobaric tagging reagents. *Molecular & Cellular Proteomics* **2004,** *3* (12), 1154-1169.

67. Oda, Y.; Huang, K.; Cross, F.; Cowburn, D.; Chait, B., Accurate quantitation of protein expression and site-specific phosphorylation. *Proceedings of the National Academy of Sciences* **1999,** *96* (12), 6591-6596.

68. Ong, S.-E.; Blagoev, B.; Kratchmarova, I.; Kristensen, D. B.; Steen, H.; Pandey, A.; Mann, M., Stable isotope labeling by amino acids in cell culture, SILAC, as a simple and accurate approach to expression proteomics. *Molecular & Cellular Proteomics* **2002,** *1* (5), 376-386.

69. Berger, S. J.; Lee, S.-W.; Anderson, G. A.; Paša-Tolić, L.; Tolić, N.; Shen, Y.; Zhao, R.; Smith, R. D., High-throughput global peptide proteomic analysis by combining stable isotope amino acid labeling and data-dependent multiplexed-MS/MS. *Analytical Chemistry* **2002,** *74* (19), 4994-5000.

70. Zhu, H.; Pan, S.; Gu, S.; Bradbury, E. M.; Chen, X., Amino acid residue specific stable isotope labeling for quantitative proteomics. *Rapid Communications in Mass Spectrometry* **2002,** *16* (22), 2115-2123.

71. Svantesson, E.; Pettersson, J.; Markides, K. E., The use of inorganic elemental standards in the quantification of proteins and biomolecular compounds by inductively coupled plasma spectrometry. *Journal of Analytical Atomic Spectrometry* **2002,** *17* (5), 491-496.

72. Sanz-Medel, A.; Montes-Bayón, M.; Bettmer, J.; Fernández-Sanchez, M. L.; Encinar, J. R., ICP-MS for absolute quantification of proteins for heteroatom-tagged, targeted proteomics. *TrAC Trends in Analytical Chemistry* **2012,** *40*, 52-63.

73. Łobiński, R.; Schaumlöffel, D.; Szpunar, J., Mass spectrometry in bioinorganic analytical chemistry. *Mass Spectrometry Reviews* **2006,** *25* (2), 255-289.

74. Sanz-Medel, A.; Montes-Bayón, M.; del Rosario Fernández de la Campa, M.; Encinar, J. R.; Bettmer, J., Elemental mass spectrometry for quantitative proteomics. *Analytical and Bioanalytical Chemistry* **2008,** *390*, 3-16.

75. Calderón‐Celis, F.; Encinar, J. R.; Sanz‐Medel, A., Standardization approaches in absolute quantitative proteomics with mass spectrometry. *Mass Spectrometry Reviews* **2018,** *37* (6), 715-737.

76. Ankney, J. A.; Muneer, A.; Chen, X., Relative and absolute quantitation in mass spectrometry–based proteomics. *Annual Review of Analytical Chemistry* **2018,** *11*, 49-77.

77. Ishihama, Y.; Oda, Y.; Tabata, T.; Sato, T.; Nagasu, T.; Rappsilber, J.; Mann, M., Exponentially modified protein abundance index (emPAI) for estimation of absolute protein amount in proteomics by the number of sequenced peptides per protein* s. *Molecular & Cellular Proteomics* **2005,** *4* (9), 1265-1272.

78. Lu, P.; Vogel, C.; Wang, R.; Yao, X.; Marcotte, E. M., Absolute protein expression profiling estimates the relative contributions of transcriptional and translational regulation. *Nature Biotechnology* **2007,** *25* (1), 117-124.

79. Brun, V.; Masselon, C.; Garin, J.; Dupuis, A., Isotope dilution strategies for absolute quantitative proteomics. *Journal of Proteomics* **2009,** *72* (5), 740-749.

80. Gerber, S. A.; Rush, J.; Stemman, O.; Kirschner, M. W.; Gygi, S. P., Absolute quantification of proteins and phosphoproteins from cell lysates by tandem MS. *Proceedings of the National Academy of Sciences* **2003,** *100* (12), 6940-6945.

81. Kirkpatrick, D. S.; Gerber, S. A.; Gygi, S. P., The absolute quantification strategy: a general procedure for the quantification of proteins and post-translational modifications. *Methods* **2005,** *35* (3), 265-273.

82. Gallien, S.; Duriez, E.; Crone, C.; Kellmann, M.; Moehring, T.; Domon, B., Targeted proteomic quantification on quadrupole-orbitrap mass spectrometer. *Molecular & Cellular Proteomics* **2012,** *11* (12), 1709-1723.

83. Schmidt, C.; Urlaub, H., Absolute quantification of proteins using standard peptides and multiple reaction monitoring. *Quantitative Methods in Proteomics* **2012**, 249-265.

84. Beynon, R. J.; Doherty, M. K.; Pratt, J. M.; Gaskell, S. J., Multiplexed absolute quantification in proteomics using artificial QCAT proteins of concatenated signature peptides. *Nature Methods* **2005,** *2* (8), 587-589.

85. Hoofnagle, A. N., Quantitative clinical proteomics by liquid chromatography–tandem mass spectrometry: assessing the platform. *Clinical Chemistry* **2010,** *56* (2), 161-164.

86. Zhou, H.; Ning, Z.; E. Starr, A.; Abu-Farha, M.; Figeys, D., Advancements in top-down proteomics. *Analytical Chemistry* **2012,** *84* (2), 720-734.

87. Gregorich, Z. R.; Ge, Y., Top‐down proteomics in health and disease: Challenges and opportunities. *Proteomics* **2014,** *14* (10), 1195-1210.

88. Brun, V.; Dupuis, A.; Adrait, A.; Marcellin, M.; Thomas, D.; Vandenesch, F. o.; Garin, J. r. m., Isotope-labeled protein standards: toward absolute quantitative proteomics. *Molecular & Cellular Proteomics* **2007,** *6* (12), 2139-2149.

89. Hanke, S.; Besir, H.; Oesterhelt, D.; Mann, M., Absolute SILAC for accurate quantitation of proteins in complex mixtures down to the attomole level. *Journal of Proteome Research* **2008,** *7* (3), 1118-1130.

90. Diehl, G.; Karst, U., On-line electrochemistry – MS and related techniques. *Analytical and Bioanalytical Chemistry* **2002,** *373* (6), 390-398.

91. Permentier, H. P.; Bruins, A. P.; Bischoff, R., Electrochemistry-mass spectrometry in drug metabolism and protein research. *Mini Reviews in Medicinal Chemistry* **2008,** *8* (1), 46-56.

92. Li, J.; Dewald, H. D.; Chen, H., Online Coupling of Electrochemical Reactions with Liquid Sample Desorption Electrospray Ionization-Mass Spectrometry. *Analytical Chemistry* **2009,** *81* (23), 9716-9722.

93. Chintalapudi, K.; Badu-Tawiah, A. K., An integrated electrocatalytic nESI-MS platform for quantification of fatty acid isomers directly from untreated biofluids. *Chemical Science* **2020,** *11* (36), 9891-9897.

94. Tang, S.; Fan, L.; Cheng, H.; Yan, X., Incorporating Electro-Epoxidation into Electrospray Ionization Mass Spectrometry for Simultaneous Analysis of Negatively and Positively Charged Unsaturated Glycerophospholipids. *Journal of the American Society for Mass Spectrometry* **2021,** *32* (9), 2288-2295.

95. Zhang, X.; Zhan, J.; Yu, Z.; Deng, J.; Li, M.; Shao, Y., Recent Advances in Real-Time Analysis of Electrochemical Reactions by Electrochemical Mass Spectrometry†. *Chinese Journal of Chemistry* **2023,** *41* (2), 214-224.

96. Hu, J.; Zhang, N.; Zhang, P. K.; Chen, Y.; Xia, X. H.; Chen, H. Y.; Xu, J. J., Coupling a Wireless Bipolar Ultramicroelectrode with Nano‐electrospray Ionization Mass Spectrometry: Insights into the Ultrafast Initial Step of Electrochemical Reactions. *Angewandte Chemie* **2020,** *132* (41), 18401-18405.

97. Brown, T. A.; Chen, H.; Zare, R. N., Identification of fleeting electrochemical reaction intermediates using desorption electrospray ionization mass spectrometry. *Journal of the American Chemical Society* **2015,** *137* (23), 7274-7277.

98. Brown, T. A.; Chen, H.; Zare, R. N., Detection of the short‐lived radical cation intermediate in the electrooxidation of N, N‐dimethylaniline by mass spectrometry. *Angewandte Chemie* **2015,** *127* (38), 11335-11337.

99. Qiu, R.; Zhang, X.; Luo, H.; Shao, Y., Mass spectrometric snapshots for electrochemical reactions. *Chemical Science* **2016,** *7* (11), 6684-6688.

100. Yu, J.; Zhou, Y.; Hua, X.; Liu, S.; Zhu, Z.; Yu, X.-Y., Capturing the transient species at the electrode–electrolyte interface by in situ dynamic molecular imaging. *Chemical Communications* **2016,** *52* (73), 10952-10955.

101. Wang, Z.; Zhang, Y.; Liu, B.; Wu, K.; Thevuthasan, S.; Baer, D. R.; Zhu, Z.; Yu, X.-Y.; Wang, F., In situ mass spectrometric monitoring of the dynamic electrochemical process at the electrode–electrolyte interface: a SIMS approach. *Analytical Chemistry* **2017,** *89* (1), 960-965.

102. Khanipour, P.; Löffler, M.; Reichert, A. M.; Haase, F. T.; Mayrhofer, K. J.; Katsounaros, I., Electrochemical real‐time mass spectrometry (EC‐RTMS): monitoring electrochemical reaction products in real time. *Angewandte Chemie International Edition* **2019,** *58* (22), 7273-7277.

103. Hasa, B.; Jouny, M.; Ko, B. H.; Xu, B.; Jiao, F., Flow Electrolyzer Mass Spectrometry with a Gas‐Diffusion Electrode Design. *Angewandte Chemie International Edition* **2021,** *60* (6), 3277-3282.

104. Liu, J.; Yu, K.; Zhang, H.; He, J.; Jiang, J.; Luo, H., Mass spectrometric detection of fleeting neutral intermediates generated in electrochemical reactions. *Chemical Science* **2021,** *12* (27), 9494-9499.

105. Hu, J.; Wang, T.; Zhang, W. J.; Hao, H.; Yu, Q.; Gao, H.; Zhang, N.; Chen, Y.; Xia, X. H.; Chen, H. Y., Dissecting the flash chemistry of electrogenerated reactive intermediates by microdroplet fusion mass spectrometry. *Angewandte Chemie International Edition* **2021,** *60* (34), 18494-18498.

106. Wan, Q.; Chen, S.; Badu-Tawiah, A. K., An integrated mass spectrometry platform enables picomole-scale real-time electrosynthetic reaction screening and discovery. *Chemical Science* **2018,** *9* (26), 5724-5729.

107. Wang, Q.; Wang, Q.; Zhang, Y.; Mohamed, Y. M.; Pacheco, C.; Zheng, N.; Zare, R. N.; Chen, H., Electrocatalytic redox neutral [3+ 2] annulation of N-cyclopropylanilines and alkenes. *Chemical Science* **2021,** *12* (3), 969-975.

108. Cheng, H.; Yang, T.; Edwards, M.; Tang, S.; Xu, S.; Yan, X., Picomole-Scale Transition Metal Electrocatalysis Screening Platform for Discovery of Mild C–C Coupling and C–H Arylation through in Situ Anodically Generated Cationic Pd. *Journal of the American Chemical Society* **2022,** *144* (3), 1306-1312.

109. Xu, C.; Zheng, Q.; Zhao, P.; Paterson, J.; Chen, H., A new quantification method using electrochemical mass spectrometry. *Journal of The American Society for Mass Spectrometry* **2019,** *30* (4), 685-693.

110. Zhao, M.; Liu, X.; Hou, Y.; Yang, T.; Xu, J.; Su, R., Combination of Electrochemistry and Mass Spectrometry to Study Nitric Oxide Metabolism and Its Modulation by Compound K in Breast Cancer Cells. *Analytical Chemistry* **2022,** *94* (12), 5122-5131.

111. D'Eramo, F.; Marioli, J. M.; Arévalo, A. A.; Sereno, L. E., HPLC Analysis of Carbohydrates with Electrochemical Detection at a Poly - 1 - naphthylamine/Copper Modified Electrode. *Electroanalysis: An International Journal Devoted to Fundamental and Practical Aspects of Electroanalysis* **1999,** *11* (7), 481-486.

112. Pappa-Louisi, A.; Papageorgiou, A.; Zitrou, A.; Sotiropoulos, S.; Georgarakis, E.; Zougrou, F., Study on the electrochemical detection of the macrolide antibiotics clarithromycin and roxithromycin in reversed-phase high-performance liquid chromatography. *Journal of Chromatography B: Biomedical Sciences and Applications* **2001,** *755* (1-2), 57-64.

113. Schmidt, D.; Roznoski, M.; Ebert, M. H., Qualitative and quantitative high performance liquid chromatographic analysis of monoamine neurotransmitters and metabolites in cerebrospinal fluid and brain tissue using reductive electrochemical detection. *Biomedical Chromatography* **1990,** *4* (5), 215-220.

114. Zhao, P.; Guo, Y.; Dewald, H. D.; Chen, H., Improvements for absolute quantitation using electrochemical mass spectrometry. *International Journal of Mass Spectrometry* **2019,** *443*, 41-45.

115. Zhao, P.; Zare, R. N.; Chen, H., Absolute quantitation of oxidizable peptides by coulometric mass spectrometry. *Journal of the American Society for Mass Spectrometry* **2019,** *30* (11), 2398-2407.

116. Poole, L. B., The basics of thiols and cysteines in redox biology and chemistry. *Free Radical Biology and Medicine* **2015,** *80*, 148-157.

117. Harriman, A., Further comments on the redox potentials of tryptophan and tyrosine. *Journal of Physical Chemistry* **1987,** *91* (24), 6102-6104.

118. Scuderi, D.; Bergès, J.; De Oliveira, P.; Houée-Levin, C., Methionine one-electron oxidation: Coherent contributions from radiolysis, IRMPD spectroscopy, DFT calculations and electrochemistry. *Radiation Physics and Chemistry* **2016,** *128*, 103-111.

119. Whiteaker, J. R.; Lin, C.; Kennedy, J.; Hou, L.; Trute, M.; Sokal, I.; Yan, P.; Schoenherr, R. M.; Zhao, L.; Voytovich, U. J., A targeted proteomics–based pipeline for verification of biomarkers in plasma. *Nature Biotechnology* **2011,** *29* (7), 625-634.

120. Kellie, J. F.; Tran, J. C.; Jian, W.; Jones, B.; Mehl, J. T.; Ge, Y.; Henion, J.; Bateman, K. P., Intact protein mass spectrometry for therapeutic protein quantitation, pharmacokinetics, and biotransformation in preclinical and clinical studies: an industry perspective. *Journal of the American Society for Mass Spectrometry* **2020,** *32* (8), 1886-1900.

121. Jenkins, R.; Duggan, J. X.; Aubry, A.-F.; Zeng, J.; Lee, J. W.; Cojocaru, L.; Dufield, D.; Garofolo, F.; Kaur, S.; Schultz, G. A., Recommendations for validation of LC-MS/MS bioanalytical methods for protein biotherapeutics. *The AAPS Journal* **2015,** *17*, 1-16.

122. Zhao, P.; Wang, Q.; Kaur, M.; Kim, Y.-I.; Dewald, H. D.; Mozziconacci, O.; Liu, Y.; Chen, H., Absolute Quantitation of Proteins by Coulometric Mass Spectrometry. *Analytical Chemistry* **2020,** *92* (11), 7877-7883.

123. Banerjee, S.; Zare, R. N., Syntheses of isoquinoline and substituted quinolines in charged microdroplets. *Angewandte Chemie International Edition* **2015,** *127* (49), 15008-15012.

124. Yan, X., Emerging microdroplet chemistry for synthesis and analysis. *International Journal of Mass Spectrometry* **2021,** *468*, 116639.

125. Yan, X.; Bain, R. M.; Cooks, R. G., Organic reactions in microdroplets: Reaction acceleration revealed by mass spectrometry. *Angewandte Chemie International Edition* **2016,** *55* (42), 12960-12972.

126. Mondal, S.; Acharya, S.; Biswas, R.; Bagchi, B.; Zare, R. N., Enhancement of reaction rate in small-sized droplets: A combined analytical and simulation study. *Journal of Chemical Physics* **2018,** *148* (24), 244704.

127. Zhou, Z.; Yan, X.; Lai, Y.-H.; Zare, R. N., Fluorescence polarization anisotropy in microdroplets. *The Journal of Physical Chemistry Letters* **2018,** *9* (11), 2928-2932.

128. Banerjee, S.; Zare, R. N., Influence of inlet capillary temperature on the microdroplet chemistry studied by mass spectrometry. *The Journal of Physical Chemistry A* **2019,** *123* (36), 7704-7709.

129. Hao, H.; Leven, I.; Head-Gordon, T., Can electric fields drive chemistry for an aqueous microdroplet? *Nature Communications* **2022,** *13* (1), 1-8.

130. Heiss, D. R.; Badu-Tawiah, A. K., In-Source Microdroplet Derivatization Using Coaxial Contained-Electrospray Mass Spectrometry for Enhanced Sensitivity in Saccharide Analysis. *Analytical Chemistry* **2021,** *93* (50), 16779-16786.

131. Sarkar, D.; Mahitha, M. K.; Som, A.; Li, A.; Wleklinski, M.; Cooks, R. G.; Pradeep, T., Metallic nanobrushes made using ambient droplet sprays. *Advanced Materials* **2016,** *28* (11), 2223-2228.

132. He, X.; Gan, Z.; Fisenko, S.; Wang, D.; El-Kaderi, H. M.; Wang, W.-N., Rapid formation of metal–organic frameworks (MOFs) based nanocomposites in microdroplets and their applications for CO2 photoreduction. *ACS Applied Materials & Interfaces* **2017,** *9* (11), 9688-9698.

133. Li, X.; Cao, Y.; Luo, K.; Sun, Y.; Xiong, J.; Wang, L.; Liu, Z.; Li, J.; Ma, J.; Ge, J., Highly active enzyme–metal nanohybrids synthesized in protein–polymer conjugates. *Nature Catalysis* **2019,** *2* (8), 718-725.

134. Zhong, X.; Chen, H.; Zare, R. N., Ultrafast enzymatic digestion of proteins by microdroplet mass spectrometry. *Nature Communications* **2020,** *11* (1), 1-9.

135. Zhao, P.; Gunawardena, H. P.; Zhong, X.; Zare, R. N.; Chen, H., Microdroplet ultrafast reactions speed antibody characterization. *Analytical Chemistry* **2021,** *93* (8), 3997-4005.

136. Burris, B. J.; Badu-Tawiah, A. K., Enzyme-Catalyzed Hydrolysis of Lipids in Immiscible Microdroplets Studied by Contained-Electrospray Ionization. *Analytical Chemistry* **2021,** *93* (38), 13001-13007.

137. Gong, C.; Li, D.; Li, X.; Zhang, D.; Xing, D.; Zhao, L.; Yuan, X.; Zhang, X., Spontaneous Reduction-Induced Degradation of Viologen Compounds in Water Microdroplets and Its Inhibition by Host–Guest Complexation. *Journal of the American Chemical Society* **2022,** *144* (8), 3510–3516.

138. Carvalho, L. B.; Capelo-Martinez, J.-L.; Lodeiro, C.; Wisniewski, J. R.; Santos, H. M., Ultrasonic-Based Filter Aided Sample Preparation as the General Method to Sample Preparation in Proteomics. *Analytical Chemistry* **2020,** *92* (13), 9164-9171.

139. Mouchahoir, T.; Schiel, J. E., Development of an LC-MS/MS peptide mapping protocol for the NISTmAb. *Analytical and Bioanalytical Chemistry* **2018,** *410* (8), 2111-2126.

140. Rivera-Albarran, M. E.; Ray, S. J., A Novel Combined Microstrip Resonator/Nanospray Ionization Source for Microwave-Assisted Trypsin Digestion of Proteins. *Journal of the American Society for Mass Spectrometry* **2020,** *31* (8), 1684-1696.

141. Wang, Y.; Zhang, W.; Ouyang, Z., Fast protein analysis enabled by high-temperature hydrolysis. *Chemical Science* **2020,** *11* (38), 10506-10516.

142. Kaplon, H.; Reichert, J. M., Antibodies to watch in 2021. *MAbs* **2021,** *13* (1), 1860476.

143. Zitvogel, L.; Kroemer, G., Antibodies regulate antitumour immunity. *Nature* **2015,** *521* (7550), 35-37.

144. Chen, L.; Han, X., Anti-PD-1/PD-L1 therapy of human cancer: past, present, and future. *Journal of Clinical Investigation* **2015,** *125* (9), 3384-91.

145. Chen, D. S.; Mellman, I., Oncology meets immunology: the cancer-immunity cycle. *Immunity* **2013,** *39* (1), 1-10.

146. Tsumoto, K.; Isozaki, Y.; Yagami, H.; Tomita, M., Future perspectives of therapeutic monoclonal antibodies. *Immunotherapy* **2019,** *11* (2), 119-127.

147. Vlasak, J.; Ionescu, R., Heterogeneity of monoclonal antibodies revealed by charge-sensitive methods. *Current Pharmaceutical Biotechnology* **2008,** *9* (6), 468-481.

148. Jenkins, N.; Murphy, L.; Tyther, R., Post-translational Modifications of Recombinant Proteins: Significance for Biopharmaceuticals. *Molecular Biotechnology* **2008,** *39* (2), 113-118.

149. Manning, M. C.; Chou, D. K.; Murphy, B. M.; Payne, R. W.; Katayama, D. S., Stability of protein pharmaceuticals: an update. *Pharmaceutical Research* **2010,** *27* (4), 544-575.

150. Gupta, S.; Jiskoot, W.; Schöneich, C.; Rathore, A. S., Oxidation and deamidation of monoclonal antibody products: potential impact on stability, biological activity, and efficacy. *Journal of Pharmaceutical Sciences* **2022,** *111* (4), 903-918.

151. Liu, H.; Gaza-Bulseco, G.; Faldu, D.; Chumsae, C.; Sun, J., Heterogeneity of monoclonal antibodies. *Journal of Pharmaceutical Sciences* **2008,** *97* (7), 2426-2447.

152. Timm, V.; Gruber, P.; Wasiliu, M.; Lindhofer, H.; Chelius, D., Identification and characterization of oxidation and deamidation sites in monoclonal rat/mouse hybrid antibodies. *Journal of Chromatography B* **2010,** *878* (9-10), 777-784.

153. Bertolotti-Ciarlet, A.; Wang, W.; Lownes, R.; Pristatsky, P.; Fang, Y.; McKelvey, T.; Li, Y.; Li, Y.; Drummond, J.; Prueksaritanont, T., Impact of methionine oxidation on the binding of human IgG1 to FcRn and Fcγ receptors. *Molecular Immunology* **2009,** *46* (8-9), 1878-1882.

154. Wang, Y.; Li, X.; Liu, Y.-H.; Richardson, D.; Li, H.; Shameem, M.; Yang, X. In *Simultaneous monitoring of oxidation, deamidation, isomerization, and glycosylation of monoclonal antibodies by liquid chromatography-mass spectrometry method with ultrafast tryptic digestion*, MAbs, Taylor & Francis: 2016; pp 1477-1486.

155. Boll, B. r.; Bessa, J.; Folzer, E.; Ríos Quiroz, A.; Schmidt, R.; Bulau, P.; Finkler, C.; Mahler, H.-C.; Huwyler, J. r.; Iglesias, A., Extensive chemical modifications in the primary protein structure of IgG1 subvisible particles are necessary for breaking immune tolerance. *Molecular Pharmaceutics* **2017,** *14* (4), 1292-1299.

156. Pavon, J. A.; Li, X.; Chico, S.; Kishnani, U.; Soundararajan, S.; Cheung, J.; Li, H.; Richardson, D.; Shameem, M.; Yang, X., Analysis of monoclonal antibody oxidation by simple mixed mode chromatography. *Journal of Chromatography A* **2016,** *1431*, 154-165.

157. Rogers, R. S.; Nightlinger, N. S.; Livingston, B.; Campbell, P.; Bailey, R.; Balland, A. In *Development of a quantitative mass spectrometry multi-attribute method for characterization, quality control testing and disposition of biologics*, MAbs, Taylor & Francis: 2015; pp 881-890.

158. Stroop, S. D., A modified peptide mapping strategy for quantifying site‐specific deamidation by electrospray time‐of‐flight mass spectrometry. *Rapid Communications in Mass Spectrometry* **2007,** *21* (6), 830-836.

159. Hirabayashi, A.; Sakairi, M.; Koizumi, H., Sonic spray ionization method for atmospheric pressure ionization mass spectrometry. *Analytical Chemistry* **1994,** *66* (24), 4557-4559.

160. Dulay, M. T.; Chamberlayne, C. F.; Zare, R. N., Optimizing Coaxial Sonic Spray Geometry for Generating Water Microdroplets. *Analytical Chemistry* **2022**.

161. Kamat, M.; Basso, K. B., Surprising Increase in Distinct Tryptic Peptide Counts at Low Temperature and Short Digestion Times. In *69th ASMS*, Pennsylvania Convention Center | Philadelphia, PA, USA, 2021.

162. Somiari, R. I.; Renganathan, K.; Russell, S.; Wolfe, S.; Mayko, F.; Somiari, S. B., A colorimetric method for monitoring tryptic digestion prior to shotgun proteomics. *International Journal of Proteomics* **2014,** *2014*.

163. Dick Jr, L. W.; Mahon, D.; Qiu, D.; Cheng, K.-C., Peptide mapping of therapeutic monoclonal antibodies: Improvements for increased speed and fewer artifacts. *Journal of Chromatography B* **2009,** *877* (3), 230-236.

164. Hall, T.; Sandefur, S. L.; Frye, C. C.; Tuley, T. L.; Huang, L., Polysorbates 20 and 80 degradation by group XV lysosomal phospholipase A2 isomer X1 in monoclonal antibody formulations. *Journal of Pharmaceutical Sciences* **2016,** *105* (5), 1633-1642.

165. Labrenz, S. R., Ester hydrolysis of polysorbate 80 in mAb drug product: evidence in support of the hypothesized risk after the observation of visible particulate in mAb formulations. *Journal of Pharmaceutical Sciences* **2014,** *103* (8), 2268-2277.

166. Picotti, P.; Aebersold, R.; Domon, B., The implications of proteolytic background for shotgun proteomics. *Molecular & Cellular Proteomics* **2007,** *6* (9), 1589-1598.

167. Kim, J.-S.; Monroe, M. E.; Camp, D. G.; Smith, R. D.; Qian, W.-J., In-source fragmentation and the sources of partially tryptic peptides in shotgun proteomics. *Journal of Proteome Research* **2013,** *12* (2), 910-916.

168. Alves, G.; Yu, Y.-K., Improving peptide identification sensitivity in shotgun proteomics by stratification of search space. *Journal of Proteome Research* **2013,** *12* (6), 2571-2581.

169. Fang, P.; Liu, M.; Xue, Y.; Yao, J.; Zhang, Y.; Shen, H.; Yang, P., Controlling nonspecific trypsin cleavages in LC-MS/MS-based shotgun proteomics using optimized experimental conditions. *Analyst* **2015,** *140* (22), 7613-7621.

170. Nigam, A.; Subramanian, M.; Koiram Rajanna, P., Non-specific digestion artifacts of bovine trypsin exemplified with surrogate peptides for endogenous protein quantitation. *Chromatographia* **2018,** *81* (1), 57-64.

171. Niu, B.; Martinelli II, M.; Jiao, Y.; Wang, C.; Cao, M.; Wang, J.; Meinke, E., Nonspecific cleavages arising from reconstitution of trypsin under mildly acidic conditions. *PloS one* **2020,** *15* (7), e0236740.

172. Fonslow, B. R.; Stein, B. D.; Webb, K. J.; Xu, T.; Choi, J.; Park, S. K.; Yates III, J. R., Digestion and depletion of abundant proteins improves proteomic coverage. *Nature Methods* **2013,** *10* (1), 54-56.

173. Huang, L.; Wang, N.; Mitchell, C. E.; Brownlee, T.; Maple, S. R.; De Felippis, M. R., A novel sample preparation for shotgun proteomics characterization of HCPs in antibodies. *Analytical chemistry* **2017,** *89* (10), 5436-5444.

174. Ohtake, S.; Shalaev, E., Effect of water on the chemical stability of amorphous pharmaceuticals: I. Small molecules. *Journal of Pharmaceutical Sciences* **2013,** *102* (4), 1139-1154.

175. Sydow, J. F.; Lipsmeier, F.; Larraillet, V.; Hilger, M.; Mautz, B.; Mølhøj, M.; Kuentzer, J.; Klostermann, S.; Schoch, J.; Voelger, H. R., Structure-based prediction of asparagine and aspartate degradation sites in antibody variable regions. *PloS one* **2014,** *9* (6), e100736.

176. Qian, J.; Yearley, E.; Tian, S.; Jing, L.; Balsaraf, A.; Lo Surdo, P.; Huang, Y.; Chandramouli, S.; Bottomley, M. J.; Moniotte, N.; Wang, Z., Non-Enzymatic and Site-Specific Glycan Shedding: A Novel Protein Degradation Pathway Observed in a Stabilized Form of RSV Prefusion F Protein. *Analytical Chemistry* **2018,** *90* (18), 10897-10902.

177. Bantscheff, M.; Lemeer, S.; Savitski, M. M.; Kuster, B., Quantitative mass spectrometry in proteomics: critical review update from 2007 to the present. *Analytical and Bioanalytical Chemistry* **2012,** *404* (4), 939-965.

178. Schubert, O. T.; Röst, H. L.; Collins, B. C.; Rosenberger, G.; Aebersold, R., Quantitative proteomics: challenges and opportunities in basic and applied research. *Nature Protocols* **2017,** *12* (7), 1289-1294.

179. Aebersold, R.; Mann, M., Mass spectrometry-based proteomics. *Nature* **2003,** *422* (6928), 198-207.

180. Bantscheff, M.; Schirle, M.; Sweetman, G.; Rick, J.; Kuster, B., Quantitative mass spectrometry in proteomics: a critical review. *Analytical and Bioanalytical Chemistry* **2007,** *389* (4), 1017-1031.

181. Lindemann, C.; Thomanek, N.; Hundt, F.; Lerari, T.; Meyer, H. E.; Wolters, D.; Marcus, K., Strategies in relative and absolute quantitative mass spectrometry based proteomics. *Biological Chemistry* **2017,** *398* (5-6), 687-699.

182. Li, Z.; Tremmel, D. M.; Ma, F.; Yu, Q.; Ma, M.; Delafield, D. G.; Shi, Y.; Wang, B.; Mitchell, S. A.; Feeney, A. K.; Jain, V. S.; Sackett, S. D.; Odorico, J. S.; Li, L., Proteome-wide and matrisome-specific alterations during human pancreas development and maturation. *Nature Communications* **2021,** *12* (1), 1-12.

183. Lange, V.; Picotti, P.; Domon, B.; Aebersold, R., Selected reaction monitoring for quantitative proteomics: a tutorial. *Molecular Systems Biology* **2008,** *4* (1), 222.

184. Zhou, S.; Hu, Y.; Veillon, L.; Snovida, S. I.; Rogers, J. C.; Saba, J.; Mechref, Y., Quantitative LC–MS/MS glycomic analysis of biological samples using aminoxyTMT. *Analytical Chemistry* **2016,** *88* (15), 7515-7522.

185. Huang, M.; Wang, Y., Targeted quantitative proteomic approach for probing altered protein expression of small GTPases associated with colorectal cancer metastasis. *Analytical Chemistry* **2019,** *91* (9), 6233-6241.

186. Sohn, C. H.; Lee, J. E.; Sweredoski, M. J.; Graham, R. L.; Smith, G. T.; Hess, S.; Czerwieniec, G.; Loo, J. A.; Deshaies, R. J.; Beauchamp, J., Click chemistry facilitates formation of reporter ions and simplified synthesis of amine-reactive multiplexed isobaric tags for protein quantification. *Journal of the American Chemical Society* **2012,** *134* (5), 2672-2680.

187. Kito, K.; Ito, T., Mass spectrometry-based approaches toward absolute quantitative proteomics. *Current Genomics* **2008,** *9* (4), 263-274.

188. Collins, B. C.; Hunter, C. L.; Liu, Y.; Schilling, B.; Rosenberger, G.; Bader, S. L.; Chan, D. W.; Gibson, B. W.; Gingras, A.-C.; Held, J. M., Multi-laboratory assessment of reproducibility, qualitative and quantitative performance of SWATH-mass spectrometry. *Nature Communications* **2017,** *8* (1), 1-12.

189. Song, X.; Chen, H.; Zare, R. N., Coulometry‐assisted quantitation in spray ionization mass spectrometry. *J. Mass Spectrom.* **2020**, e4628.

190. Kang, J.; Lemaire, H.-G.; Unterbeck, A.; Salbaum, J. M.; Masters, C. L.; Grzeschik, K.-H.; Multhaup, G.; Beyreuther, K.; Müller-Hill, B., The precursor of Alzheimer's disease amyloid A4 protein resembles a cell-surface receptor. *Nature* **1987,** *325* (6106), 733-736.

191. Haass, C.; Selkoe, D. J., Cellular processing of β-amyloid precursor protein and the genesis of amyloid β-peptide. *Cell* **1993,** *75* (6), 1039-1042.

192. Selkoe, D. J.; Hardy, J., The amyloid hypothesis of Alzheimer's disease at 25 years. *EMBO Molecular Medicine* **2016,** *8* (6), 595-608.

193. Fagan, A. M.; Xiong, C.; Jasielec, M. S.; Bateman, R. J.; Goate, A. M.; Benzinger, T. L.; Ghetti, B.; Martins, R. N.; Masters, C. L.; Mayeux, R., Longitudinal change in CSF biomarkers in autosomal-dominant Alzheimer's disease. *Science Translational Medicine* **2014,** *6* (226), 226ra30-226ra30.

194. Shankar, G. M.; Bloodgood, B. L.; Townsend, M.; Walsh, D. M.; Selkoe, D. J.; Sabatini, B. L., Natural oligomers of the Alzheimer amyloid-β protein induce reversible synapse loss by modulating an NMDA-type glutamate receptor-dependent signaling pathway. *Journal of Neuroscience* **2007,** *27* (11), 2866-2875.

195. Pérez-Grijalba, V.; Pesini, P.; Allué, J. A.; Sarasa, L.; Montañés, M.; Lacosta, A.-M.; Casabona, D.; San-José, I.; Boada, M.; Tárraga, L., Aβ 1-17 is a major amyloid-β fragment isoform in cerebrospinal fluid and blood with possible diagnostic value in Alzheimer's disease. *Journal of Alzheimer's Disease* **2015,** *43* (1), 47-56.

196. Bros, P.; Delatour, V.; Vialaret, J.; Lalere, B.; Barthelemy, N.; Gabelle, A.; Lehmann, S.; Hirtz, C., Quantitative detection of amyloid-β peptides by mass spectrometry: state of the art and clinical applications. *Clinical Chemistry and Laboratory Medicine (CCLM)* **2015,** *53* (10), 1483-1493.

197. Grasso, G., Mass spectrometry is a multifaceted weapon to be used in the battle against Alzheimer's disease: Amyloid beta peptides and beyond. *Mass Spectrometry Reviews* **2019,** *38* (1), 34-48.

198. Iino, T.; Watanabe, S.; Yamashita, K.; Tamada, E.; Hasegawa, T.; Irino, Y.; Iwanaga, S.; Harada, A.; Noda, K.; Suto, K., Quantification of Amyloid-β in Plasma by Simple and Highly Sensitive Immunoaffinity Enrichment and LC-MS/MS Assay. *The Journal of Applied Laboratory Medicine* **2021**.

199. Lame, M. E.; Chambers, E. E.; Blatnik, M., Quantitation of amyloid beta peptides Aβ1–38, Aβ1–40, and Aβ1–42 in human cerebrospinal fluid by ultra-performance liquid chromatography–tandem mass spectrometry. *Analytical Biochemistry* **2011,** *419* (2), 133-139.

200. Permentier, H. P.; Bruins, A. P., Electrochemical oxidation and cleavage of proteins with on-line mass spectrometric detection: development of an instrumental alternative to enzymatic protein digestion. *Journal of the American Society for Mass Spectrometry* **2004,** *15*, 1707-1716.

201. Roeser, J.; Permentier, H. P.; Bruins, A. P.; Bischoff, R., Electrochemical oxidation and cleavage of tyrosine-and tryptophan-containing tripeptides. *Analytical Chemistry* **2010,** *82* (18), 7556-7565.

202. Pagala, V. R.; High, A. A.; Wang, X.; Tan, H.; Kodali, K.; Mishra, A.; Kavdia, K.; Xu, Y.; Wu, Z.; Peng, J., Quantitative protein analysis by mass spectrometry. In *Protein-Protein Interactions*, Springer: 2015; pp 281-305.

203. Na, C. H.; Peng, J., Analysis of ubiquitinated proteome by quantitative mass spectrometry. In *Quantitative Methods in Proteomics*, Springer: 2012; pp 417-429.

204. Garcia, B. A., Quantitative proteomics for understanding modified proteins and proteomes. *The FASEB Journal* **2018,** *32*, 474.1-474.1.

205. Cox, J.; Hein, M. Y.; Luber, C. A.; Paron, I.; Nagaraj, N.; Mann, M., Accurate proteome-wide label-free quantification by delayed normalization and maximal peptide ratio extraction, termed MaxLFQ. *Molecular & Cellular Proteomics* **2014,** *13* (9), 2513-2526.

206. Miao, W.; Li, L.; Wang, Y., High-throughput targeted quantitative analysis of the interaction between HSP90 and kinases. *Analytical Chemistry* **2019,** *91* (18), 11507-11509.

207. Yang, L.; Gregorich, Z. R.; Cai, W.; Zhang, P.; Young, B.; Gu, Y.; Zhang, J.; Ge, Y., Quantitative proteomics and immunohistochemistry reveal insights into cellular and molecular processes in the infarct border zone one month after myocardial infarction. *Journal of Proteome Research* **2017,** *16* (5), 2101-2112.

208. Coradin, M.; Karch, K. R.; Garcia, B. A., Monitoring proteolytic processing events by quantitative mass spectrometry. *Expert Review of Proteomics* **2017,** *14* (5), 409-418.

209. Schwanhäusser, B.; Busse, D.; Li, N.; Dittmar, G.; Schuchhardt, J.; Wolf, J.; Chen, W.; Selbach, M., Correction: Corrigendum: Global quantification of mammalian gene expression control. *Nature* **2013,** *495* (7439), 126-127.

210. Silva, J. C.; Gorenstein, M. V.; Li, G.-Z.; Vissers, J. P.; Geromanos, S. J., Absolute Quantification of Proteins by LCMSE: A Virtue of Parallel ms Acquisition* S. *Molecular & Cellular Proteomics* **2006,** *5* (1), 144-156.

211. Gilgunn, S.; Bones, J., Challenges to industrial mAb bioprocessing—removal of host cell proteins in CHO cell bioprocesses. *Current Opinion in Chemical Engineering* **2018,** *22*, 98-106.

212. Lim, A.; Doyle, B. L.; Kelly, G. M.; Reed‐Bogan, A. M.; Breen, L. H.; Shamlou, P. A.; Lambooy, P. K., Characterization of a cathepsin D protease from CHO cell‐free medium and mitigation of its impact on the stability of a recombinant therapeutic protein. *Biotechnology Progress* **2018,** *34* (1), 120-129.

213. Tscheliessnig, A. L.; Konrath, J.; Bates, R.; Jungbauer, A., Host cell protein analysis in therapeutic protein bioprocessing–methods and applications. *Biotechnology Journal* **2013,** *8* (6), 655-670.

214. Goepfert, P. A.; Fu, B.; Chabanon, A.-L.; Bonaparte, M. I.; Davis, M. G.; Essink, B. J.; Frank, I.; Haney, O.; Janosczyk, H.; Keefer, M. C., Safety and immunogenicity of SARS-CoV-2 recombinant protein vaccine formulations in healthy adults: interim results of a randomised, placebo-controlled, phase 1–2, dose-ranging study. *The Lancet Infectious Diseases* **2021,** *21* (9), 1257-1270.

215. Li, X.; Wang, F.; Li, H.; Richardson, D. D.; Roush, D. J., The measurement and control of high-risk host cell proteins for polysorbate degradation in biologics formulation. *Antibody Therapeutics* **2022,** *5* (1), 42-54.

216. Gao, X.; Rawal, B.; Wang, Y.; Li, X.; Wylie, D.; Liu, Y.-H.; Breunig, L.; Driscoll, D.; Wang, F.; Richardson, D. D., Targeted host cell protein quantification by LC–MRM enables biologics processing and product characterization. *Analytical Chemistry* **2019,** *92* (1), 1007-1015.

217. Husson, G.; Delangle, A.; O'hara, J.; Cianferani, S.; Gervais, A.; Van Dorsselaer, A.; Bracewell, D.; Carapito, C., Dual data-independent acquisition approach combining global HCP profiling and absolute quantification of key impurities during bioprocess development. *Analytical chemistry* **2018,** *90* (2), 1241-1247.

218. Gupta, S.; Jiskoot, W.; Schöneich, C.; Rathore, A. S., Oxidation and Deamidation of Monoclonal Antibody Products: Potential Impact on Stability, Biological Activity, and Efficacy. *Journal of Pharmaceutical Sciences* **2021**.

219. Gervais, D., Protein deamidation in biopharmaceutical manufacture: understanding, control and impact. *Journal of Chemical Technology & Biotechnology* **2016,** *91* (3), 569-575.

220. Vigneswara, V.; Cass, S.; Wayne, D.; Bolt, E. L.; Ray, D. E.; Carter, W. G., Molecular ageing of alpha-and Beta-synucleins: protein damage and repair mechanisms. *PLoS One* **2013,** *8* (4), e61442.

221. Hains, P. G.; Truscott, R. J., Age-dependent deamidation of lifelong proteins in the human lens. *Investigative Ophthalmology & Visual Science* **2010,** *51* (6), 3107-3114.

222. Bults, P.; Bischoff, R.; Bakker, H.; Gietema, J. A.; van de Merbel, N. C., LC-MS/MS-based monitoring of in vivo protein biotransformation: quantitative determination of trastuzumab and its deamidation products in human plasma. *Analytical Chemistry* **2016,** *88* (3), 1871-1877.

223. Ai, Y.; Zhao, P.; Fnu, P. I. J.; Chen, H., Absolute quantitation of tryptophan-containing peptides and amyloid β-peptide fragments by coulometric mass spectrometry. *Journal of the American Society for Mass Spectrometry* **2021,** *32* (7), 1771-1779.

224. Wang, Q.; Liu, Z.; Liu, Y.; Chen, H., Absolute Quantitation of N-Nitrosamines by Coulometric Mass Spectrometry without Using Standards. *Journal of the American Society for Mass Spectrometry* **2022**.

225. Kim, P.; Kaszuba, A.; Jang, H.-I.; Kim, Y.-I., Purification of GST-fused cyanobacterial central oscillator protein KaiC. *Appl. Biochem. Microbiol.* **2020,** *56* (4), 395-399.

226. Kim, Y.-I.; Boyd, J. S.; Espinosa, J.; Golden, S. S., Detecting KaiC phosphorylation rhythms of the cyanobacterial circadian oscillator in vitro and in vivo. *Methods Enzymol.* **2015,** *551*, 153-173.

227. Yan, B.; Steen, S.; Hambly, D.; Valliere-Douglass, J.; Bos, T. V.; Smallwood, S.; Yates, Z.; Arroll, T.; Han, Y.; Gadgil, H., Succinimide formation at Asn 55 in the complementarity determining region of a recombinant monoclonal antibody IgG1 heavy chain. *Journal of Pharmaceutical Sciences* **2009,** *98* (10), 3509-3521.

228. Jiskoot, W.; Randolph, T. W.; Volkin, D. B.; Middaugh, C. R.; Schöneich, C.; Winter, G.; Friess, W.; Crommelin, D. J.; Carpenter, J. F., Protein instability and immunogenicity: roadblocks to clinical application of injectable protein delivery systems for sustained release. *Journal of Pharmaceutical Sciences* **2012,** *101* (3), 946-954.

229. Cao, M.; Xu, W.; Niu, B.; Kabundi, I.; Luo, H.; Prophet, M.; Chen, W.; Liu, D.; Saveliev, S. V.; Urh, M.; Wang, J., An Automated and Qualified Platform Method for Site-Specific Succinimide and Deamidation Quantitation Using Low-pH Peptide Mapping. *Journal of Pharmaceutical Sciences* **2019,** *108*, 3540-3549.

230. Cao, M.; Mulagapati, S. H. R.; Vemulapalli, B.; Wang, J.; Saveliev, S. V.; Urh, M.; Hunter, A.; Liu, D., Characterization and quantification of succinimide using peptide mapping under low-pH conditions and hydrophobic interaction chromatography. *Analytical Biochemistry* **2019,** *566*, 151-159.

231. Liigand, P.; Kaupmees, K.; Kruve, A., Influence of the amino acid composition on the ionization efficiencies of small peptides. *Journal of Mass Spectrometry* **2019,** *54* (6), 481-487.